THE CHARACTERISTIC IMPEDANCE AND PHASE VELOCITY OF A SHIELDED HELICAL TRANSMISSION LINE

DEPARTMENT OF ELECTRICAL ENGINEERING
CARNEGIE INSTITUTE OF TECHNOLOGY
PITTSBURGH, PENNSYLVANIA

THE CHARACTERISTIC IMPEDANCE AND PHASE VELOCITY of a SHIELDED HELICAL TRANSMISSION LINE

by

Herbert S. Kirschbaum

Progress Report of Work Done Under

Office of Naval Research Contracts N7onr 30306 and N7onr 30308

Edward R. Schatz, Supervisor
Everard M. Williams
Herbert S. Kirschbaum

Department of Electrical Engineering
Carnegie Institute of Technology
Pittsburgh 13, Pennsylvania

Acknowledgment

The author wishes to express his appreciation to Professor E. K. Williams for suggesting this problem and to Professors E. R. Schatz and R. L. Bright for helpful suggestions and criticisms.

TABLE OF CONTENTS

Synopsis

This report gives the results of a theoretical and experimental investigation of the properties of a shielded helix when used as a transmission line. Such a structure is dispersive and because of the presence of both TM and TE modes it cannot be said to have a true characteristic impedance. However, such an impedance is defined in terms of a distributed capacitance and inductance. These parameters, the capacitance and the inductance, are determined for the case of infinite wave length for round wire helices. The equations are developed for a uniform dielectric inside the shield and for two dielectrics, one inside the helix and the other between the helix and shield. These analytic results are shown to agree very well with the experimental results obtained by the author and by other investigators.

As a check, an attempt is made to solve the wave equation for a tape helix, the tape being assumed to be anisotropic to the extent that it can conduct only in the helix direction. The results of this work show that the phase velocity varies as the frequency varies. In addition, this work shows the phase velocity and characteristic impedance of a narrow tape helix compare very favorably with these same properties of a wire helix, the wire diameter being equal to the tape width.

LIST OF FIGURES

LIST OF TABLES

Chapter I.

Introduction

A brief description is given herein of the various aspects of the problem of the shielded helical transmission line, followed by a discussion of the theoretical and experimental results which have been presented elsewhere. This is followed by a discussion of the results of the present investigation.

I-1. The Helical Transmission Line Problem

Helical structures have long been used in various ways as electromagnetic devices. In particular, they occur in the windings of core type transformers, video delay lines, traveling wave tubes and as antenna structures. As a result of the interest in this structure, numerous reports have appeared describing the efforts made to analyze and measure the properties of a helix used as an electromagnetic device.

A helical structure can take many forms. Some of these are: a helix of infinite extent existing in an unbounded uniform medium; a helix of infinite extent in which the medium inside the helix radius is different from that outside; a shielded helix with either a uniform medium inside the shield or as in the previous situation, two media present. The greatest effort has been confined, in the past, to the first one of these forms, namely, the infinite helix in an unbounded uniform medium. The problem, in this case, is one of finding those solutions of the homogeneous Maxwell equations which satisfy the boundary conditions at the helix and at infinity. From these solutions, the various modes of operation of the helix can be evaluated.

In the case of a shielded helical transmission line, the problem is one of finding those solutions of the homogeneous Maxwell equations which satisfy the boundary conditions at the helix and at the shield. When used as

a transmission line, the greatest interest is centered upon the characteristic impedance and phase constant of the helical line. Strictly speaking, the impedance concept is not a correct one when applied to a helical transmission line, since the waves present are a mixture of both transverse magnetic and transverse electric waves. Any impedances so developed apply only to relatively low frequencies, and they completely break down at a frequency where the circumference of the helix is equal to about one to two wave lengths. Beyond this frequency, the helix operates in many different modes, each with its own phase velocity. It has also been shown[11] that if the wave length is less than twice the pitch, no free modes of any sort can exist on a helix immersed in an unbounded uniform medium. This probably applies also to the shielded helix if the shield is not too close to the helix.

I-2. Previous Work

As has been noted above, most of the work done on the helix concerned a helix immersed in an unbounded uniform medium. Very little has been done with regard to the shielded helix used as a transmission line. These analyses whether on the shielded or unshielded helix can, in general, be classified into four classifications. These are the infinitesimally thin wire approximation, the exact approach, the sheath or butt helix approximation, and the various approximations to a round wire or narrow tape helix. These various helices are illustrated in Figure 1. In the thin wire approximation, it is assumed that the current flows along a line helix and that the electric field in the helix direction is zero along this line. Such an approach inevitably leads to a phase velocity in the helix direction equal to the

---

11 - Superscript numbers refer to the Bibliography and references at the end of this report.

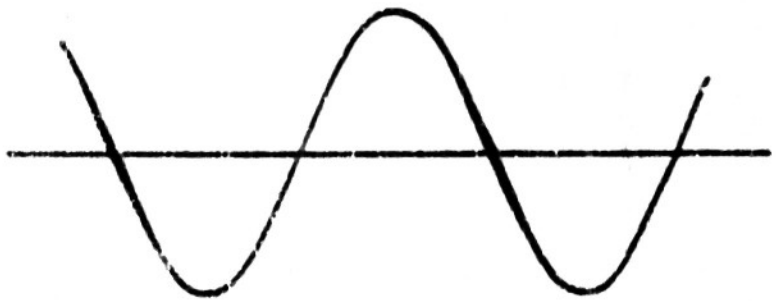

(a): LINE HELIX

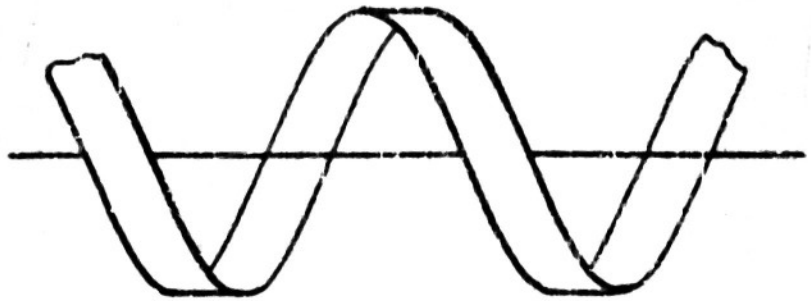

(b): TAPE HELIX

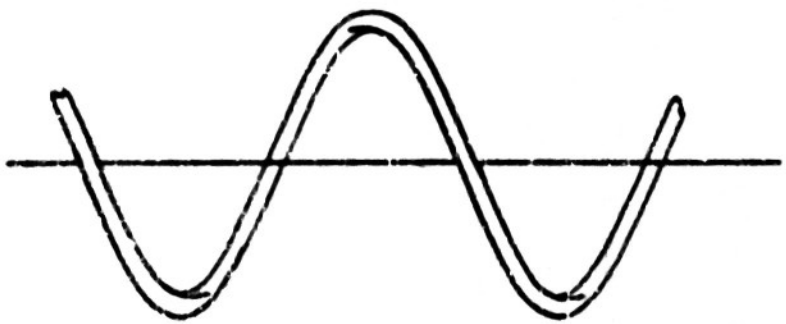

(c): ROUND WIRE HELIX

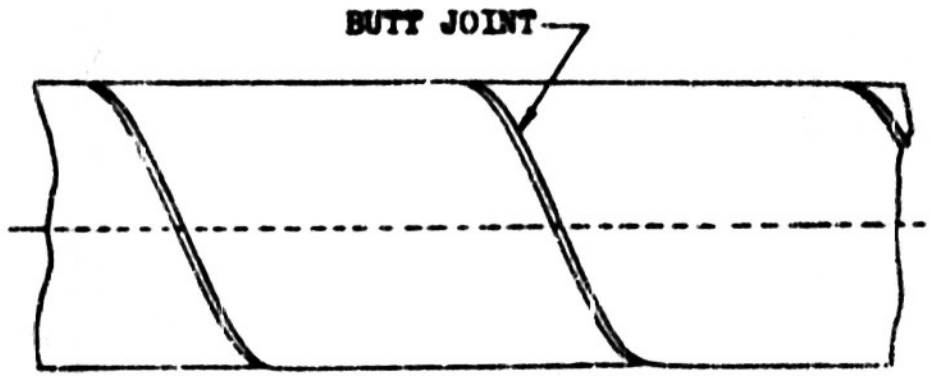

(d): BUTTED TAPE HELIX

FIGURE 1: VARIOUS TYPES OF HELICES

velocity of light. Since this work will show that the wire dimensions have a significant effect upon the phase velocity, such a model is unsuitable. Furthermore, the characteristic impedance of such a shielded line helix is infinite.

The exact approach was used by Nicholson.[9] He used a coordinate system which described the surface of a helical wire and derived the form of Maxwell's equations in that system. His results are of doubtful validity since he assumed his coordinate system to be orthogonal, which it is not, as shown by Bagby[10]. Furthermore, he assumed rather than determined the phase velocity. An exact approach of this sort in which a helical coordinate system is used offers no advantages in the case of a shielded helix since, in this case, the shield does not form a coordinate surface. As an added complication, Maxwell's equations in such a coordinate system cannot be solved by known methods and an approximate solution must be found. Sensiper[11] also used an exact approach for a tape helix and found that the propagation constant was determined by an infinite determinantal transcendental equation. He abandoned this method in favor of an approximate approach.

Various authors[6,12,13] have studied the propagation of electromagnetic waves on shielded and unshielded helices by assuming the helix to be replaced by an anisotropic conducting sheet which could conduct in the helix direction only. Such a sheet actually forms a butt wound helix. By its very nature, such a model is not a satisfactory approximation to a wire or narrow tape helix except in cases where the helix pitch is so small that the turns butt together. The main feature of attraction which the butt tape model presents is the fact that it can be solved exactly.

The approximation to an actual wire helix was used by Buchholz[15] in obtaining the inductance of a twin helical line inside a shielding sheath. He used an integral equation approach to find the vector potential caused

by equal and opposite direct currents flowing in two parallel helices. From this, he determined the flux linkages with an actual round wire from which followed the inductance.

Sensiper[11] very completely analyzed the various modes with which a thin tape unshielded helix can propagate electromagnetic waves. His approximation consisted of satisfying the boundary condition with regard to the electric field on the center line of the tape only, and satisfying the boundary conditions with regard to the magnetic field over the entire tape surface. In order to satisfy the latter condition, he assumed a uniform distribution of current density across the tape. However, he did not consider the effect of a shield or the effect of two different dielectric media, one inside the helix and one external to it.

Tien[16] carried forward a similar analysis in attempting to evaluate the effect of dielectric material outside the helix. His results were intended for application to traveling wave tubes, and he assumed the phase velocity was that for a butted tape helix.

Various authors carried on experimental work on helices. Only those whose work concerned shielded helices at low frequencies are discussed in Chapter III on experimental results.

This section is not intended as a detailed review of all the pertinent literature. However, the references mentioned will serve as a guide to still other work on the helix in general.

I-3. Results of the Present Investigation

This investigation treats the shielded helix as a distributed circuit transmission line. The inductance and capacitance parameters are derived for a quasi-round wire helix for infinite wave length. While these parameters have real meaning for direct current only, they should prove useful

up to fairly high frequencies as is shown later by the work on the butted tape helix. These inductance and capacitance parameters are used to derive expressions for the characteristic impedance and phase velocity of a shielded helix.

The wave equation is solved for a thin tape and the low frequency characteristic impedance and phase velocity are derived. These are shown to agree closely with those obtained from the distributed inductance and capacitance parameters for a round wire.

The results of the analytical work are compared with experimental results obtained by this author and others, and shown to agree very closely.

Chapter II.

Analytical Results

Because of complexity involved in the development of the transmission line parameters, these derivations have been placed in two Appendices. These are Appendices B and C. In this section, a brief description will be given of the methods used to develop the expressions for the transmission line parameters along with the final results. This will be followed by an application of these results to the problem of determining the characteristic impedance of the helical transmission line and also its phase velocity. These results are compared in Chapter III with experimental results performed by this author and other investigators.

The results of a wave equation solution are also presented for helical tapes, the solutions being derived for a butted tape helix and for a very narrow tape helix. It is shown also that the phase velocity is a function of frequency.

Finally there is a brief discussion of the losses in the wire and sheath.

Two of the parameters with which the behavior of a transmission line can be described are the distributed capacitance in, say, farads per meter of line length and the distributed inductance in, say, henries per meter of line length. Since the transmission line of this report consists of a helix formed of round wire surrounded by a perfectly conducting sheath, there are two possible definitions of line length. The first of these might be measured in the axial direction. The second might be measured in the helix direction. Since the propagation of energy along such a line

is actually in the axial direction, the former definition of line length is preferred. The capacitance and inductance parameters are developed per meter in the helix direction and then written in terms of line length in the axial direction.

II-1. The Distributed Capacitance

(a) Description of the Helix

The transmission line with which this report is concerned consists of a helix of round wire formed by winding it upon a supporting tube or rod of dielectric material. The return conductor consists of a conducting sheath which is outside the helix and coaxial with the axis of the helix. The space between the helix and the sheath may be free space or may be filled with some dielectric such as oil, polystyrene, etc. For the purposes of determining the capacitance per unit length, the transmission line is assumed to be infinitely long.

(b) Formulation of the Problem

In Appendix B a rather complete formulation of the problem of the capacitance is presented. It will suffice here to present some of the more salient features of the derivation. The method of approach used is to disregard the actual boundary at the surface of the wire and to replace it with a boundary that closely approximates the surface of the wire. The necessity for doing this lies in the intractability of Laplace's equation when written in a coordinate system which will describe the surface of the helical wire. Furthermore, any such coordinate system would not contain the sheath as one of its coordinate surfaces.

Laplace's equation is solved in a circular cylindrical coordinate system. A potential function is then derived which satisfies Laplace's equation and which also satisfies certain boundary conditions. These boundary conditions are: that the potential at the sheath is zero and that the discontinuity in the radial component of the displacement vector, at the helix radius, be equal to the surface charge density on a very narrow tape helix. When the width of this tape is allowed to approach zero, the tape helix degenerates into a line helix of infinitesimal cross section having a uniform charge of Q_f coulombs per meter in the helix direction. The potential function so derived approaches infinity as one approaches the line helix.

Considering only a region in the immediate vicinity of the line, the equipotential surfaces are very close to right circular cylinders formed into the shape of a helix. This is the case since, as the line charge is approached very closely, the helical line appears to approach an infinitely long straight line of charge and it is known that the equipotential surfaces around such a line of charge are right circular cylinders. One of these equipotential surfaces is chosen as the surface of the wire. Although such a surface does not coincide with the actual wire surface, the agreement between it and the wire for very small wires is sufficiently close for practical applications. The potential of this equipotential surface when divided by the charge in coulombs per meter yields the reciprocal of the distributed capacitance.

(c) The Analytical Results

The procedure outline in section II-1(b) is carried out in detail in Appendix B. The results of this work are given on the next page in several forms,

$$\frac{1}{C} = \frac{R_1}{\epsilon_2 \tau \cos\psi}\left\{\log_e\frac{R_2}{R_1} + 2\sum_{m=1}^{\infty}\frac{\left[1-\frac{I_m(bR_1)K_m(bR_2)}{I_m(bR_2)K_m(bR_1)}\right]I_m(bR_1)K_m(bR_1)\cos\left(\frac{br}{\cos\psi}\right)}{\frac{\epsilon_1}{\epsilon_2}+\left(\frac{\epsilon_1}{\epsilon_2}-1\right)\left[1-\frac{I_m'(bR_1)K_m(bR_2)}{I_m(bR_2)K_m'(bR_1)}\right]bR_1 I_m(bR_1)K_m'(bR_1)}\right\} \tag{1}$$

or,

$$\frac{1}{C_z} = \frac{1}{2\pi\epsilon_2}\left\{\log_e\frac{R_2}{R_1} + 2\sum_{m=1}^{\infty}\frac{\left[1-\frac{I_m(bR_1)K_m(bR_2)}{I_m(bR_2)K_m(bR_1)}\right]I_m(bR_1)K_m(bR_1)\cos\left(\frac{br}{\cos\psi}\right)}{\frac{\epsilon_1}{\epsilon_2}+\left(\frac{\epsilon_1}{\epsilon_2}-1\right)\left[1-\frac{I_m'(bR_1)K_m(bR_2)}{I_m(bR_2)K_m'(bR_1)}\right]bR_1 I_m(bR_1)K_m'(bR_1)}\right\} \tag{2}$$

where C is the capacitance per meter in the helix direction and C_z is the capacitance per meter in the axial direction. The I_m and K_m functions are modified Bessel functions of order m and of the first and second kinds, respectively. Their properties are discussed briefly in Appendix A. The other dimensions are defined in Figures 2 and 3. Any consistent system of length units may be used since all lengths enter as dimensionless ratios. The permitivities ϵ_1 and ϵ_2 are those of regions 1 and 2 defined in Figure 3. Normally ϵ_1 is greater than ϵ_2, but in the case where they are equal, (2) reduces to

$$\frac{1}{C_z} = \frac{1}{2\pi\epsilon_2}\left\{\log_e\frac{R_2}{R_1} + 2\sum_{m=1}^{\infty}\left[1-\frac{I_m(bR_1)K_m(bR_2)}{I_m(bR_2)K_m(bR_1)}\right]I_m(bR_1)K_m(bR_1)\cos\left(\frac{br}{\cos\psi}\right)\right\} \tag{3}$$

If the helix pitch τ is sufficiently small, the summation in the pair of brackets can be replaced by a closed form. A complete discussion of this

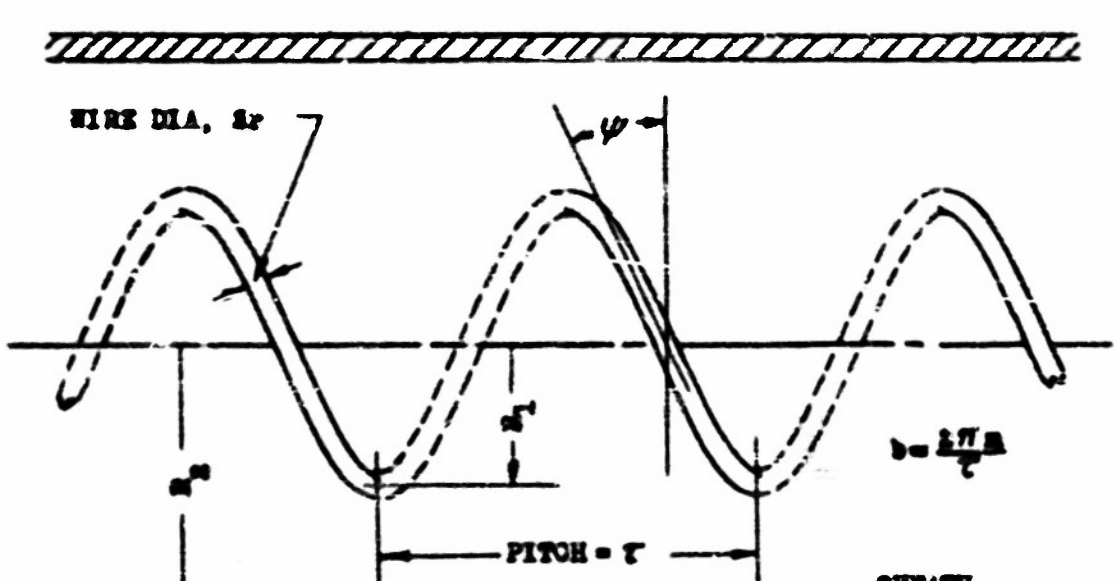

FIGURE 2: HELICAL WIRE INSIDE SHEATH

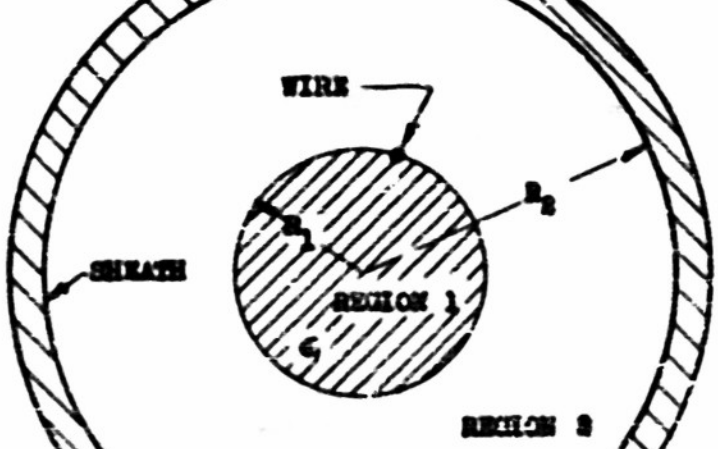

FIGURE 3: DEFINITION OF REGIONS 1 and 2

is given in Appendix B-4. For this case, (2) becomes,

$$\frac{1}{C_2} = \frac{1}{2\pi\epsilon_2}\left\{\text{Log}_e\frac{R_2}{R_1} - \frac{2\epsilon_2}{\epsilon_1+\epsilon_2}\sin\psi\cdot\text{Log}_e\left[2\sin\left(\frac{\pi r}{\tau\cos\psi}\right)\right]\right\} \tag{4}$$

Figure 4 shows approximately the range of $\frac{R_1}{\tau}$ for which (4) can be used and still be within a specified percentage of (3). This figure actually shows the error to be expected in the characteristic impedance resulting from the use of (4) and a similar expression for inductance. Since the capacitance, inductance and impedance expressions are very similar, the curves in Figure 4 give a good indication of the ranges of helix dimensions for which (4) is applicable.

If on the other hand the helix pitch τ approaches infinity, the inner conductor becomes a straight wire parallel to the axis and displaced from it by a distance R_1. Within the radius R_1 the permittivity is ϵ_1, and between R_1 and R_2 it is ϵ_2. For very long pitches the capacitance becomes approximately

$$\frac{1}{C_2} = \frac{1}{2\pi\epsilon_2}\left\{\text{Log}_e\frac{R_2}{R_1} + \frac{2\epsilon_2}{\epsilon_1+\epsilon_2}\sum_{m=1}^{\infty}\frac{\left[1-\left(\frac{R_1}{R_2}\right)^{2m}\right]\cos\left(\frac{mr}{R_1}\right)}{m\left[1-\left(\frac{\epsilon_1-\epsilon_2}{\epsilon_1+\epsilon_2}\right)\left(\frac{R_1}{R_2}\right)^{2m}\right]}\right\} \tag{5}$$

For the case in which $\epsilon_1 = \epsilon_2$ this becomes,

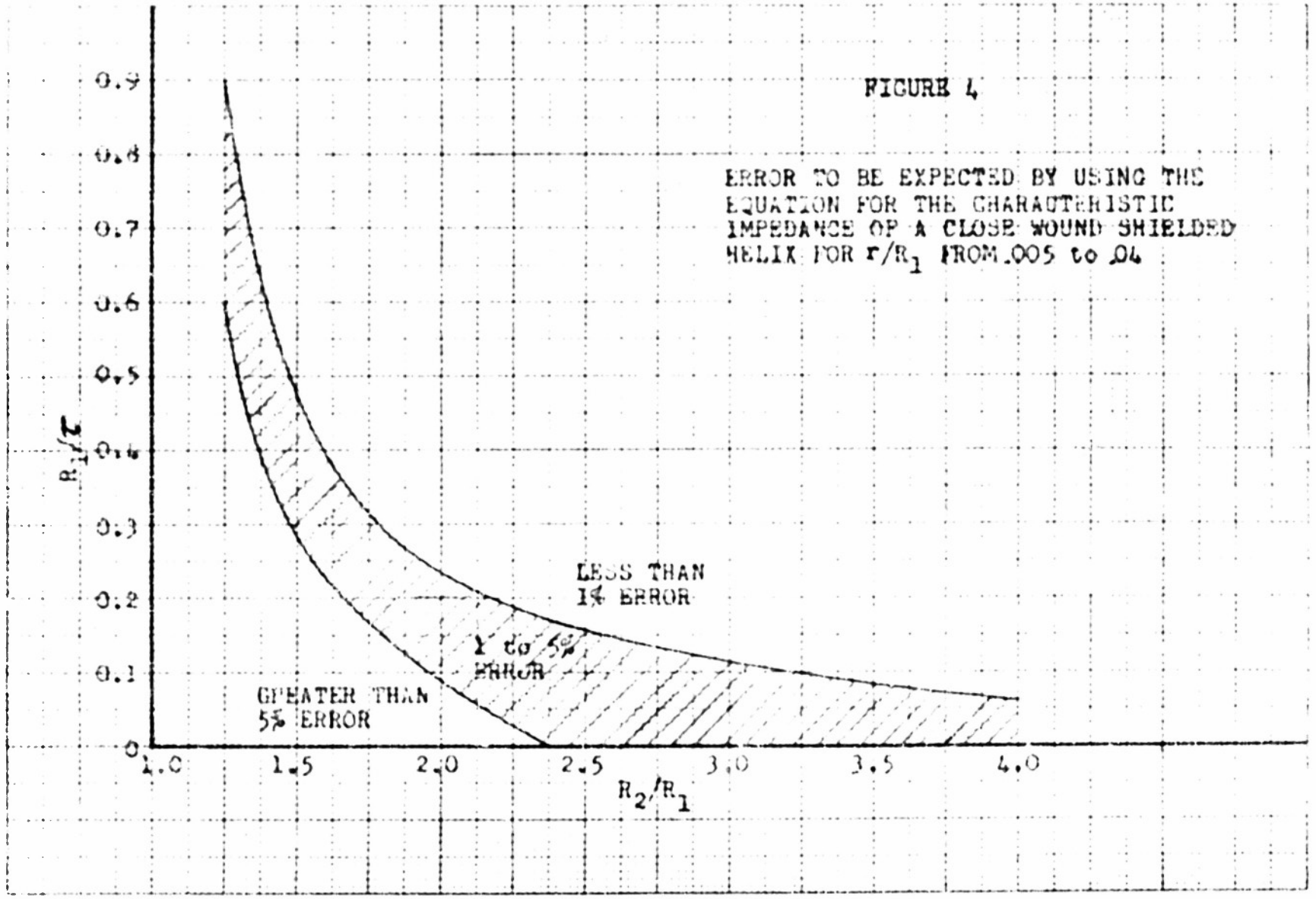
FIGURE 4
ERROR TO BE EXPECTED BY USING THE EQUATION FOR THE CHARACTERISTIC IMPEDANCE OF A CLOSE WOUND SHIELDED HELIX FOR r/R1 FROM .005 to .04
0.9
0.8
0.7
0.6
0.5
0.4
0.3
0.2
0.1
0
R1/Z
LESS THAN 1% ERROR
1 to 5% ERROR
GREATER THAN 5% ERROR
1.0
1.5
2.0
2.5
3.0
3.5
4.0
R2/R1

$$\frac{1}{C_2} = \frac{1}{2\pi\epsilon_2}\left\{\text{Log}_e\frac{R_2}{R_1} + \sum_{m=1}^{\infty}\left[1-\left(\frac{R_1}{R_2}\right)^{2m}\right]\frac{\cos\left(\frac{mr}{R_1}\right)}{m}\right\} \tag{6}$$

This can be written in closed form by applying formula 418 on page 85 of reference (4). Upon doing this,

$$\frac{1}{C_2} = \frac{1}{2\pi\epsilon_2}\left\{\text{Log}_e\frac{R_2}{R_1} + \frac{1}{2}\text{Log}_e\left[\frac{1-2\left(\frac{R_1}{R_2}\right)^2\cos\frac{r}{R_1}+\left(\frac{R_1}{R_2}\right)^4}{2\left(1-\cos\frac{r}{R_1}\right)}\right]\right\} \tag{7}$$

For very small $\frac{r}{R_1}$ as compared with unity, this becomes,

$$\frac{1}{C_2} = \frac{1}{2\pi\epsilon_2}\left\{\text{Log}_e\frac{R_2}{r}\left(1-\frac{R_1^2}{R_2^2}\right)\right\} \tag{8}$$

The exact expression for the capacitance between two parallel cylinders which are not coaxial is given in reference (18) page 76. The capacitance there derived, in the notation of this author, is,

$$\frac{1}{C_2} = \frac{1}{2\pi\epsilon_2}\,\text{Cosh}^{-1}\left\{\frac{R_2}{2r}\left(1-\frac{R_1^2}{R_2^2}\right)+\frac{r}{2R_2}\right\} \tag{9}$$

This expression will approach (8) as (r/R_2) becomes very small. Depending upon the range of applicability, any one of the capacitances presented above may be used with the inductance per meter to arrive at a characteristic impedance and phase velocity for the transmission line. Since this report is concerned mainly with characteristic impedance and phase velocity, no calculations of capacitance as such were made. In the sections on impedance and phase velocity, the above expressions were used, where applicable, to determine a family of impedance and phase velocity curves.

II-2. The Distributed Inductance.

(a) Formulation of the Problem

In Appendix C, a rather complete formulation of the problem of the distributed inductance is given. It will suffice here to present some of the more salient features of the derivation which appear in Appendix C. As in the case of the capacitance, the actual wire is not used to form the boundary of the helix. Instead, a different surface which closely approximates the actual wire is used in place of the wire. It is shown in Appendix C that the inductance of the helix can be arrived at by knowing completely the vector potential in the region surrounding the helix. This inductance neglects any internal flux in the wire. This assumption is based upon the fact that at the frequencies at which this structure is used, the current in the wire will be confined to the surface of the wire. This vector potential is arrived at by solving in cylindrical coordinates what might be called the vector equivalent of Laplace's equation, along with the requirement that the divergence of the vector potential be zero. These two equations, which must be satisfied in the magnetostatic case, are,

$$\nabla \times \nabla \times \underline{A} = 0 \tag{10}$$

$$\nabla \cdot \underline{A} = 0 \qquad (11)$$

Where $\underline{A}$ is the vector potential in the current free region surrounding the helix. This vector potential and the magnetic field which can be derived from it must satisfy certain boundary conditions. The most important of these is, that the magnetic field outside the sheath be zero and that the discontinuity in the tangential component of the $\underline{H}$ vector at the helix radius R_1 be numerically equal to the current density in a very narrow tape helix at R_1. When the width of the tape is allowed to approach zero, the tape degenerates into a line helix of infinitesimal cross section carrying a current of I amperes. The vector potential so derived approaches infinity as one approaches the helical line. If one approaches the line sufficiently close, the distance between the line and the observer becomes small compared with the radius of curvature of the line. In this case the helical line may be approximated by an infinite straight line carrying current. The surfaces of equi-vector-potential which surround such a straight line of current are known to be right circular cylinders. A round wire carrying current in which the current density in the wire is a function of the radius only, has equi-vector-potential surfaces which are right circular cylinders. In fact the wire surface itself is an equi-vector-potential surface. Therefore, as an approximation, one of the equi-vector-potential surfaces which surrounds the line helix is used as the surface of the wire. This approximation approaches perfection as the wire radius approaches zero. As is shown in Appendix C, the magnitude of the vector potential in the helix direction at the wire surface when multiplied by (μ_0/I) yields the inductance per meter in the helix direction. In this report μ_0 is the permeability of free space expressed in rationalized M.K.S. units.

(b) The Analytical Results

The procedure outlined in section II-2(a) is carried out in detail in Appendix C. The results of this work are given below in several forms.

$$L = \frac{\mu_0 R_1 \cos\psi}{\tau}\left\{\frac{1}{2}\left(1-\frac{R_1^2}{R_2^2}\right)+\tan^2\psi\cdot\log_e\frac{R_2}{R_1} -2\sum_{m=1}^{\infty}\left[1-\frac{I_m'(bR_1)K_m'(bR_2)}{I_m'(bR_2)K_m'(bR_1)}\right]I_m'(bR_1)K_m'(bR_1)\cos\left(\frac{br}{\cos\psi}\right)\right\} \qquad (12)$$

where L is the inductance in henries per meter in the helix direction. The other dimensions are defined in Figure 2. Any consistent system of length may be used since all lengths enter as dimensionless ratios. The primes on the Bessel functions denote differentiation with respect to the argument ($b\rho$). If L_z is used to denote the inductance per meter in the axial direction, (12) becomes

$$L_z = 2\pi\mu_0\left(\frac{R_1}{\tau}\right)^2\left\{\frac{1}{2}\left(1-\frac{R_1^2}{R_2^2}\right)+\tan^2\psi\cdot\log_e\frac{R_2}{R_1} -2\sum_{m=1}^{\infty}\left[1-\frac{I_m'(bR_1)K_m'(bR_2)}{I_m'(bR_2)K_m'(bR_1)}\right]I_m'(bR_1)K_m'(bR_1)\cos\left(\frac{br}{\cos\psi}\right)\right\} \qquad (13)$$

If the helix pitch is sufficiently small, the summation in the brackets can be replaced by a closed form. A complete discussion of this is given in Appendix C-6. For this case (13) becomes,

$$L_2 = 2\pi\mu_0\left(\frac{R_1}{\tau}\right)^2\left\{\frac{1}{2}\left(1-\frac{R_1^2}{R_2^2}\right)+\tan^2\psi\left[\log_e\frac{R_2}{R_1}-\frac{1}{\sin\psi}\log_e\left(2\sin\left(\frac{\pi r}{\tau\cos\psi}\right)\right)\right]\right\} \qquad (14)$$

Figure 4 shows the range of $\frac{R}{\tau}$ for which (14) can be used with reasonable accuracy. Although this figure is strictly applicable to the characteristic impedance, it is sufficiently accurate to indicate for what range of good results can be expected from (14).

For a very close wound helix of small wire, the second term within the bracket becomes negligible and the above expression reduces to,

$$L_2 = \pi\mu_0\left(\frac{R_1}{\tau}\right)^2\left(1-\frac{R_1^2}{R_2^2}\right) \qquad (15)$$

This checks previously derived results for very close wound helices in shielding cans. (See reference (19)).

On the other hand, if the pitch of the helix becomes very large it approaches a straight wire parallel to the axis of the sheath and displaced from the axis by a distance of R_1. Hence for a very long pitch the inductance becomes approximately,

$$L_2 = \frac{\mu_0}{2\pi}\left\{\log_e\frac{R_2}{R_1}+\sum_{m=1}^{\infty}\left[1-\left(\frac{R_1}{R_2}\right)^{2m}\right]\frac{\cos\left(\frac{mr}{R_1}\right)}{m}\right\} \qquad (16)$$

This can be expressed in closed form by applying formula 418 on page 85 of reference (4). Upon doing this,

$$L_z = \frac{\mu_0}{2\pi}\left\{\log_e \frac{R_2}{R_1} + \frac{1}{2}\log_e\left[\frac{1-2\left(\frac{R_1}{R_2}\right)^2\cos\frac{r}{R_1}+\left(\frac{R_1}{R_2}\right)^4}{2\left(1-\cos\frac{r}{R_1}\right)}\right]\right\} \tag{17}$$

For very small $\frac{r}{R_1}$ as compared with unity, this becomes,

$$L_z = \frac{\mu_0}{2\pi}\left\{\log_e \frac{R_2}{r}\left(1-\frac{R_1^2}{R_2^2}\right)\right\} \tag{18}$$

When this expression is used along with (8) to compute the characteristic impedance of this degenerate helix ($\tau = \infty$), there results an expression which is in agreement with the accepted[21] impedance for this structure. This validates equation (14) for the case of infinitely long pitch.

The expressions in this section for the inductance and in the previous section for the capacitance are based upon very small wire radii. However, if the pitch of the helix becomes of the same order of magnitude as the wire diameter, the wire radius, while still very small compared to R_1, can hardly be said to be small compared with the pitch. In this case the equipotential surfaces do not satisfactorily approximate the surface of the wire. This difficulty is vitiated by noting that for very small pitches all terms but the first within the braces of equation (13) become negligibly small. Since the first term is independent of the wire diameter it may be concluded that for very close wound small wire helices the distributed inductance is independent of the wire shape. The same may also

be said to be true of the distributed capacitance.

Depending upon the range of applicability, any one of the above inductances may be used with the appropriately chosen capacitance to arrive at a characteristic impedance and phase velocity for the transmission line. Since this report is concerned mainly with the characteristic impedance and phase velocity of a helical transmission line, no calculations of inductance as such were made. In the section on impedance and phase velocity, the above expressions were used where applicable to determine a family of impedance and phase velocity curves.

II-3. Characteristic Impedance and Phase Velocity

(a) Definitions

When a distributed circuit transmission line which has an inductance L_z per unit length and a capacitance C_z per unit length is studied, it is found that it can sustain traveling waves of current and voltage. In the absence of losses, it is found that these waves travel unattenuated with a velocity v_z which is independent of frequency. At any point the ratio of voltage to current is also a constant Z_0 which is independent of frequency. These two constants, the phase velocity and characteristic impedance are related to the inductance and capacitance parameters as follows:

$$Z_0 = \sqrt{\frac{L_z}{C_z}} \tag{20}$$

$$v_z = \frac{1}{\sqrt{L_z C_z}} \tag{21}$$

The inductance and capacitance parameters were derived upon the assumption

of infinite wave length. Consequently these constants have meaning only so long as the wave length is quite long compared with the pitch of the helix. The basis for this assertion is the fact that the mutual effect of the turns of the helix upon any one given turn become smaller as the distance between them increases. Therefore, it is the turns closest a given one that have the greatest effect upon its inductance and capacitance. If the wave length is long, the turns in the vicinity of any one given turn are essentially at constant potential and carry essentially constant current and the above parameters have real meaning.

In Appendix D an attempt is made to solve the wave equation in order to find the phase velocity. Intractable difficulties are encountered in trying to satisfy the boundary conditions. However, a helix is studied for which the wave equation can be solved approximately and although this helix is not a very good model for a wire helix, its behavior sheds some light on the range of applicability of the above parameters with respect to frequency. This will be discussed in a later section.

(b) <u>The Characteristic Impedance</u>

By using (2) and (13) in (20) one obtains for the characteristic impedance,

$$Z_0 = \frac{R_1}{\tau}\sqrt{\frac{\mu_0}{\epsilon_2}}\cdot\sqrt{F_1 F_2} \qquad (22)$$

where,

$$F_1 = \left\{ \log_e \frac{R_2}{R_1} + 2 \sum_{m=1}^{\infty} \frac{\left[1 - \frac{I_m(bR_1) K_m(bR_2)}{I_m(bR_2) K_m(bR_1)} \right] I_m(bR_1) K_m(bR_1) \cos\left(\frac{br}{\cos\psi}\right)}{\frac{\epsilon_1}{\epsilon_2} + \left(\frac{\epsilon_1}{\epsilon_2} + 1\right) \left[1 - \frac{I_m'(bR_1) K_m(bR_2)}{I_m(bR_2) K_m'(bR_1)} \right] (bR_1) I_m(bR_1) K_m'(bR_1)} \right\} \tag{23}$$

$$F_2 = \left\{ \frac{1}{2}\left(1 - \frac{R_1^2}{R_2^2}\right) + \tan^2\psi - \log_e \frac{R_2}{R_1} - 2 \sum_{m=1}^{\infty} \left[1 - \frac{I_m'(bR_1) K_m'(bR_2)}{I_m'(bR_2) K_m'(bR_1)} \right] I_m'(bR_1) K_m'(bR_1) \cos\left(\frac{br}{\cos\psi}\right) \right\} \tag{24}$$

The expression given by (22) is of course very general and for certain ratios of (R/τ) simpler results can be used. For (R_1/τ) sufficiently large, the factors F_1 and F_2 become,

$$F_1 = \left\{ \log_e \frac{R_2}{R_1} - \frac{2\epsilon_2}{\epsilon_1 + \epsilon_2} \sin\psi \cdot \log_e \left[2 \sin\left(\frac{\pi r}{\tau \cos\psi}\right) \right] \right\} \tag{25}$$

$$F_2 = \left\{ \frac{1}{2}\left(1 - \frac{R_1^2}{R_2^2}\right) + \tan^2\psi \cdot \left[\log_e \frac{R_2}{R_1} - \frac{1}{\sin\psi} \cdot \log_e \left(2 \sin\left(\frac{\pi r}{\tau \cos\psi}\right) \right) \right] \right\} \tag{26}$$

On the other hand for $\frac{R_1}{\tau}$ sufficiently small, using (5) and (18),

$$Z_o = \frac{1}{2\pi} \sqrt{\frac{\mu_2}{\epsilon_2}} \cdot \sqrt{G_1 G_2} \tag{27}$$

where,

$$G_1 = \left\{ \log_e \frac{R_2}{R} + \frac{2\epsilon_2}{\epsilon_1 + \epsilon_2} \sum_{m=1}^{\infty} \frac{\left[1 - \left(\frac{R_1}{R_2}\right)^{2m} \right] \cos\left(\frac{mr}{R_1}\right)}{m \left[1 - \frac{\epsilon_1 - \epsilon_2}{\epsilon_1 + \epsilon_2} \left(\frac{R_1}{R_2}\right)^{2m} \right]} \right\} \tag{28}$$

$$G_2 = \left\{ \log_e \frac{R_1}{r} \left(1 - \frac{R_1^2}{R_2^2} \right) \right\} \tag{29}$$

(c) An Example

As an example consider a helical transmission line for which the dimensions are tabulated in Table 1.

Table 1

Dimensions Of Helical Transmission Lines Used In Example

$R_1 = 0.385"$	$\epsilon_1 = 2.6\epsilon_0$
$R_2 = 0.750"$	$\epsilon_2 = 1.0\epsilon_0$
$r = 0.010"$	$\epsilon_0 = 8.854 \times 10^{-12}$ fd/m.
τ = variable	

These dimensions were chosen since they correspond to those for a series of helices tested by the author.

Figure 5 shows the impedance as calculated from the close wound helix approximation which is embodied in equations (22), (25) and (26). This approximation was applied over the range of $\frac{R_1}{\tau}$ from 0.02 to 10.0. Of course, at the lower end of the range the helix can hardly be said to be close wound. Also in Figure 5 is plotted the exact impedance as embodied in (22), (23) and (24). It is interesting to note that at $\frac{R_1}{\tau} = 0.02$ they differ by only 6%.

(d) Impedance Curves For Wire Helices

By appling the above equations in appropriate regions, families

FIGURE 5:

CHARACTERISTIC IMPEDANCE OF A SHIELDED HELICAL TRANSMISSION LINE WITH,

$R_2/R_1 = 1.95$

$K_1/K_2 = 2.6$

$r/R_1 = 0.026$

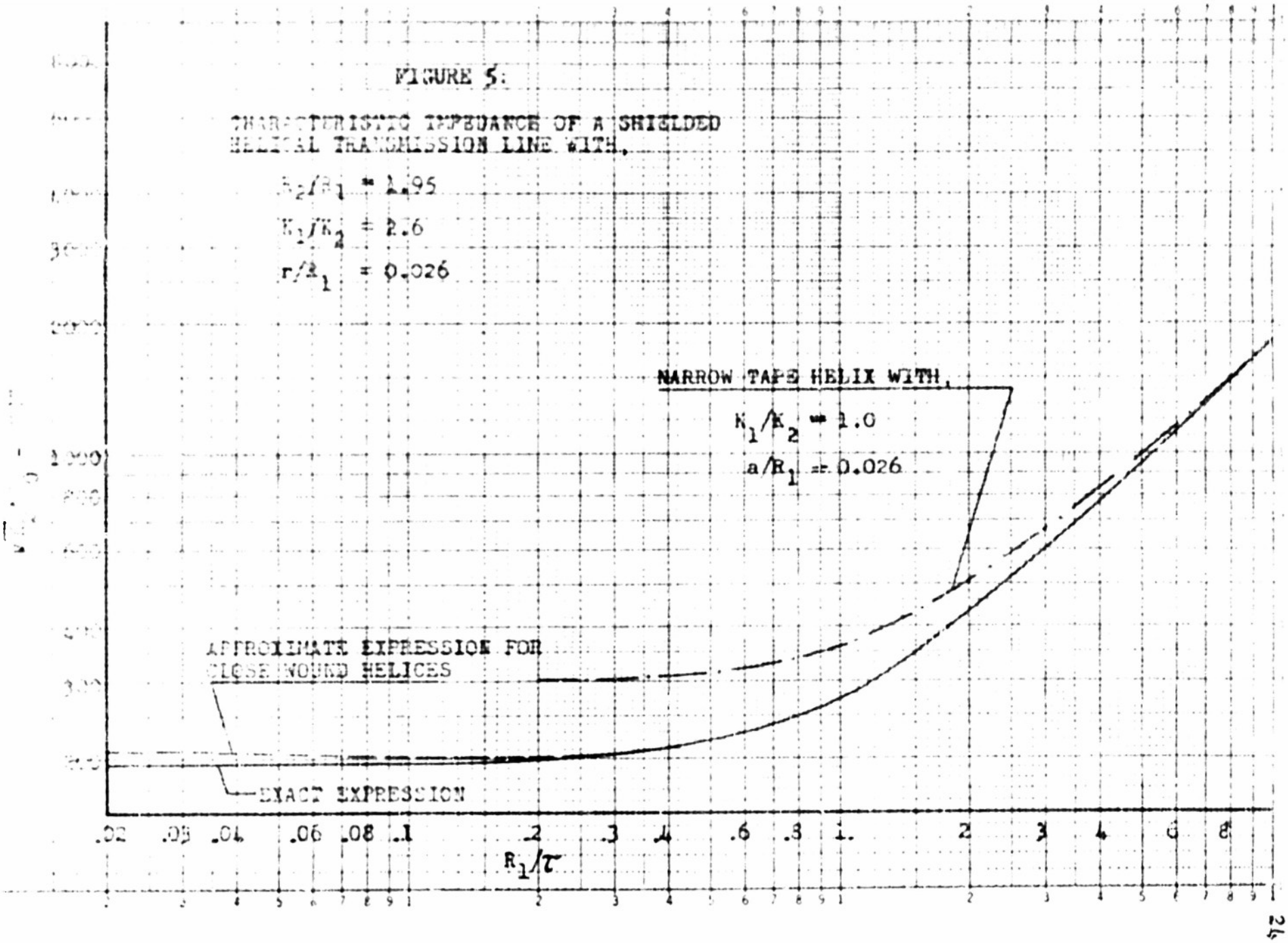

of impedance curves have been prepared. They cover the case where $K_1 = K_2$ and where $K_1 = 2.6K_2$, K_1 and K_2 being the relative permittivities in regions 1 and 2 respectively. The latter choice was made since the relative dielectric constant of polystyrene is 2.6.

The first group of curves give the impedance of a helical transmission line for $K_1 = K_2$ and $\frac{R_2}{R_1}$ from 4.0 down to 1.25. These curves cover the range of $\frac{R_1}{\tau}$ from 0.20 up to that value of $\frac{R_1}{\tau}$ at which the turns butt together. These are Figures 6 to 9.

The second group of curves are for $K_1 = 2.6K_2$ all other dimensionless ratios being the same as for the first group. These are Figures 10 to 13.

(e) Phase Velocity

By using (2) and (13) in (21), one obtains for the phase velocity in the axial direction,

$$N_z = \frac{\tan\psi}{\sqrt{\mu_0 \epsilon_2}} \sqrt{\frac{F_1}{F_2}} \tag{30}$$

where F_1 and F_2 are given by either (23) and (24) or by (25) and (26) above. The latter pair are for close wound helices. On the other hand if $\frac{R_1}{\tau}$ is sufficiently small, using (5) and (18),

$$N_z = \frac{1}{\sqrt{\mu_0 \epsilon_2}} \sqrt{\frac{G_1}{G_2}} \tag{31}$$

where G_1 and G_2 are given by (28) and (29). In the event $\epsilon_1 = \epsilon_2$ equation (31) reduces to the velocity of light in a medium characterised by the permeability μ_0 and the permittivity ϵ_2.

FIGURE 6:

CHARACTERISTIC IMPEDANCE OF SHIELDED HELICAL TRANSMISSION LINE WITH,

$\mu/\mu_0 = 1.0$

$\epsilon/\epsilon_0 = 1.105$

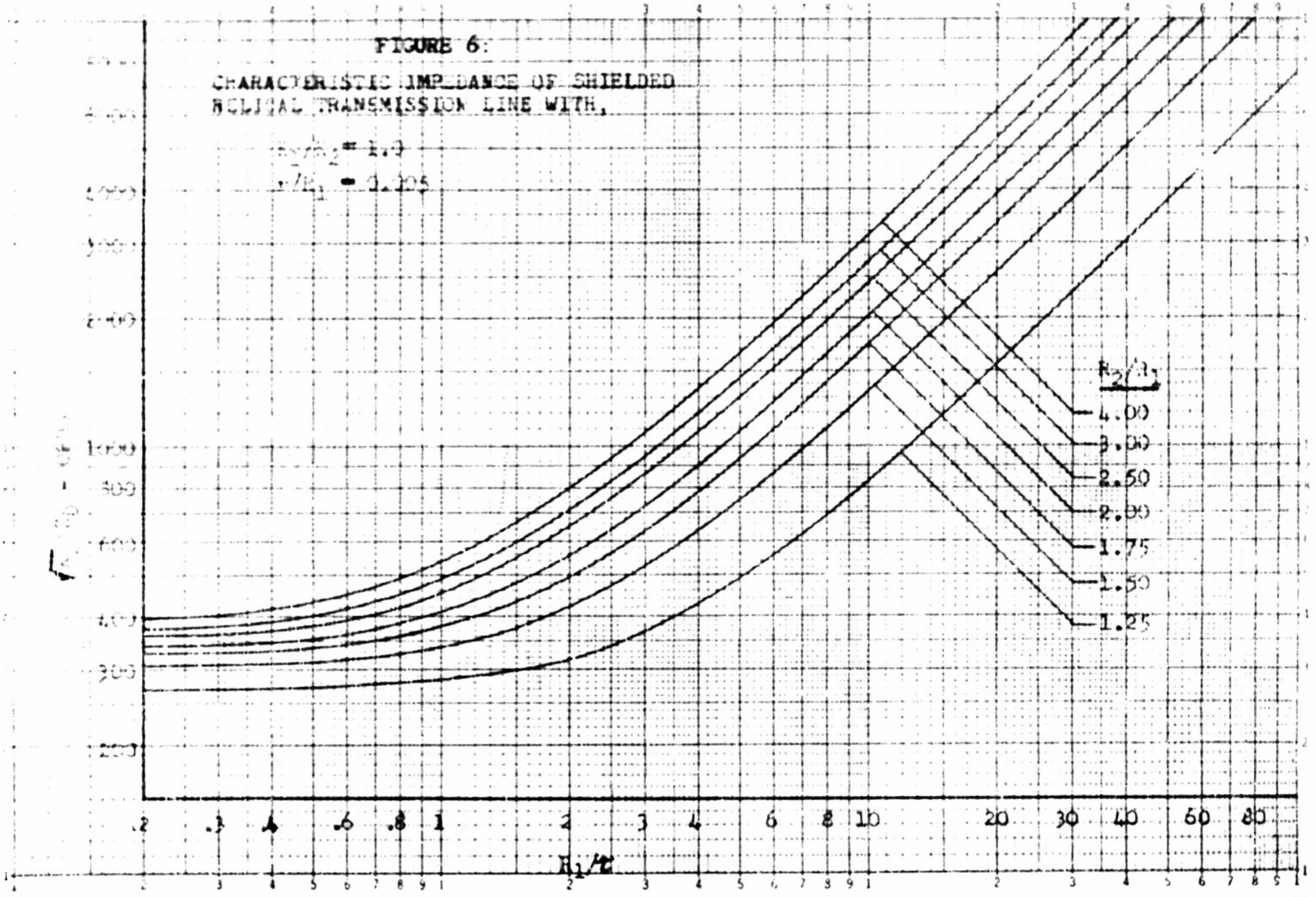

FIGURE 7:

CHARACTERISTIC IMPEDANCE OF SHIELDED HELICAL TRANSMISSION LINE WITH,

$R_1/R_2 = 1.0$

$r/R_1 = 0.01$

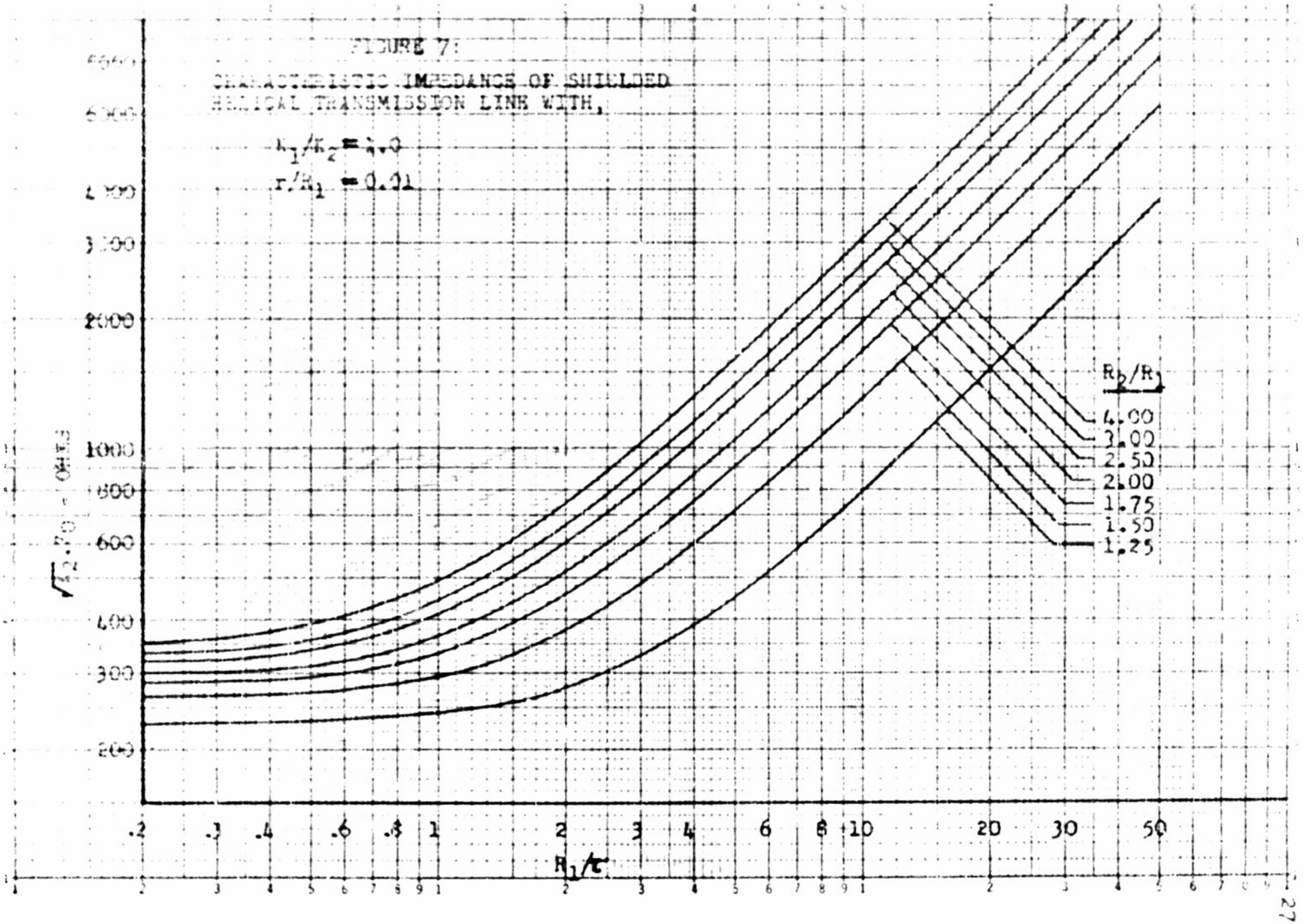

FIGURE 8:

CHARACTERISTIC IMPEDANCE OF SHIELDED HELICAL TRANSMISSION LINE WITH,

$K_1/K_2 = 1.0$

$\tau/R_1 = 0.02$

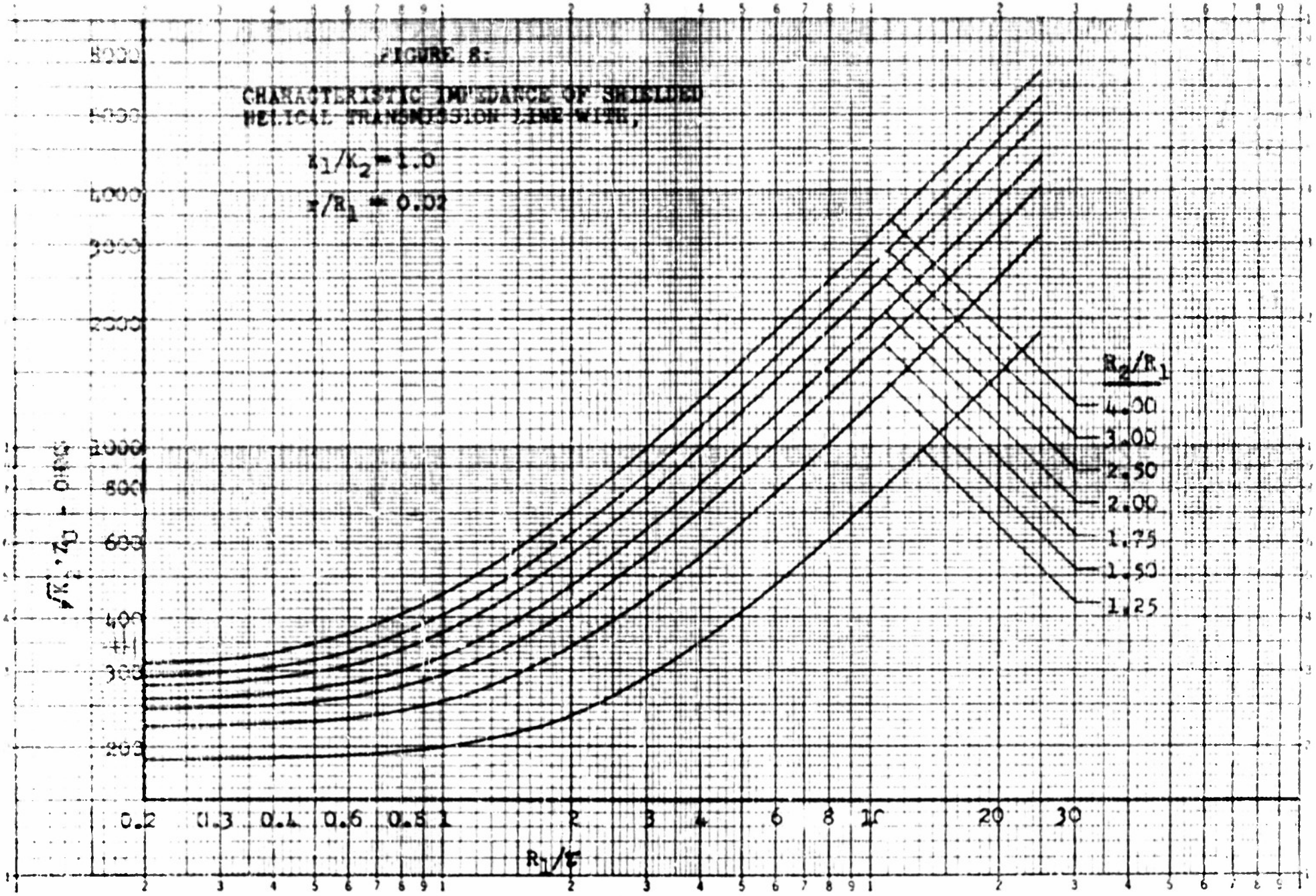

FIGURE 9:

CHARACTERISTIC IMPEDANCE OF SHIELDED HELICAL TRANSMISSION LINE WITH,

$K_1/K_2 = 1.0$

$r/R_1 = 0.04$

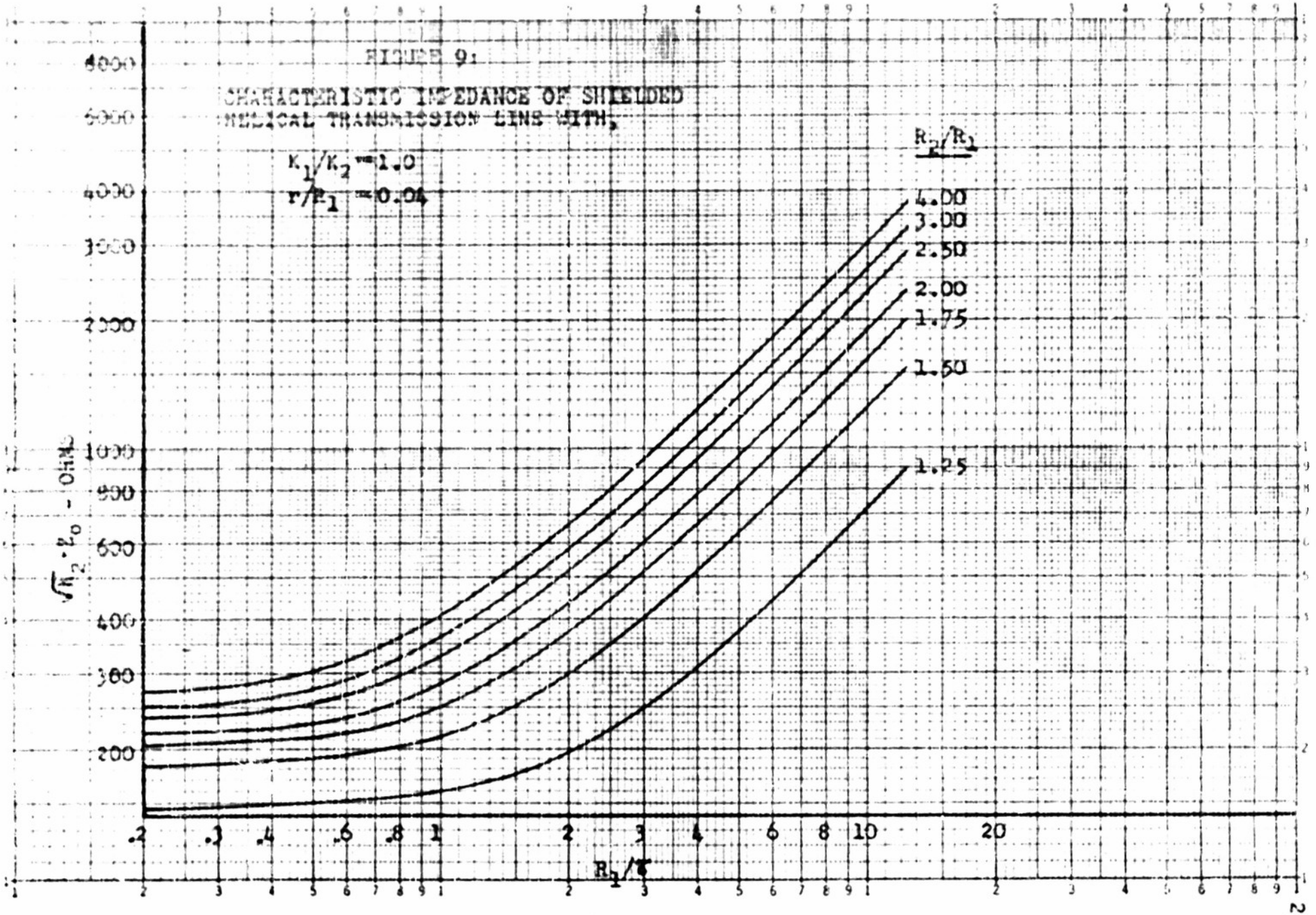

FIGURE 10:

CHARACTERISTIC IMPEDANCE OF SHIELDED HELICAL TRANSMISSION LINE WITH,

$t_1/t_2 = 2.5$

$r/R_1 = 0.005$

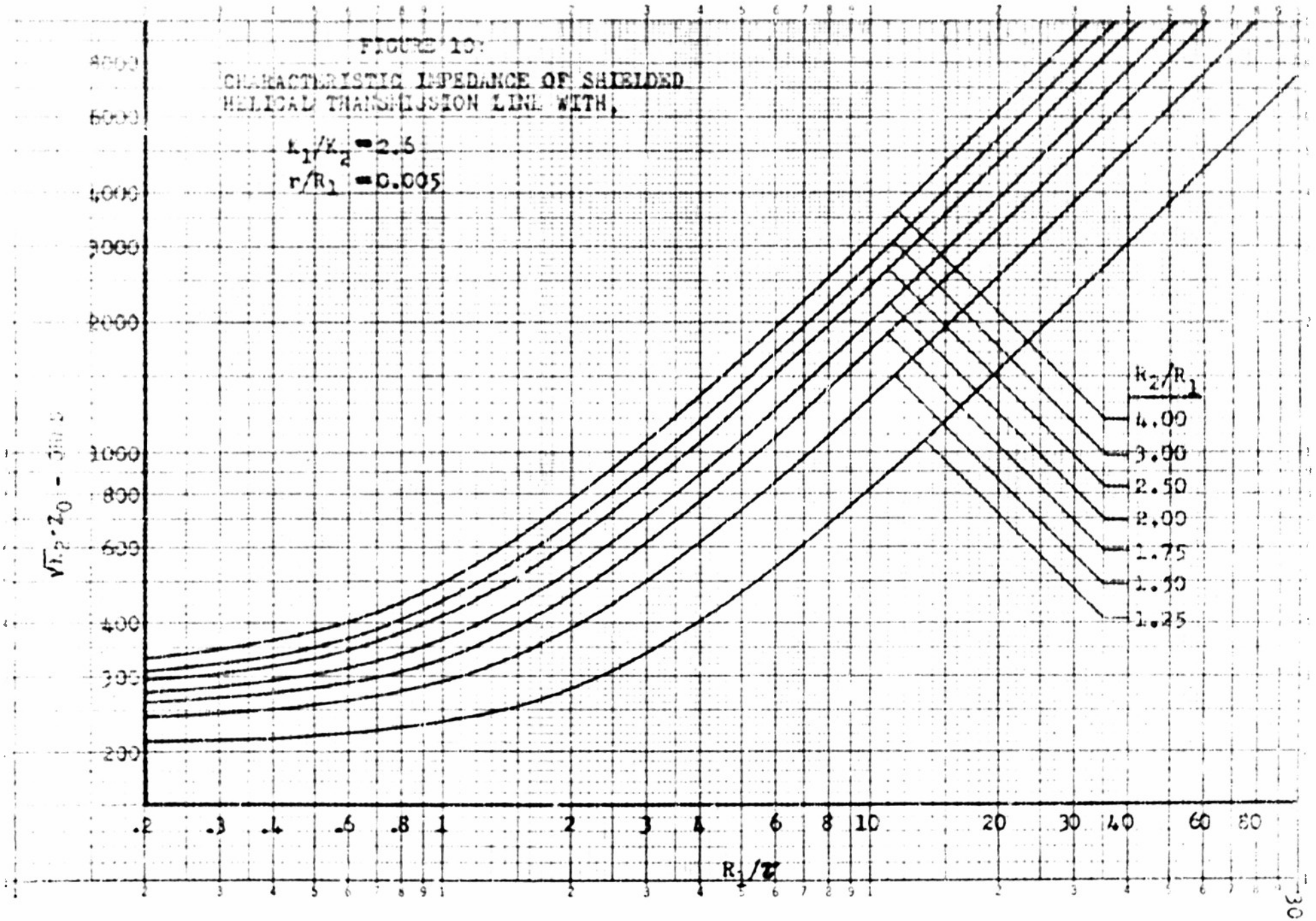

FIGURE 11:

CHARACTERISTIC IMPEDANCE OF SHIELDED HELICAL TRANSMISSION LINE WITH,

$R_1/R_2 = 2.6$

$r/R_1 = 0.01$

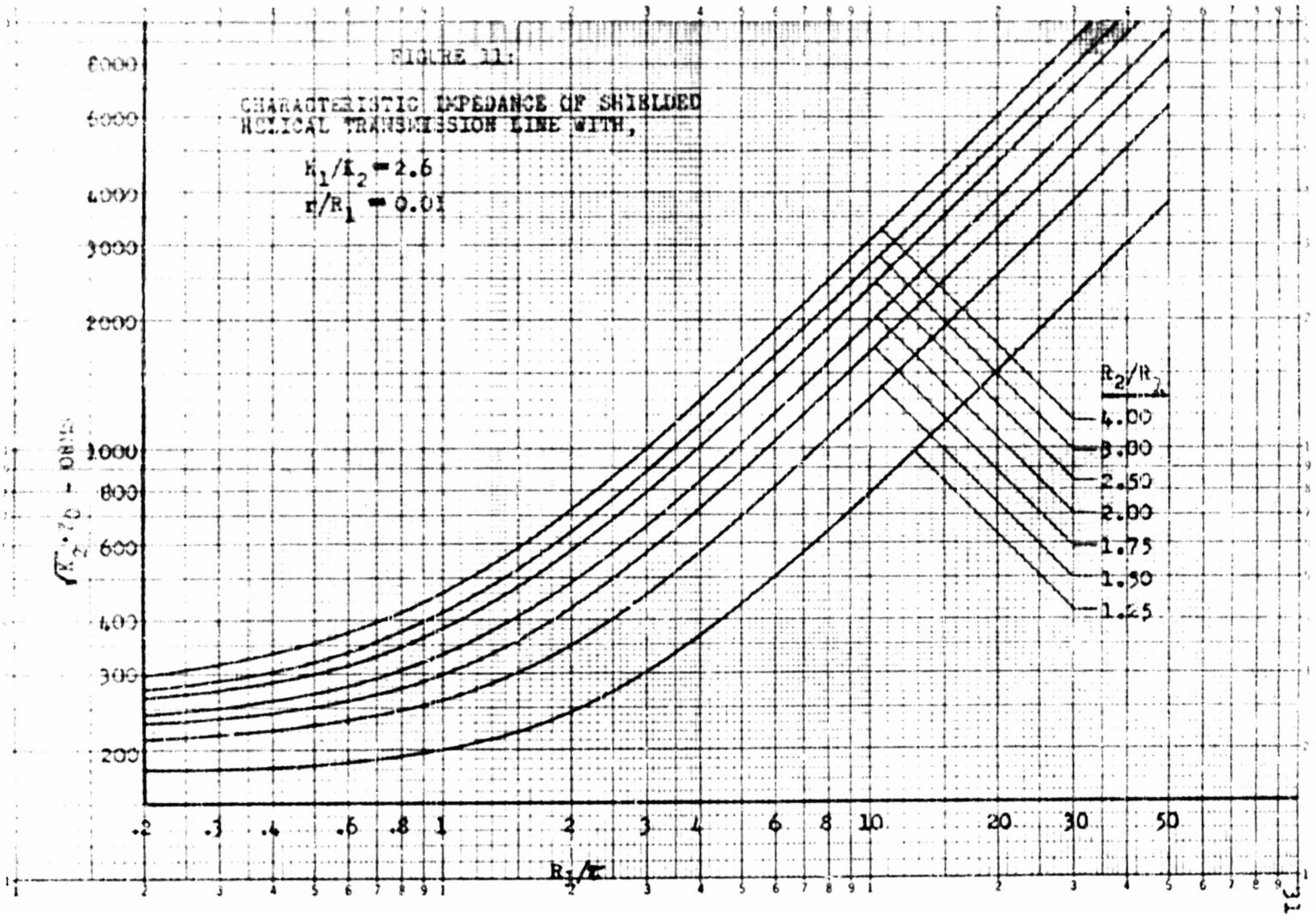

FIGURE 12:

CHARACTERISTIC IMPEDANCE OF SHIELDED HELICAL TRANSMISSION LINE WITH,

$K_1/K_2 = 2.6$

$r/R_1 = 0.02$

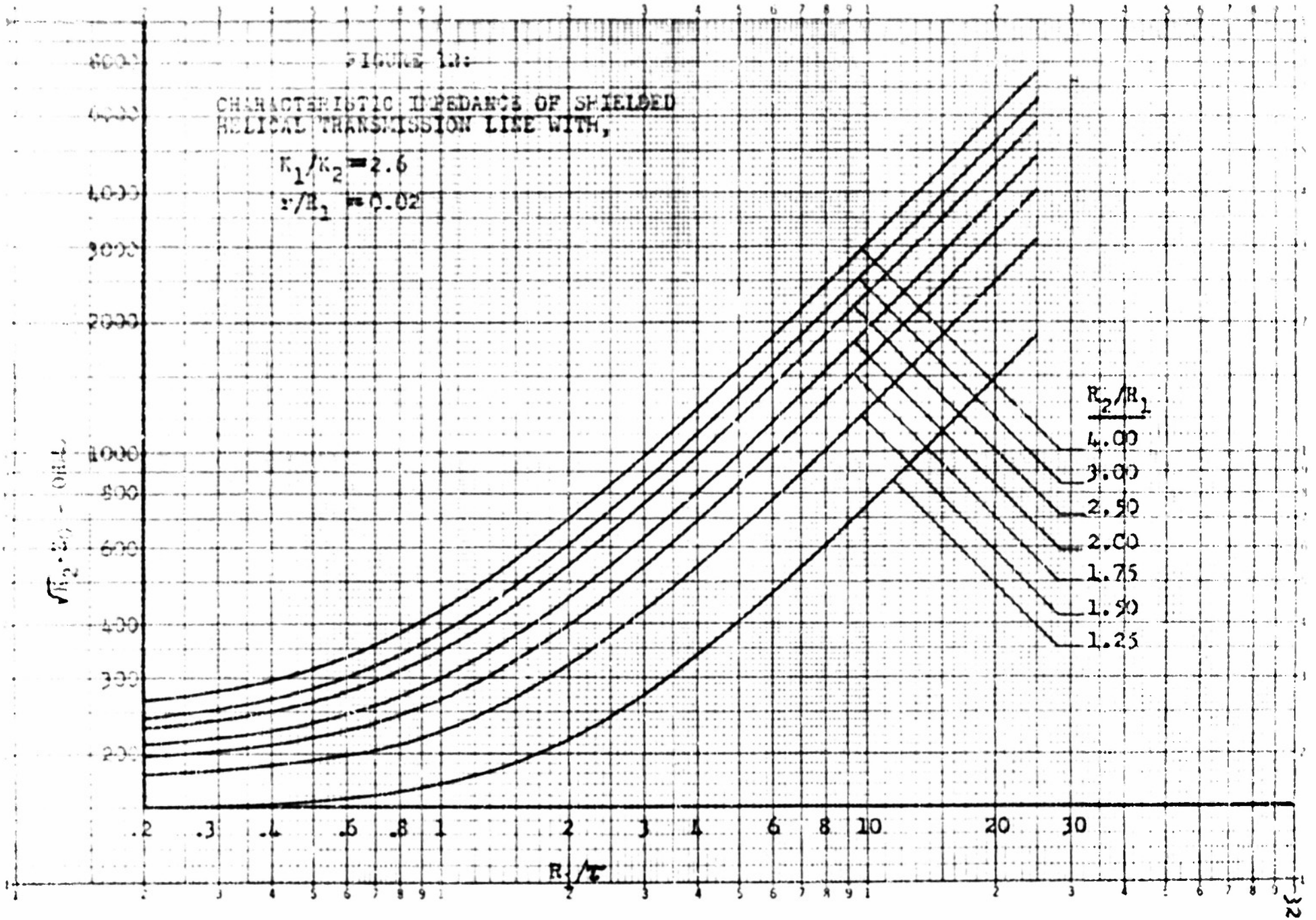

FIGURE 13:

CHARACTERISTIC IMPEDANCE OF SHIELDED HELICAL TRANSMISSION LINE WITH,

$K_1/K_2 = 2.6$

$r/R_1 = 0.04$

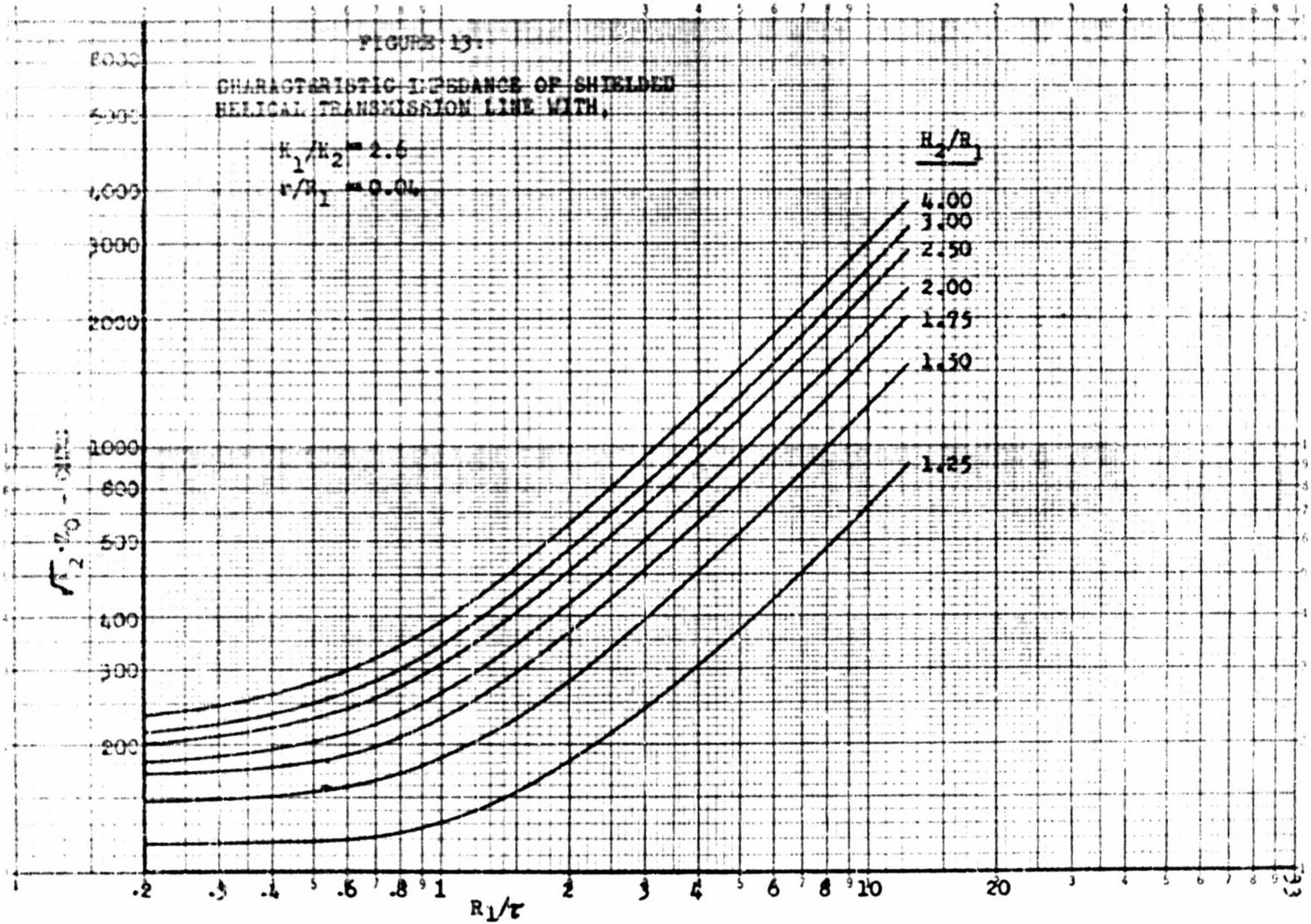

FIGURE 14:

PHASE VELOCITY OF SHIELDED HELICAL TRANSMISSION LINES WITH.

$\kappa_1/\kappa_2 = 1.0$

$r/R_1 = 0.005$

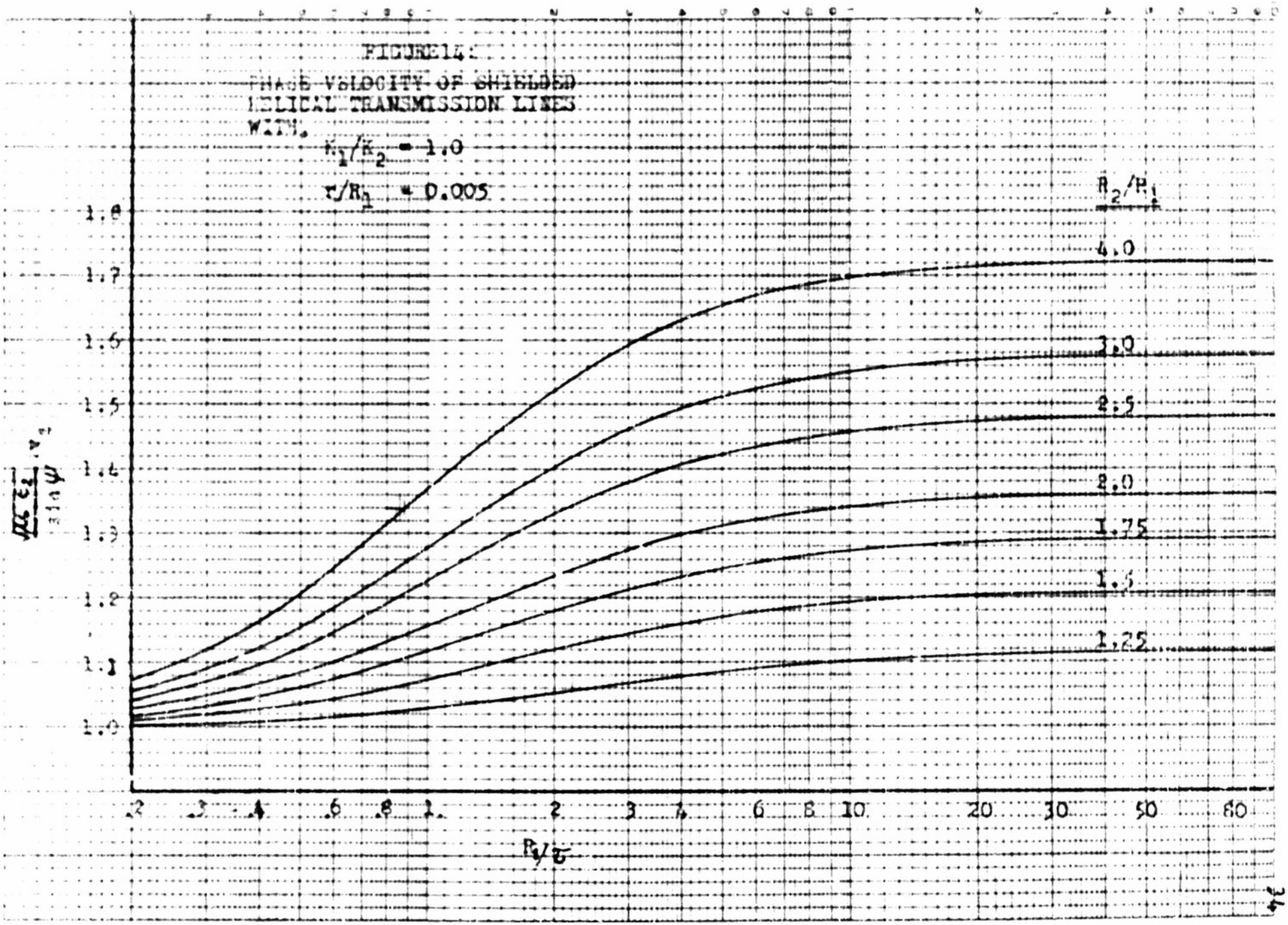

FIGURE 15:

PHASE VELOCITY OF SHIELDED HELICAL TRANSMISSION LINES WITH,

$K_1/K_2 = 1.0$

$r/R_1 = 0.01$

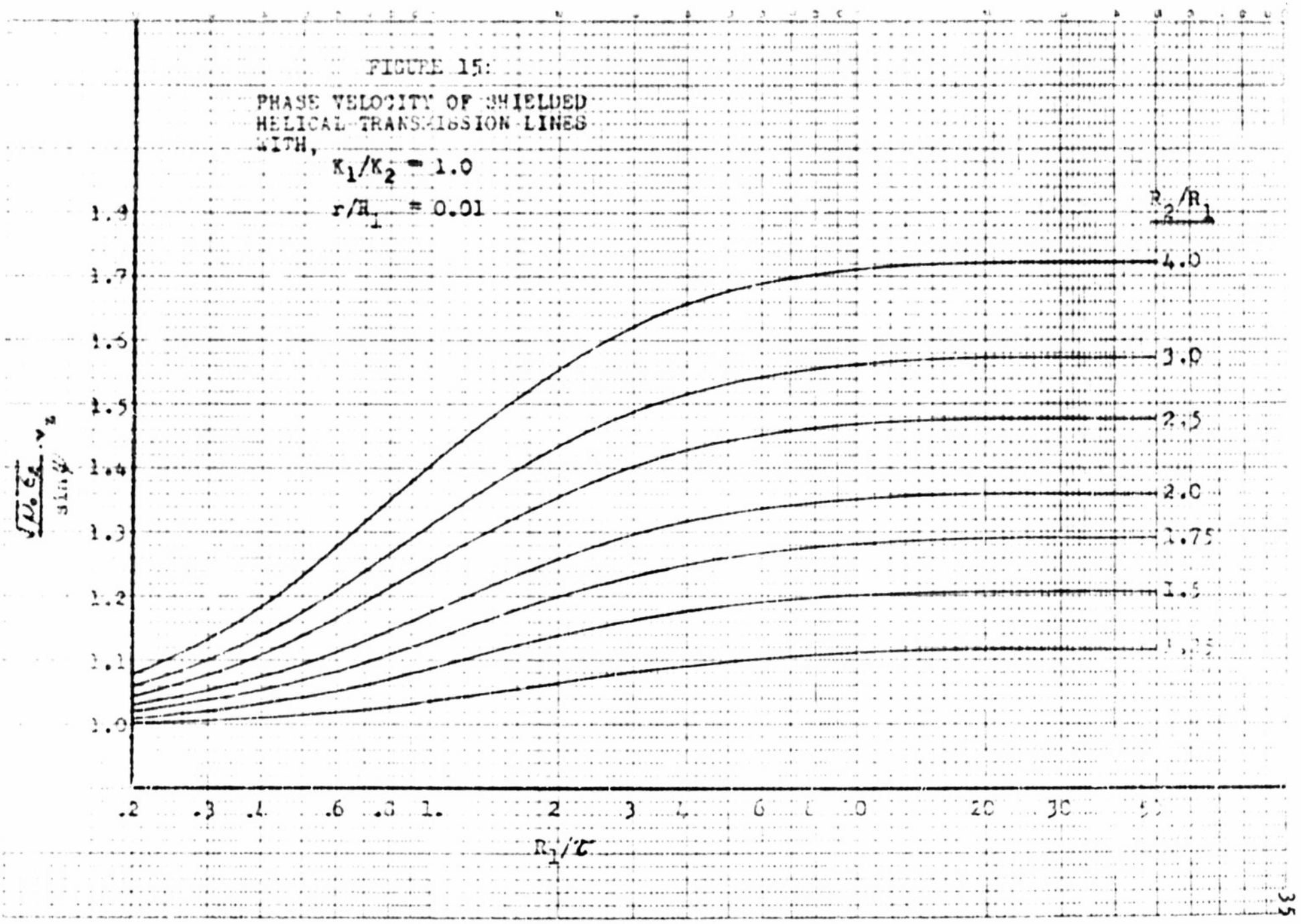

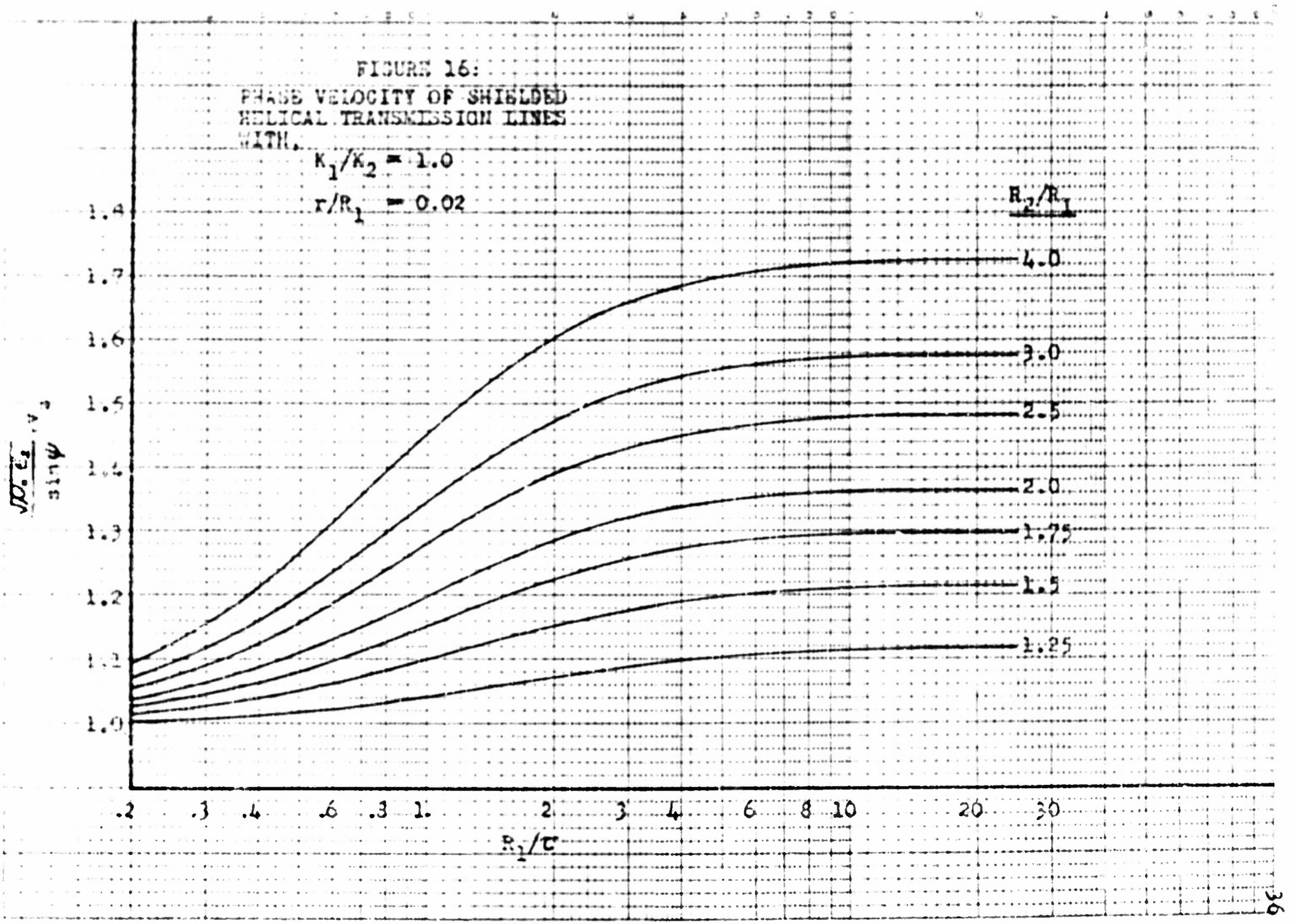
FIGURE 16:
PHASE VELOCITY OF SHIELDED HELICAL TRANSMISSION LINES WITH.
$K_1/K_2 = 1.0$
$r/R_1 = 0.02$
R_2/R_1
4.0
3.0
2.5
2.0
1.75
1.5
1.25
$\frac{v_p}{\sin\psi\sqrt{\varepsilon_r}}$
1.4
1.7
1.6
1.5
1.3
1.2
1.0
.2
.3
.4
.6
.8
1.
2
3
4
6
8
10
20
30
R_1/τ

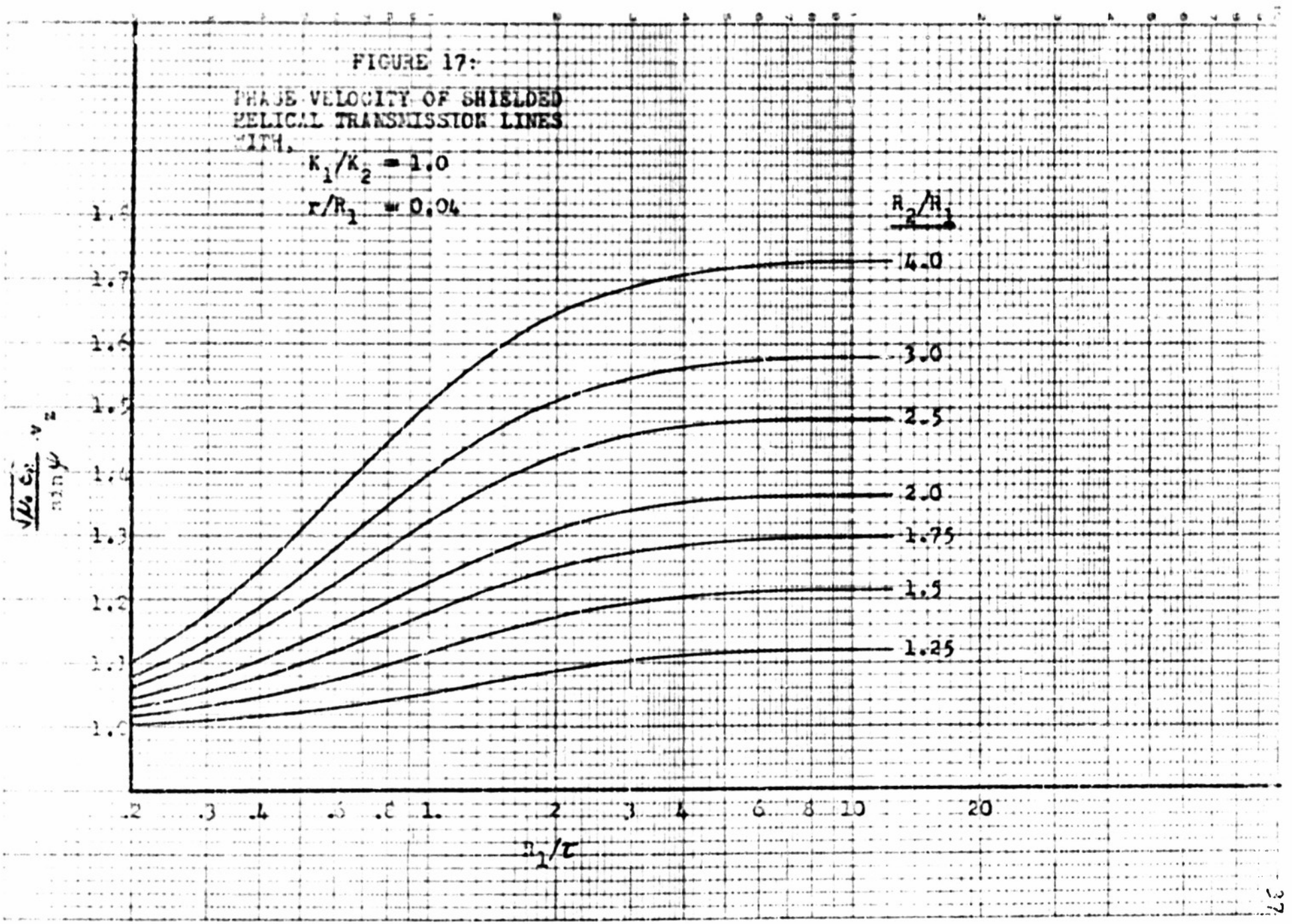
FIGURE 17:
PHASE VELOCITY OF SHIELDED HELICAL TRANSMISSION LINES WITH,
$K_1/K_2 = 1.0$
$r/R_1 = 0.04$
R_2/R_1
4.0
3.0
2.5
2.0
1.75
1.5
1.25
$\frac{\sqrt{\mu_0 \epsilon_0}}{\sin\psi} \cdot v_z$
R_1/τ
.2
.3
.4
.5
.6
1.
2
3
4
6
8
10
20

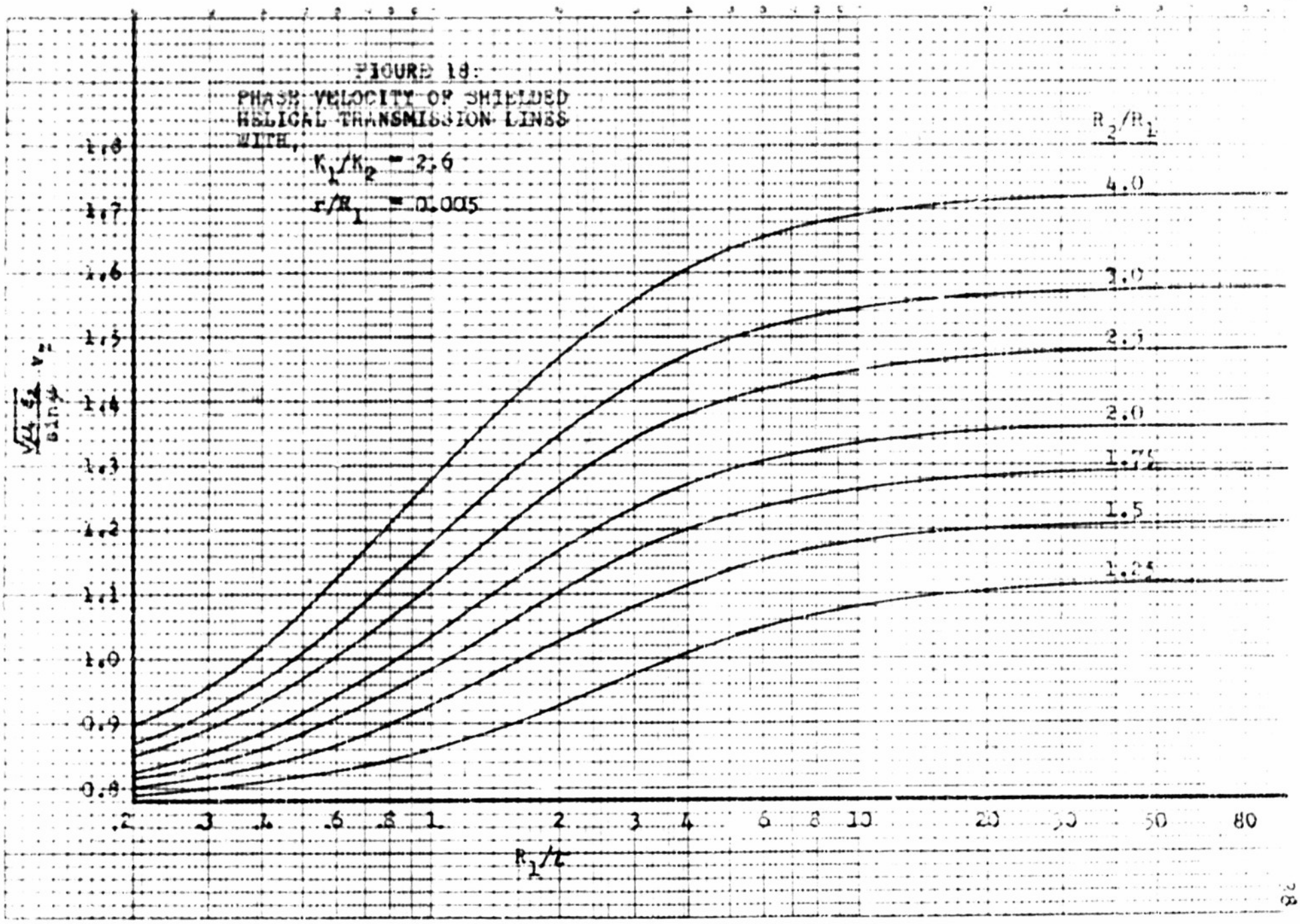
FIGURE 18:
PHASE VELOCITY OF SHIELDED
HELICAL TRANSMISSION LINES
WITH,
$K_1/K_2 = 2.6$
$r/R_1 = 0.005$
R_2/R_1
4.0
3.0
2.5
2.0
1.75
1.5
1.25
$\frac{v}{\sin\psi}$
1.8
1.7
1.6
1.5
1.4
1.3
1.2
1.1
1.0
0.9
0.8
.2
.3
.4
.6
.8
1
2
3
4
6
8
10
20
30
50
80
R_1/t

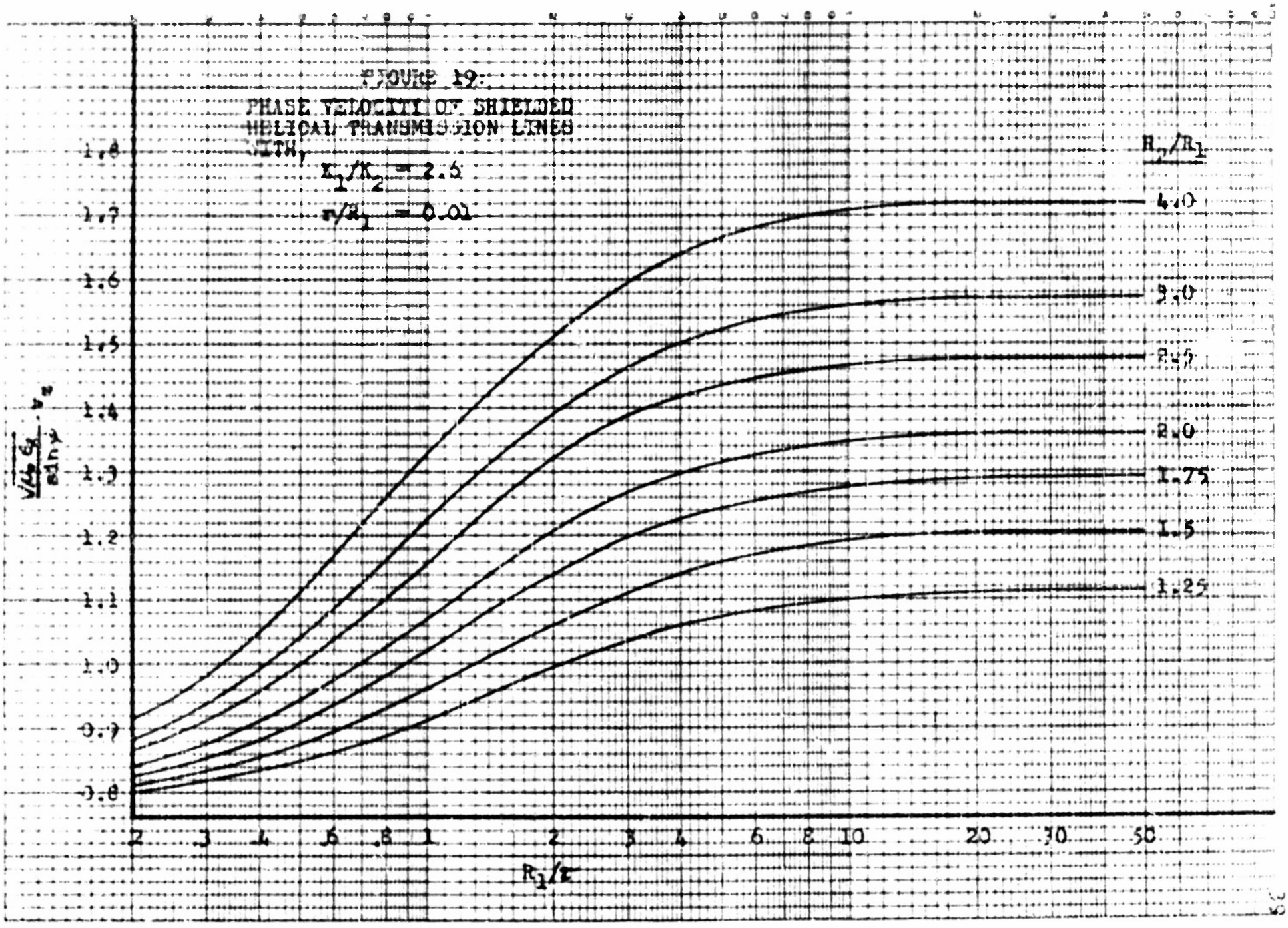
FIGURE 19:
PHASE VELOCITY OF SHIELDED
HELICAL TRANSMISSION LINES
WITH
$K_1/K_2 = 2.6$
$r/R_1 = 0.01$
R_2/R_1
4.0
3.0
2.5
2.0
1.75
1.5
1.25
$\frac{\sqrt{\mu_0 \epsilon_0}}{\sin\psi} \cdot v_p$
1.8
1.7
1.6
1.5
1.4
1.3
1.2
1.1
1.0
0.9
0.8
2
3
4
5
6
8
1
2
3
4
6
8
10
20
30
50
R_1/r

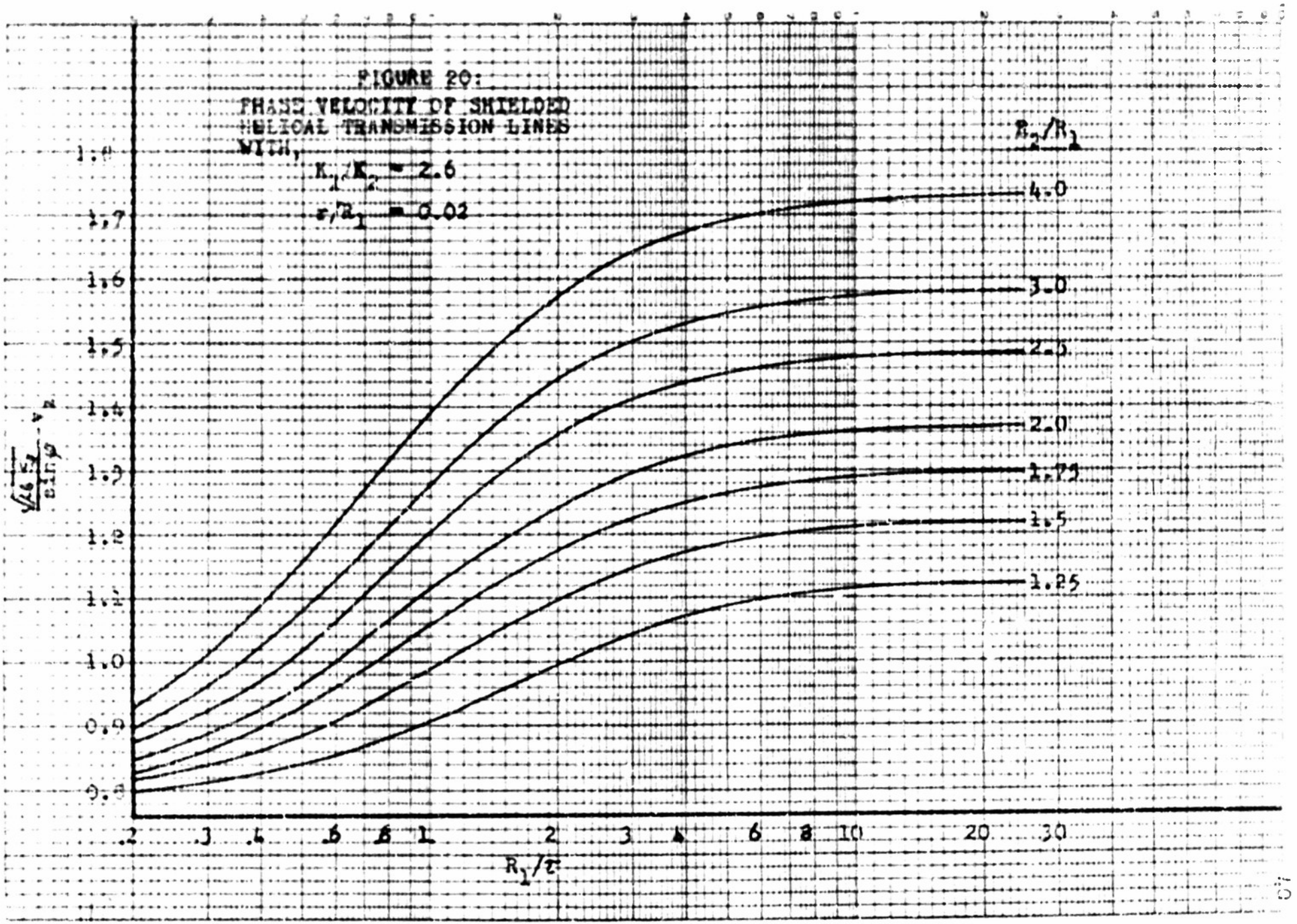
FIGURE 20:
PHASE VELOCITY OF SHIELDED HELICAL TRANSMISSION LINES WITH,
$K_1/K_2 = 2.6$
$s/R_1 = 0.02$
R_2/R_1
4.0
3.0
2.5
2.0
1.75
1.5
1.25
$\frac{\sqrt{\epsilon_r}}{\sin\psi} \frac{v}{c}$
1.8
1.7
1.6
1.5
1.4
1.3
1.2
1.1
1.0
0.9
0.8
.2
.3
.4
.6
.8
1
2
3
4
6
8
10
20
30
R_1/τ

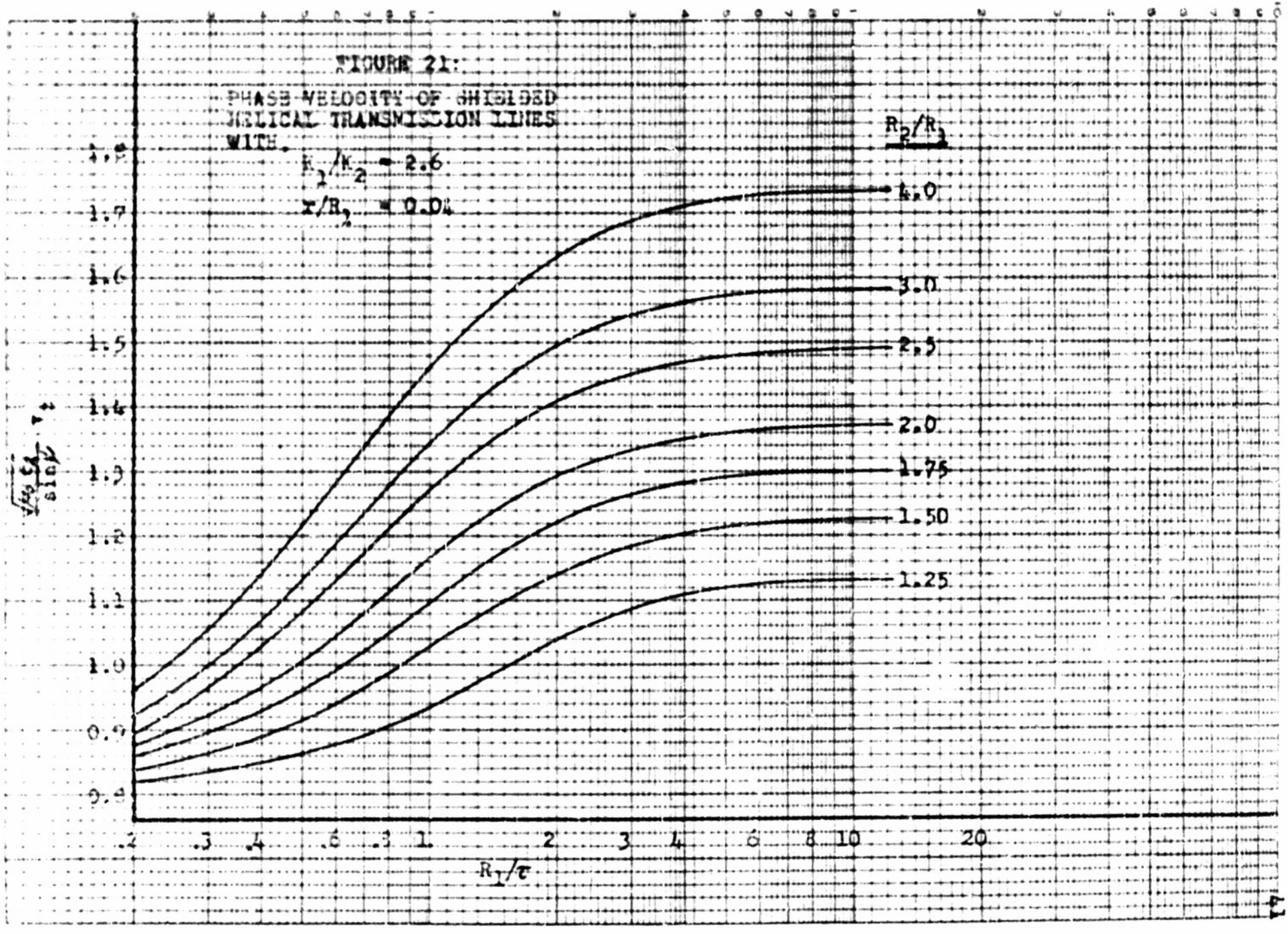
FIGURE 21:
PHASE VELOCITY OF SHIELDED HELICAL TRANSMISSION LINES WITH,
$\epsilon_2/\epsilon_2 = 2.6$
$t/R_2 = 0.04$
R_2/R_1
4.0
3.0
2.5
2.0
1.75
1.50
1.25
$\frac{v_p}{\sin\psi}\sqrt{\frac{\epsilon_2}{\mu_2}}$
1.8
1.7
1.6
1.5
1.4
1.3
1.2
1.1
1.0
0.9
0.8
.2
.3
.4
.6
.8
1.
2
3
4
6
8
10
20
R_1/τ

(f) Phase Velocity Curves

By applying the above equations in the appropriate range of $\frac{R_1}{\tau}$, families of phase velocity curves have been prepared. They cover the cases $K_1 = K_2$ and $K_1 = 2.6\,K_2$. The latter choice was made since the relative permittivity of polystyrene is about 2.6.

The first group of curves give $\frac{\sqrt{\mu_0 \epsilon_2}}{\sin\psi}$ as a function of $\frac{R_1}{\tau}$ for $K_1 = K_2$. These curves cover the range of R_2/R_1 from 4.0 down to 1.25 and the range of $\frac{R_1}{\tau}$ from 0.20 up to that value of $\frac{R_1}{\tau}$ at which the turns butt together. These are Figures 14 to 17. The second group of curves are for $K_1 = 2.6K_2$, all other dimensionless ratios being the same as for the first group. These are Figures 18 to 21.

II-4 The Wave Equation Solution for Tape Helices

(a) The Butted Tape Helix

An attempt is made in Appendix D to solve the wave equation for a tape helix inside a perfectly conducting sheath. This is done for the case $K_1 = K_2$.

The tape was chosen because of the relative ease of satisfying the boundary conditions. It was also felt that for very small conductor cross section the phase velocity would not be affected very significantly by the conductor shape. In principle, the boundary conditions at the tape and the sheath are met, leading to a determinental equation from which the propagation constant can be found. However, the resulting determinental equation has an infinite number of rows and columns and as a result, it is not feasible to find the propagation constant or phase velocity in this manner. If one considers a very wide tape helix such that the adjacent turns butt against each other, and further imposes upon the tape the property that it can conduct only in the helix direction, the determinental equation

has one row and column. As shown in Appendix D, it is,

$$\left| \frac{\gamma_0^2 R_1^2 \left[1 - \frac{I_0(\gamma_0 R_1) K_0(\gamma_0 R_2)}{I_0(\gamma_0 R_2) K_0(\gamma_0 R_1)} \right] K_0(\gamma_0 R_1) I_0(\gamma_0 R_1)}{\beta_0^2 R_1^2 \left[1 - \frac{I_0'(\gamma_0 R_1) K_0'(\gamma_0 R_2)}{I_0'(\gamma_0 R_2) K_0'(\gamma_0 R_1)} \right] K_0'(\gamma_0 R_1) I_0'(\gamma_0 R_1)} \cdot \frac{\sin^2 \psi}{\cos \psi} + \cos \psi \right| = 0 \qquad (32)$$

where, $\gamma_0^2 = \beta^2 - \beta_0^2$

$\beta_0^2 = \omega^2 \mu_0 \epsilon_0$

$\beta = \frac{\omega}{v_p}$

While it is obvious that a tape helix which completely covers the cylinder at radius R_1 is a poor approximation of a wire helix, its behavior for small helix angles should be similar to the behavior of a very close wound wire helix. Equation (32) can be written,

$$\tan^2 \psi - \frac{\beta_0^2 R_1^2}{\gamma_0^2 R_1^2} \cdot \frac{I_0(\gamma_0 R_1) K_1(\gamma_0 R_1)}{I_0(\gamma_0 R_1) K_0(\gamma_0 R_1)} \cdot \frac{\left[1 - \frac{I_1(\gamma_0 R_1) K_1(\gamma_0 R_2)}{I_1(\gamma_0 R_2) K_1(\gamma_0 R_1)} \right]}{\left[1 - \frac{I_0(\gamma_0 R_1) K_0(\gamma_0 R_2)}{I_0(\gamma_0 R_2) K_0(\gamma_0 R_1)} \right]} = 0 \qquad (33)$$

For any given frequency and helix angle, this is a transcendental equation in the unknown γ_0. If this can be solved, the propagation constant β and the velocity v_p will follow immediately. This equation can be put in the form,

$$(\gamma_0 R_1)^2 \frac{I_0(\gamma_0 R_1) K_0(\gamma_0 R_2)}{I_1(\gamma_0 R_1) K_1(\gamma_0 R_2)} \cdot \frac{\left[1 - \frac{I_0(\gamma_0 R_1) K_0(\gamma_0 R_2)}{I_0(\gamma_0 R_2) K_0(\gamma_0 R_1)}\right]}{\left[1 - \frac{I_1(\gamma_0 R_1) K_1(\gamma_0 R_2)}{I_1(\gamma_0 R_2) K_1(\gamma_0 R_1)}\right]} = \left(\beta_0 R_1 \cot\psi\right)^2 \tag{34}$$

It is obvious from (34) that if one assumes some particular value for $(\gamma_0 R_1)$ a corresponding value of $(\beta_0 R_1 \cot\psi)$ can be calculated. This calculated value of $(\beta_0 R_1 \cot\psi)$ when divided by the assumed $(\gamma_0 R_1)$ yields a quantity $\frac{\beta_0}{\gamma_0}\cot\psi$ which can be plotted as a function of $\beta_0 R_1 \cot\psi$. This is done in Figure 22 for ratios of $\frac{R_2}{R_1}$ from 1.25 to 4.0.

It is of interest to find the velocity v_2 as ω is allowed to approach zero. When this is done,

$$\lim_{\omega \to 0} v_2 = \frac{1}{\sqrt{\mu_0 \epsilon_2}} \frac{1}{\sqrt{1 + \frac{1}{2}\left(1 - \frac{R_1^2}{R_2^2}\right)\frac{\cot^2\psi}{\log_e \frac{R_2}{R_1}}}} \tag{35}$$

One result which can be obtained from Figure 22 is that the phase velocity is not independent of frequency. At very low frequencies it is given by (35) and at very high frequencies, since $\frac{\beta_0}{\gamma_0}\cot\psi$ approaches unity, it is given by

$$\lim_{\omega \to \infty} v_2 = \frac{\sin\psi}{\sqrt{\mu_0 \epsilon_2}} \tag{36}$$

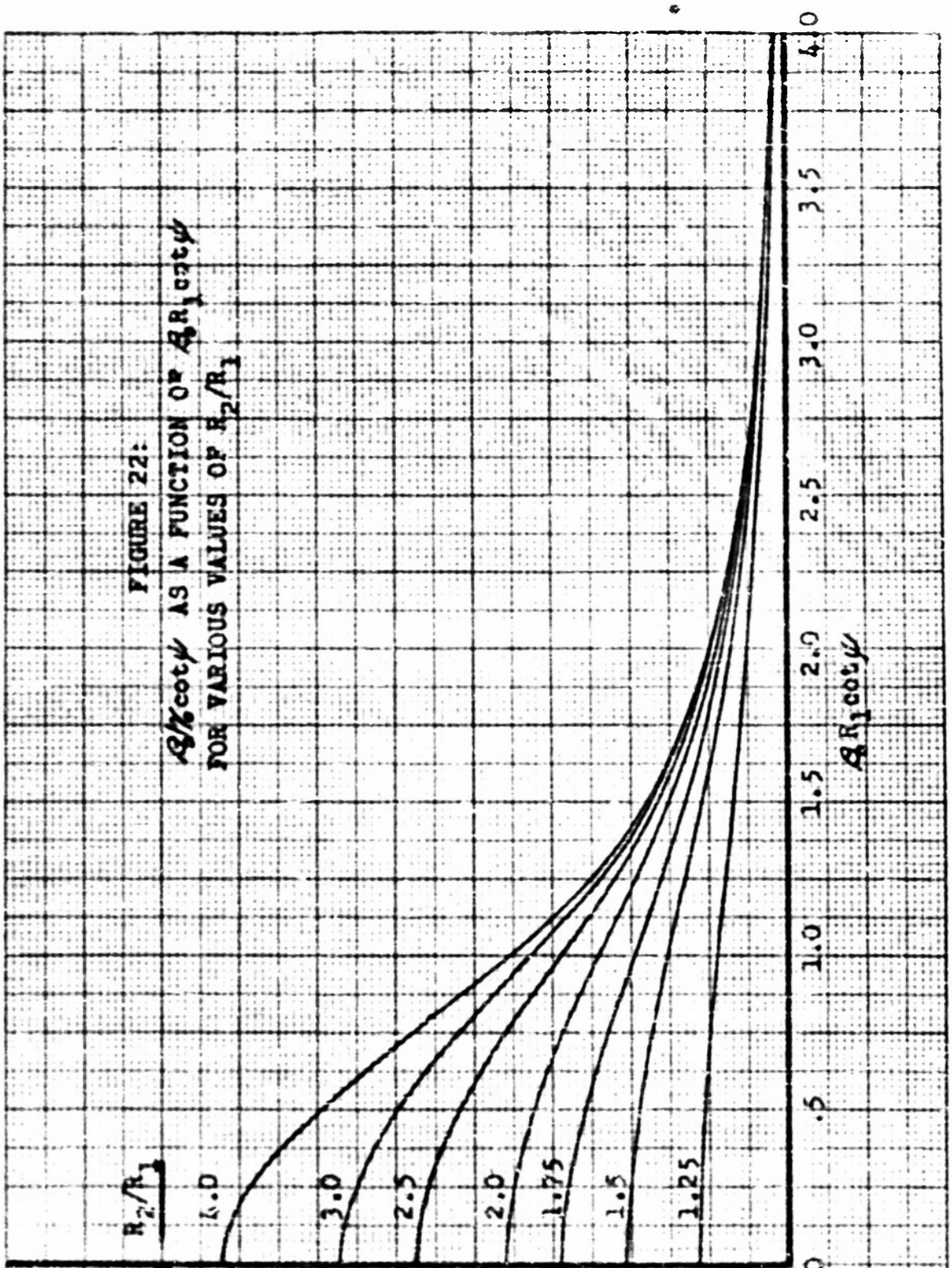
FIGURE 22:
$\theta/\kappa \cot\psi$ AS A FUNCTION OF $\Delta R_1 \cot\psi$
FOR VARIOUS VALUES OF R_2/R_1
R_2/R_1
4.0
3.0
2.5
2.0
1.75
1.5
1.25
1.0
$\theta/\kappa \cot\psi$
$\Delta R_1 \cot\psi$
0
.5
1.0
1.5
2.0
2.5
3.0
3.5
4.0

This is the velocity which a wave would have if it were to propagate in the helix direction with the velocity of light.

Table 2

Butted Tape Helical Transmission Line Dimensions

$R_1 = 0.375$ inches $\quad \epsilon_1 = \epsilon_o$

$R_2 = 0.750$ " $\quad \epsilon_2 = \epsilon_o$

$\tau = 0.0625$ " $\quad \epsilon_o = 8.854 \times 10^{-12}$ Fd./m.

As an example consider a butt tape helix having the dimensions listed in Table 2. The two limiting velocities from (35) and (36) are, respectively 10.81×10^6 and 7.96×10^6 meters per second. The phase velocity at other frequencies is shown in Figure 23. These have been normalized by dividing them by the velocity given by (36).

In order to show the effect of wire size, the phase velocity as computed from equation (30) for this same helix made from round wire instead of tape, has been plotted in Figure 24. Over the range of wire sizes considered the agreement with (35) is very good. As one allows the wire size to approach zero, equation (30) will approach (36). This portion is shown dotted in Figure 24 since no calculations were made below $r/R_1 = 0.005$.

Thus (35) appears to be a fairly accurate expression for very close wound helices. It does however fail to agree with the true phase velocity as the pitch increases as shown in Figure 25. For this case, equation (35) gives too high a result over a considerable portion of the range . The maximum deviation is about 17% at $(R_1/\tau) = 0.4$. Even though (35) would be of limited usefulness in the design of wire helices, it would be

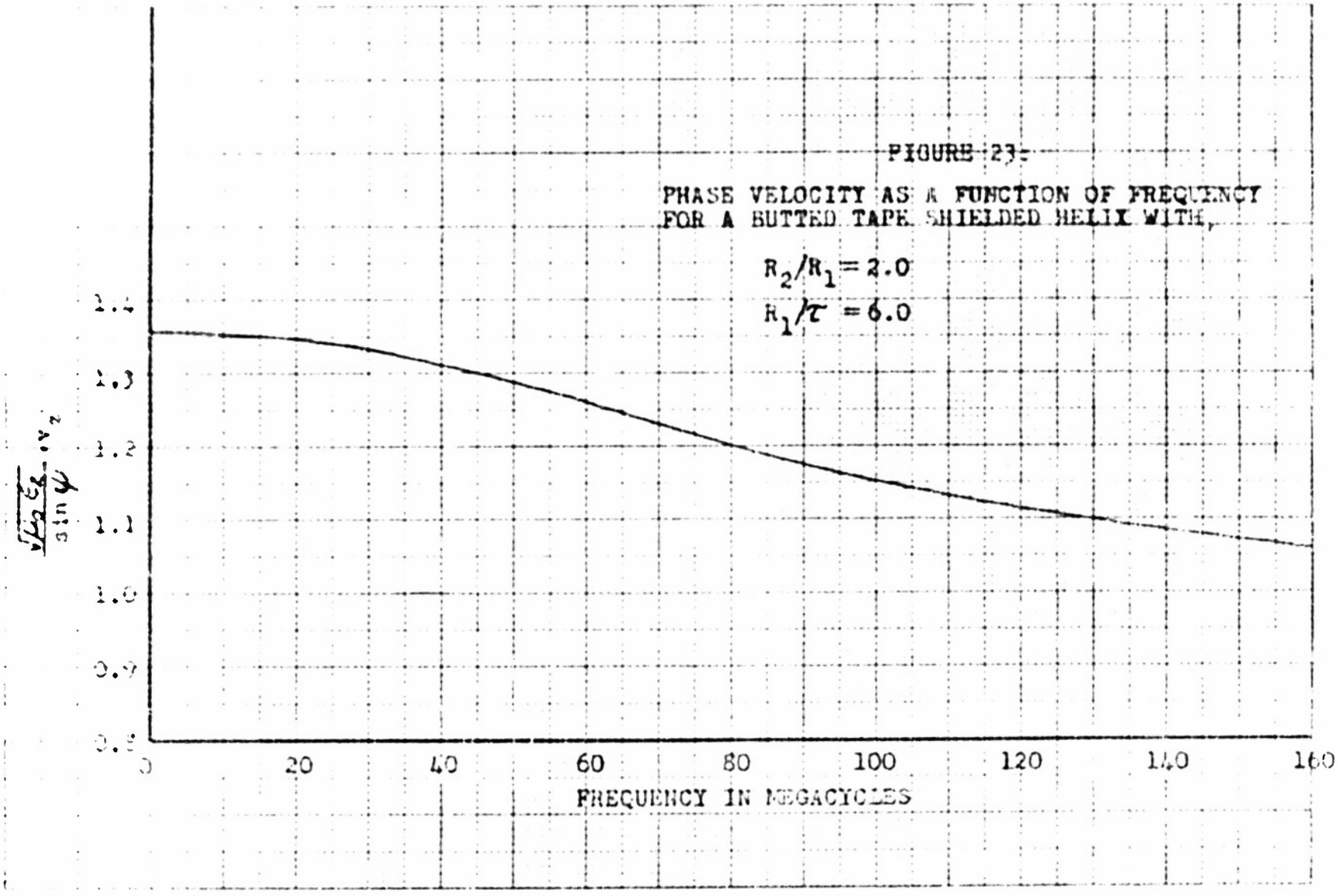
PIGURE 23-
PHASE VELOCITY AS A FUNCTION OF FREQUENCY
FOR A BUTTED TAPE SHIELDED HELIX WITH,
$R_2/R_1 = 2.0$
$R_1/\tau = 6.0$
$\frac{\sqrt{\mu_2 \epsilon_2}}{\sin \psi} \cdot v_z$
1.4
1.3
1.2
1.1
1.0
0.9
0.8
0
20
40
60
80
100
120
140
160
FREQUENCY IN MEGACYCLES

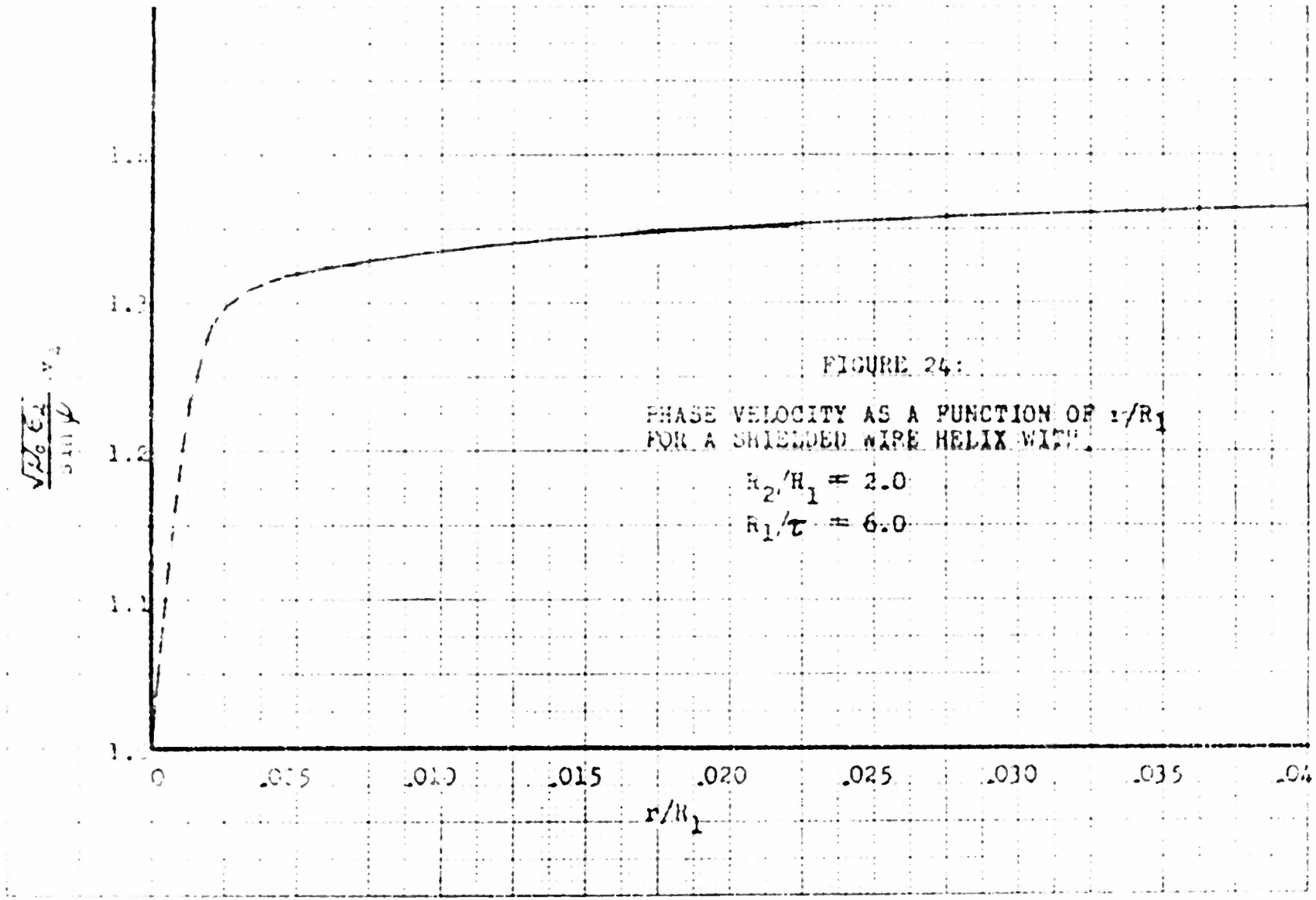

FIGURE 24:

PHASE VELOCITY AS A FUNCTION OF r/R_1
FOR A SHIELDED WIRE HELIX WITH

$R_2/R_1 = 2.0$

$R_1/\tau = 6.0$

FIGURE 25:

PHASE VELOCITY OF SHIELDED HELICAL TRANSMISSION LINES WITH,

$R_2/R_1 = 1.95$

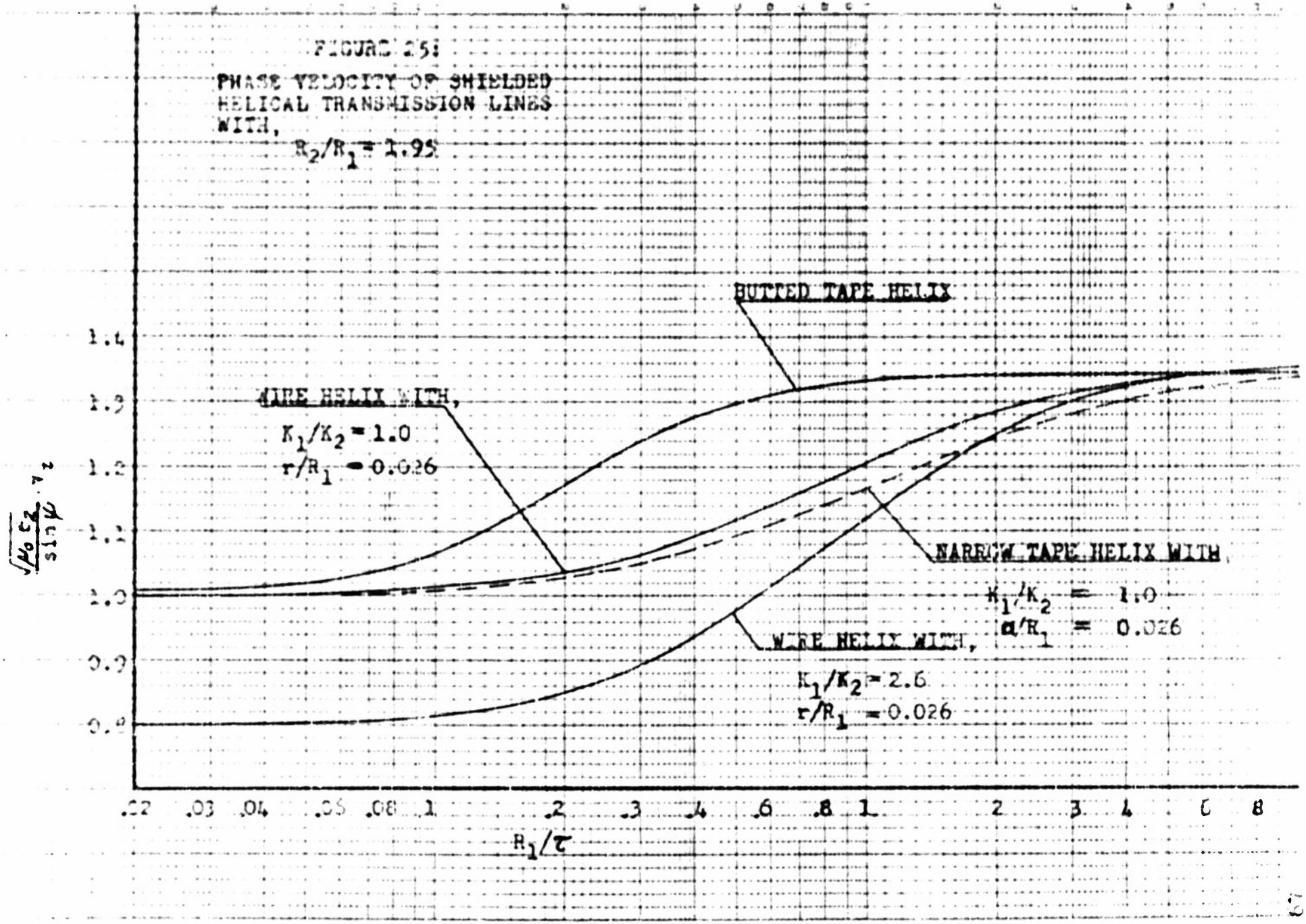

quite useful for tape helices where the tape width is such as to very nearly result in a butt helix. This equation has been used successfully in the design of a tape helix (see reference (20)).

(b) The Phase Velocity and Characteristic Impedance of a Narrow Tape Helix.

In Appendix D are derived expressions for the characteristic impedance and phase velocity of a narrow tape helix. These expressions which were derived for an anisotiopic tape which can conduct only in the helix direction, apply to low frequencies only since they were derived on the basis of zero frequency.

The phase velocity is given by,

$$\frac{\sqrt{\mu_0 \epsilon_2}}{\sin\psi} \cdot v_2 = \sqrt{\frac{S_1 + S_2 \sin\psi}{[1+S_1]\sin^2\psi + S_2 \sin\psi}} \tag{37}$$

where,

$$S_1 = \frac{2 \log_e\left(\frac{R_2}{R_1}\right)}{\left(1 - \frac{R_1^2}{R_2^2}\right)\cot^2\psi} \tag{38}$$

$$S_2 = \frac{2 \log_e\left(\frac{\epsilon}{\gamma}\right) + \frac{\xi^2}{24}}{\left(1 - \frac{R_1^2}{R_2^2}\right)\cot^2\psi} \tag{39}$$

$$\xi = \frac{2\pi a}{\tau \cos\psi} \tag{40}$$

$a = \frac{1}{2}$ the tape width (41)

The characteristic impedance is given by,

$$Z_o = \frac{\sin\psi}{2\pi}\sqrt{\frac{\mu_o}{\epsilon_2}}\left[\frac{\sqrt{\mu_o\epsilon_2}}{\sin\psi}\cdot\sqrt{2}\right]\left\{\left[\log_e\frac{R_1}{R_1} + \sin\psi\left\{\left[\log_e\left(\frac{1}{\xi}\right) + \frac{\xi^2}{68}\right]\right\}\right\} \qquad (42)$$

Both of these expressions apply to the case where the helix is immersed in a homogeneous isotropic medium characterized by permeability μ_o and permittivity ϵ_2.

Expression (37) was used to calculate the dashed curve of Figure 25. There is very good agreement between it and the curve for the wire helix having a wire diameter equal to the tape width. As was pointed out in Appendix D, equation (37) should give a result slightly lower than the correct result.

Equation (42) was used to calculate the dot-and-dashed curve on Figure 5. It agrees extremely well with the round wire helix at values of $\frac{R_1}{\tau} > 10$, these values being off the curve sheet. The reason for the discrepancy for low values of $\frac{R_1}{\tau}$ lies in the fact that the curve for the round wire helix includes the effect of a polystyrene core upon which the helix is wound, whereas the tape helix curve does not. If this dot-and-dashed curve is compared with the curve $\frac{R_2}{R_1} = 2.0$ of Figure 8, it is found that the agreement is quite good.

II-5 Conduction Losses in the Wire and Shield

Probably the most important losses in the helical structure are those which occur in the wire and shield. The results which are developed in Appendices B, C and D and which are presented in this chapter are based upon the assumption that the wire and sheath are lossless. The presence

of conduction loss in the wire and sheath will change the results of the analysis presented up to this point. With moderate amounts of loss, however, its effect upon the previous results will so small as to be negligible. This is fortunate, for an exact solution of the problem with a wire and shield of finite conductivity is extremely difficult.

If the radius of the wire is very small as compared to the helix radius, the wire may be considered to be essentially straight. In this case the well known theory of skin effect in round straight wires can be applied (see reference (22), chapter 15). This theory neglects the effect of other current carrying conductors in the neighborhood of the conductor under consideration, this effect being called the "proximity effect". For a close wound helix there are many turns of wire in close proximity to the one under consideration. Fortunately the proximity effect of those conductors on the one side of any given conductor is cancelled by those conductors on the other side of the given conductor. Unless the shield is very close to the helix the proximity effect of the shield currents is negligible and will be omitted.

From reference (22) there is obtained the skin effect ratio,

$$\left[\frac{R_{ac}}{R_{dc}}\right] = Re. \left\{\frac{\alpha r}{2} \frac{I_0(\alpha r)}{I_1(\alpha r)}\right\} \tag{43}$$

where,

$$\alpha = \sqrt{j\omega\mu_1\sigma} = (1+j)\sqrt{\frac{\omega\mu_1\sigma}{2}} \tag{44}$$

σ = the conductivity of the material of the wire (45)

r = the radius of the wire (46)

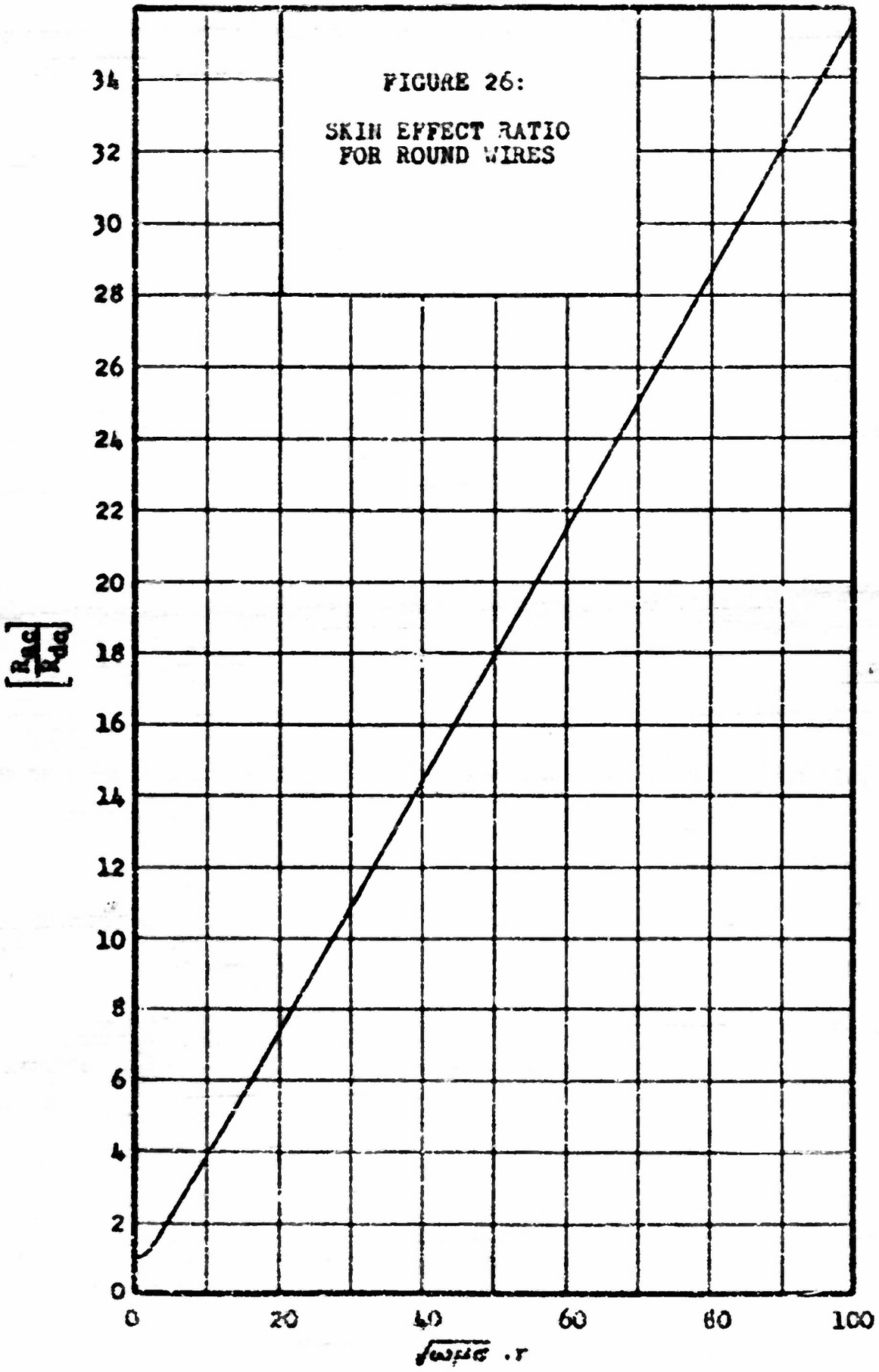
FIGURE 26:
SKIN EFFECT RATIO
FOR ROUND WIRES
$\left[\frac{R_{ac}}{R_{dc}}\right]$
0
2
4
6
8
10
12
14
16
18
20
22
24
26
28
30
32
34
0
20
40
60
80
100
$\sqrt{\omega\mu\sigma}\cdot r$

This ratio is plotted in Figure 26 as a function of $|\alpha r|$. For values of the argument in excess of 100, the skin effect ratio is given very closely by,

$$\left[\frac{R_{ac}}{R_{dc}}\right] \cong \frac{|\alpha r|}{2\sqrt{2}} \tag{47}$$

Since the resistance per unit length of a round wire for uniform current distribution is given by,

$$R_{dc} = \frac{1}{\pi r^2 \sigma} \tag{48}$$

the resistance of the wire per unit length in the helix direction is given by,

$$R_w = \frac{1}{\pi r^2 \sigma}\left[\frac{R_{ac}}{R_{dc}}\right] \tag{49}$$

From this the resistance of the wire per unit length in the axial direction is,

$$R_{w_z} = \frac{\csc \psi}{\pi r^2 \sigma}\left[\frac{R_{ac}}{R_{dc}}\right] \tag{50}$$

In order to calculate the losses in the sheath, it is necessary to know the current distribution on the surface of the sheath. If the losses are small, they will have a negligibly small effect upon the current distribution as calculated upon the basis of infinite conductivity.

Equations (146) and (147) of Appendix C can be used to arrive at the surface current density for a quasi-static case of alternating currents.

That is, for a frequency low enough that the current and charge distributions are essentially the same as for the static case. Hence from (146) and (147) the surface current densities are,

$$\delta_{\phi rms} = \frac{-I_{rms}}{\tau}\left\{\frac{R_1^2}{R_2^2} + 2\sum_{m=1}^{\infty}\frac{R_1}{R_2}\cdot\frac{I_m'(bR_1)}{I_m'(bR_2)}\cos(bz-m\phi)\right\} \tag{51}$$

$$\delta_{z rms} = \frac{-I_{rms}}{\tau}\left\{1 + 2\sum_{m=1}^{\infty}\frac{R_1}{R_2}\cdot\frac{I_m'(bR_1)}{I_m'(bR_2)}\cos(bz-m\phi)\right\} \tag{52}$$

where I_{rms} is the effective value of the current flowing in the wire.

If the frequency is sufficiently high, the depth of penetration of current into the surface of the sheath will be small compared with the radius of the sheath. For this case the skin depth will essentially be the same as for a plane conducting sheet. It is for that case,

$$\delta = \sqrt{\frac{2}{\omega\mu\sigma}} \tag{53}$$

The skin depth has the property that if all the current flowing in the sheath were to flow with uniform distribution in a surface layer of thickness δ, the loss would be exactly equal to the actual loss.

Now consider a ring of very small length Δz and thickness δ taken out of the sheath as shown in Figure 27(a). Since the surface densities δ_ϕ and δ_z are orthogonal the total loss will be equal to the

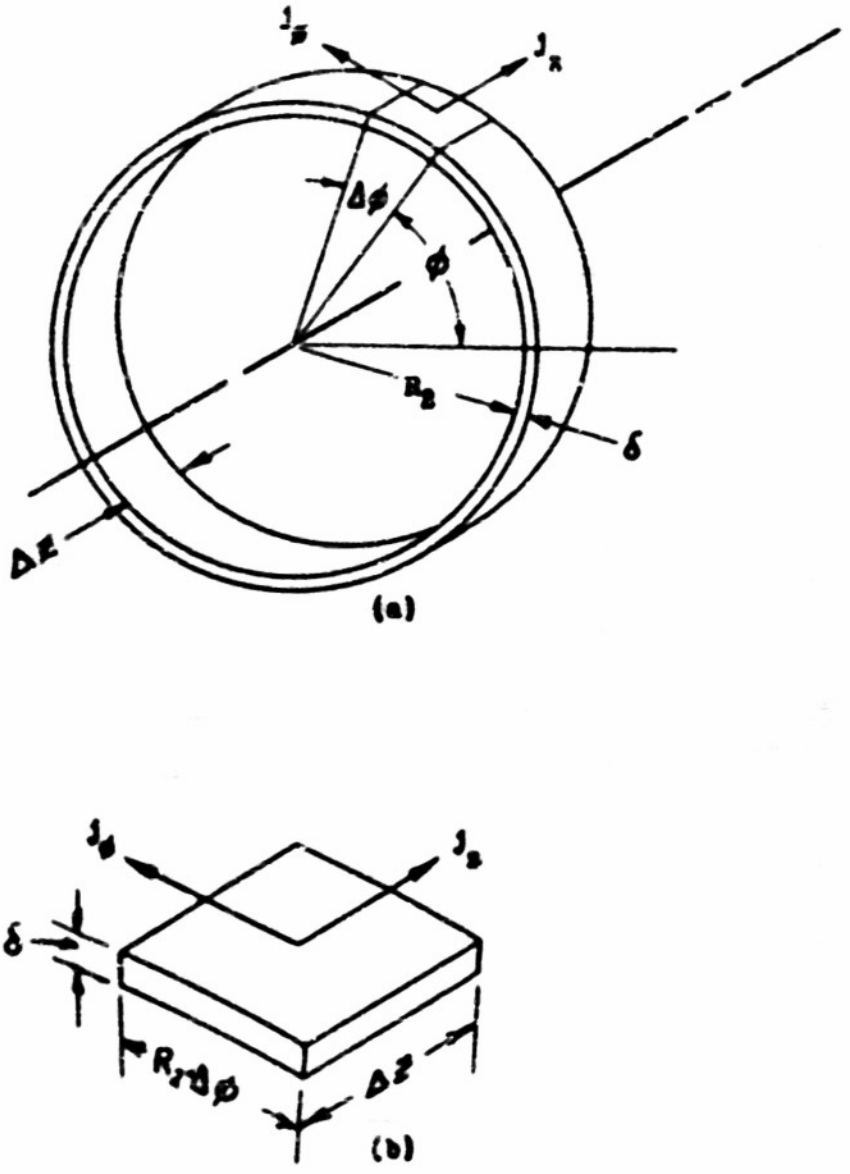

FIGURE 27: RING TAKEN OUT OF CURATH

arithmetic sum of the loss due to each individual component. For the z component of current density, the total rms current flowing in the differential slab as shown in Figure 27(b) is,

$$J_{z\,rms}(R_2\,d\phi) \tag{54}$$

This flows in a slab that has resistance,

$$\frac{\Delta z}{\delta(R_2 d\phi)\sigma} \tag{55}$$

and the loss in this slab due to the z component of current is,

$$J^2_{z\,rms}\,\frac{(R_2 d\phi)\cdot\Delta z}{\delta\,\sigma} \tag{56}$$

where the $J_{z\,rms}$ of (56) is obtained from (52) for some particular value of z and ϕ. If this expression is integrated with respect to ϕ from 0 to 2π the result will be the loss in the ring due to the z component of current. No generallity is lost by taking the position of the ring as being at z equals zero. Denoting the loss in this ring due to J_z as P_z there results,

$$P_z = I^2_{rms}\,\frac{\Delta z}{2\pi R_2\,\delta\,\sigma}\left\{1 + 2\sum_{m=1}^{\infty}\left[\frac{R_1}{R_2}\,\frac{I'_m(bR_1)}{I'_m(bR_2)}\right]^2\right\} \tag{57}$$

In exactly the same manner the loss in the ring due to the ϕ component of current density is,

$$P_\phi = I_{rms}^2 \frac{2\pi R_2 \cdot \Delta Z}{\delta \sigma} \left\{ \left(\frac{R_1}{R_2}\right)^4 + 2 \sum_{m=1}^{\infty} \left[\frac{R_1}{R_2} \frac{I_m'(bR_1)}{I_m'(bR_2)} \right]^2 \right\} \tag{58}$$

The total loss in the ring will be the arithmetic sum of equations (57) and (58). The loss in this particular ring will be no different than the loss in any other similar ring taken out of the sheath. Hence by dividing the sum of (57) and (58) by (ΔZ) the sheath loss per unit length in the axial direction is obtained.

If this is then divided by the rms wire current, an equivalent sheath resistance referred to the wire is obtained. Denoting this by R_{sz}, there results for the resistance per unit length in the axial direction due to sheath losses,

$$R_{sz} = \frac{1}{2\pi R_2 \delta \sigma} \left\{ \left[1 + \left(\frac{R_1}{R_2}\right)^4 \cot^2 \psi \right] + 2 \csc^2 \psi \sum_{m=1}^{\infty} \left[\frac{R_1}{R_2} \cdot \frac{I_m'(bR_1)}{I_m'(bR_2)} \right]^2 \right\} \tag{59}$$

This resistance when added to the resistance of equation (50) gives the total resistance per unit of length in the axial direction.

Chapter III

Experimental Results

Other authors have conducted experimental work on the impedance and phase velocity of shielded helices. However, this author has conducted similar experimental work because the reports of the previous investigators left some doubts concerning the manner of testing or the actual dimensions, etc., of their helices. As will be shown, the work of all the investigators agrees closely with the analytic results presented in the previous chapter. After a discussion of the present author's work, the investigations of the other investigators will be presented.

III-1 The Method of Testing

The method of testing used by the present author does not measure the characteristic impedance and phase velocity directly. These are determined from a measurement of the open circuit and short circuit driving point impedances of the transmission line. Figure 28 shows the results of a typical set of measurements on a given lossless helical transmission line of axial length l_2 . From transmission line theory applied to a lossless transmission line, the open and short circuit impedances are pure reactance. They are,

$$X_{sc} = j\sqrt{\frac{L_2}{C_2}}\tan\left(2\pi f l_2\sqrt{L_2 C_2}\right) \tag{1}$$

$$X_{oc} = -j\sqrt{\frac{L_2}{C_2}}\cot\left(2\pi f l_2\sqrt{L_2 C_2}\right) \tag{2}$$

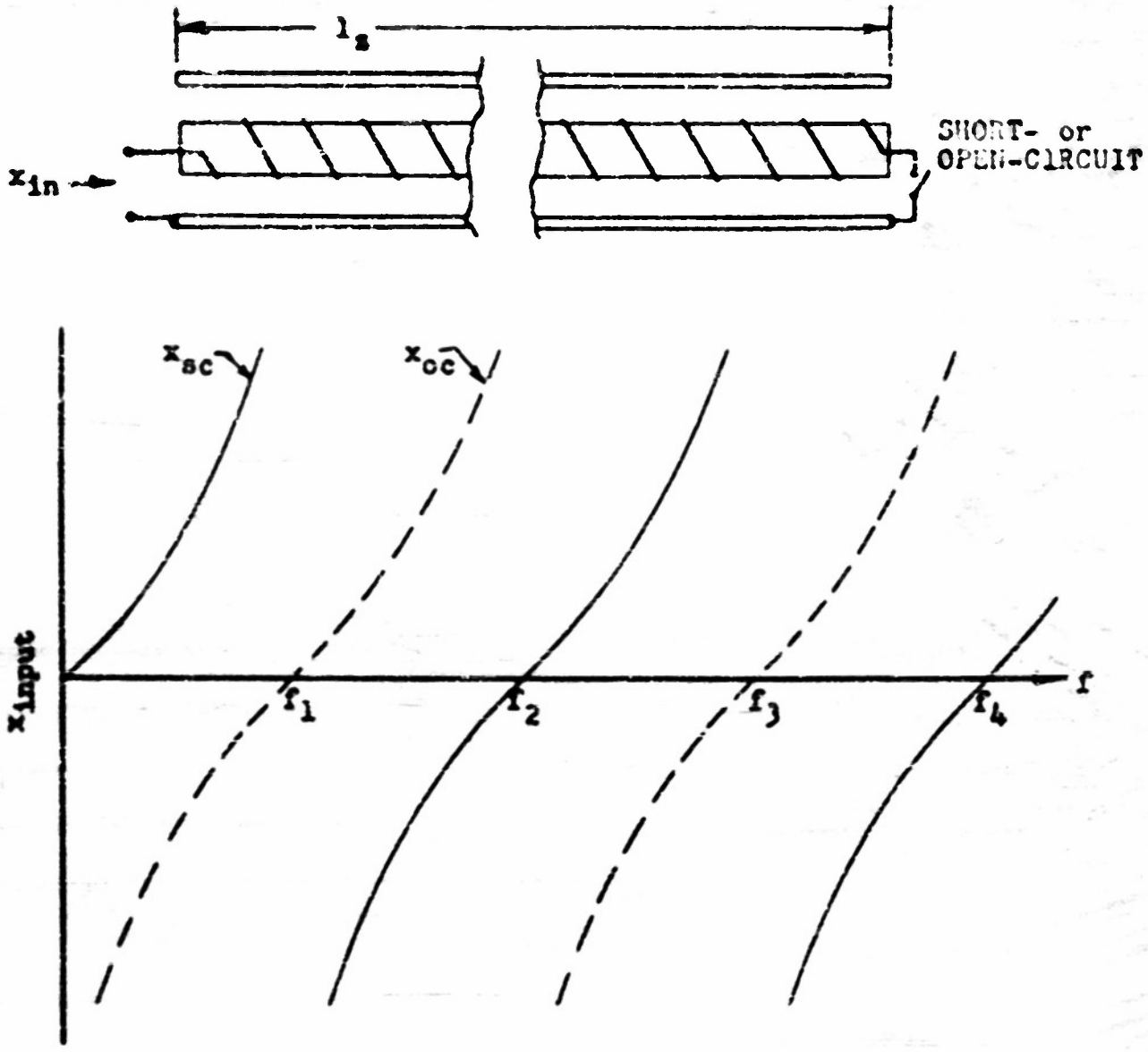

$$Z_0 = \sqrt{|x_{sc}|\,|x_{oc}|}$$

$$v_s = 4f_1 l_s$$

FIGURE 26: OPEN AND SHORT CIRCUIT TEST FOR CHARACTERISTIC IMPEDANCE AND PHASE VELOCITY

where X_{sc} and X_{oc} are the short circuit and open circuit driving point impedances respectively. The parameters L_z and C_z are the distributed inductance and capacitance per unit of length in the axial direction.
From (1) and (2),

$$Z_0 = \sqrt{\frac{L_z}{C_z}} = \sqrt{|X_{sc}| \cdot |X_{oc}|} \tag{3}$$

$$\nu_z = \frac{1}{\sqrt{L_z C_z}} = 4 f_1 l_z \tag{4}$$

where f_1 is the frequency of the first "pole" in the short circuit driving point impedance. This frequency is also that at which the transmission line is one quarter of a wave-length long. Thus by measuring the open and short circuit driving point impedances for frequencies up to that at which the line becomes one quarter of a wave-length long, the characteristic impedance and phase velocity can be determined from (3) and (4).

The analytic results of Chapter II were arrived at by assuming infinite wave-length. Because of this, the experimental results are confined to frequencies for which the transmission line is equal to or less than one quarter wave-length long.

The driving point impedances were measured with either a General Radio 916A bridge or a General Radio 821A twin-T-bridge. In either case, the oscillator used was a General Radio 684A oscillator. Since the bridge measurements are dependent upon a knowledge of the applied frequency, this oscillator was calibrated from 0.7 Mc up to 5 Mc. In no case did its scale reading differ by more than 0.35% from its true frequency. Because of the

very good accuracy in the region of calibration, it was used with confidence up to about 10 Mc. The 916A bridge is accurate to within ± 2%. The 821A twin T bridge is considerably more accurate than this because it employs a highly precise capacitor in a "substitution" circuit.

III-2 Description of the Helices and Experimental Results

All of the helices tested had the same R_1, R_2 and wire radius r_0. These were respectively 0.385", 0.750" and 0.010". The winding pitch was varied from 1/32 inch up to 1-1/2 inches. The outer conductor or sheath consisted of a 1.5" copper tube 72" long with a wall thickness of 1/8 inch. The first two helices, Nos. 1 and 2, were wound on a polystyrene tube having a 3/4 inch outside diameter and a 1/16 inch wall. These helices were 72 inches long and were supported concentrically in the copper tube by three polystyrene supports placed at both ends and the middle. These supports were 1/8 inch thick and their effect was assumed to be negligible. The helix was made very long in order to eliminate from consideration any end effects, the analysis of Chapter II being based upon an infinitely long helix. Helices 3 to 8 were the same as 1 and 2 in all respects except that they were wound on 3/4 inch solid polystyrene rod and were 71 inches long. Figure 29 (a photograph of helix No. 8) shows a portion of the copper sheath, the rod with the wire helix wound on it, and the end support. Table 3 gives the R_1/τ of the various helices along with the calculated and measured properties.

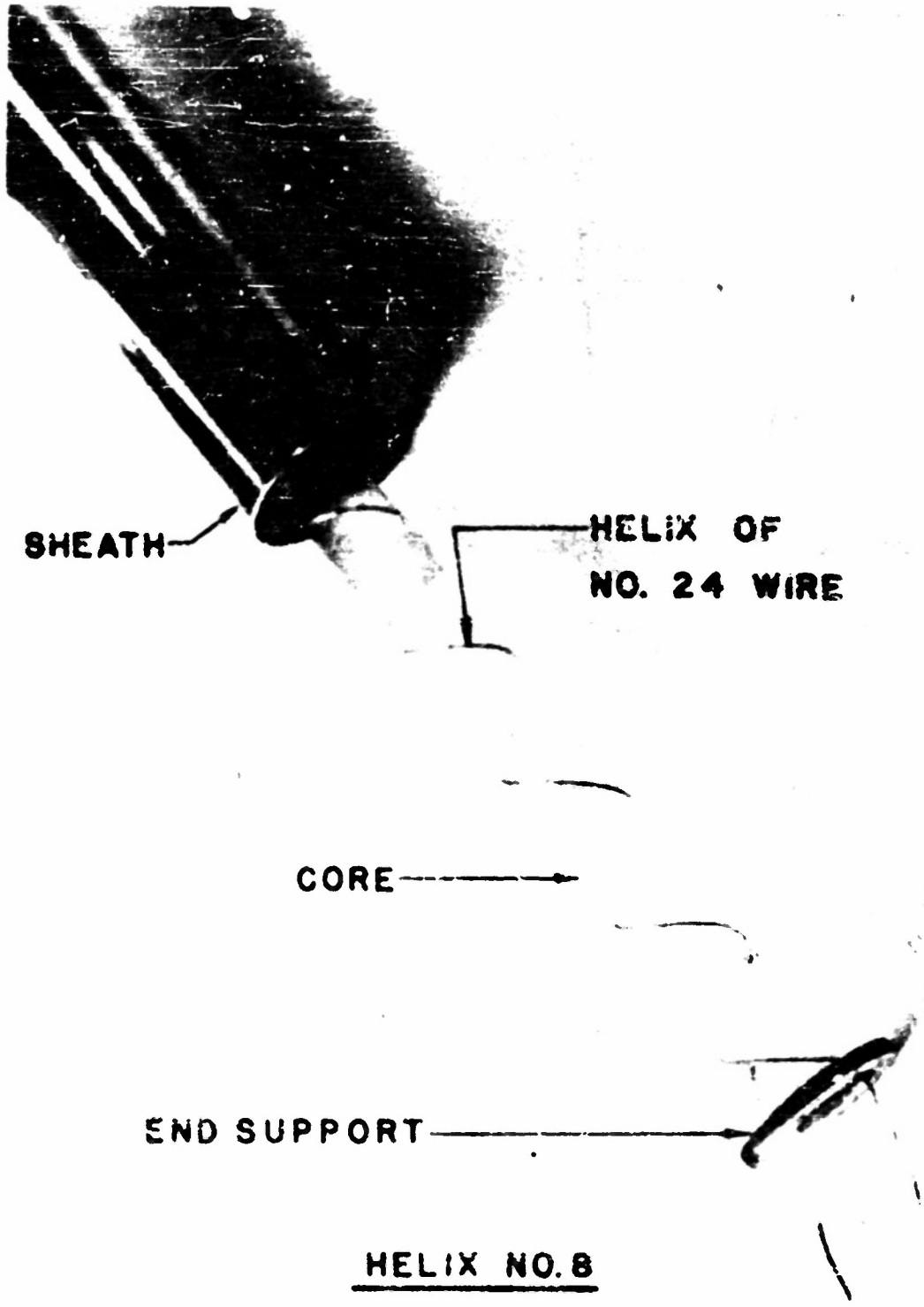

HELIX NO. 8

FIGURE 29

Table 3

Comparison of Test and Analytic Results

As Obtained by the Author

Helix Number	Pitch, Inches	$\frac{R_1}{\tau}$	Characteristic Imp. Ohms		$\frac{\sqrt{\mu_0 \epsilon_r}}{\sin \psi} \cdot v_s$	
			Calculated	Measured	Calculated	Measured
1	0.50	0.770	247*	248	1.068*	1.038
2	1.00	0.385	210*	216.2	0.930*	0.930
3	0.03125	12.32	2260	2250	1.347	1.328
4	0.0625	6.16	1140	1137	1.342	1.321
5	0.125	3.08	603	605.5	1.302	1.272
6	0.250	1.54	356	364.5	1.206	1.181
7	0.500	0.77	247	257.3	1.068	1.052
8	1.50	0.257	201	212.3	0.874	0.881

*Calculated for a solid core

These results are plotted in Figures 30 and 31. At the lower end of the range of R_1/τ, the measured impedances lie somewhat above the calculated impedances. This is probably because of the fact that the theoretical result is based upon the assumption that the dielectric material of the supporting rod extends out to a radius R_1. In actuality, it falls short of this by an amount equal to the wire radius. In Figure 31 the phase velocity compares very favorably with the theoretical curve, the maximum deviation being 3%. One thing apparent from the test results is that it makes very little difference whether the helix is wound on a solid rod or upon a tube.

III-3 Experimental Results of Other Investigators

(a) The Results of E. Keutner

The report by E. Keutner of the tests on a series of shielded

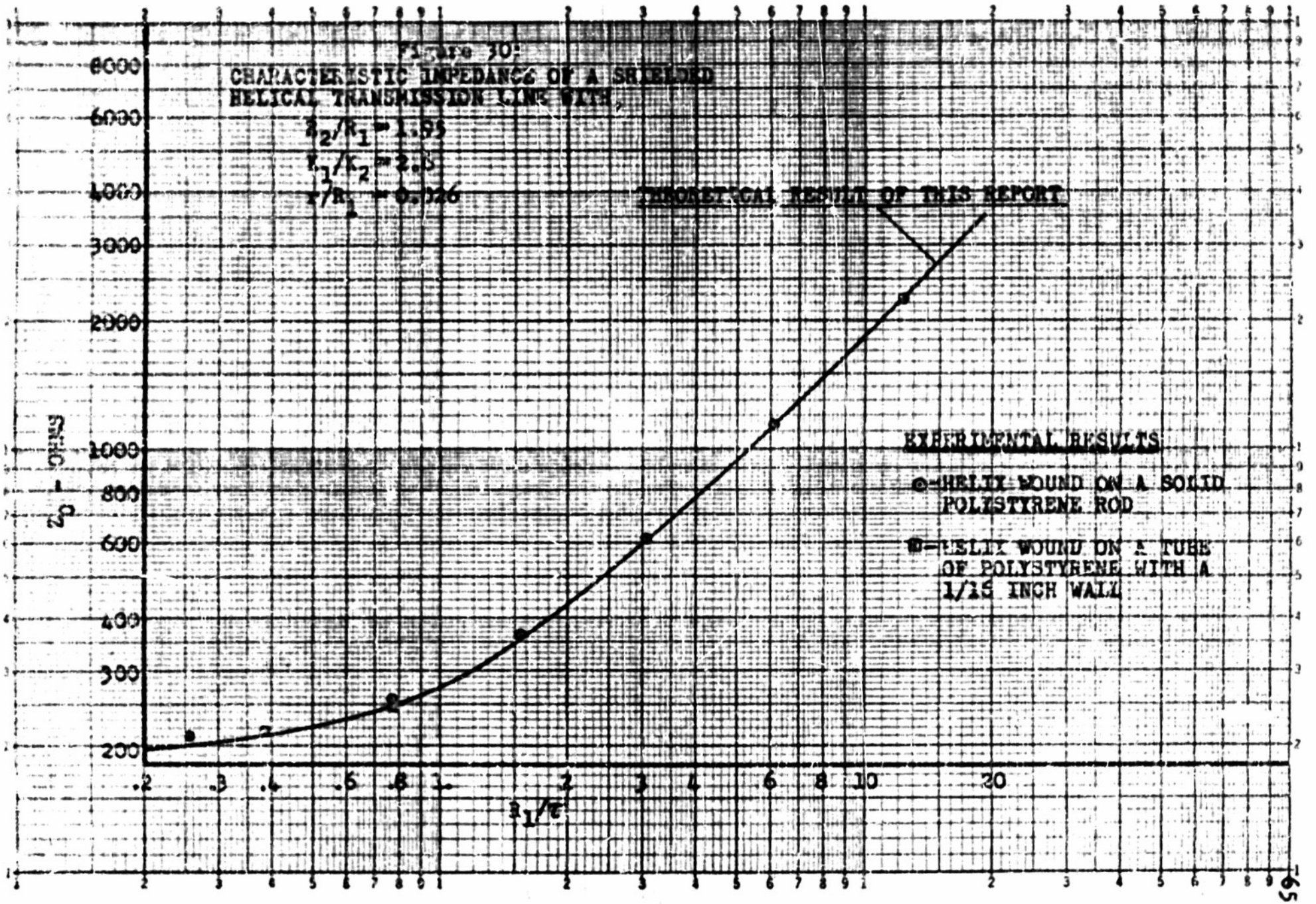
Figure 30
CHARACTERISTIC IMPEDANCE OF A SHIELDED HELICAL TRANSMISSION LINE WITH
$a_2/a_1 = 1.95$
$a_3/a_2 = 2.5$
$\tau/a_1 = 0.026$
THEORETICAL RESULT OF THIS REPORT
EXPERIMENTAL RESULTS
⊙-HELIX WOUND ON A SOLID POLYSTYRENE ROD
⊗-HELIX WOUND ON A TUBE OF POLYSTYRENE WITH A 1/15 INCH WALL
Z_0 OHMS
a_1/τ
6000
5000
4000
3000
2000
1000
800
600
400
300
200
.2
.3
.4
.6
.8
1
2
3
4
6
8
10
20

Figure 32.

PHASE VELOCITY OF A SHIELDED HELICAL TRANSMISSION LINE WITH $R_2/R_1 = 1.95$

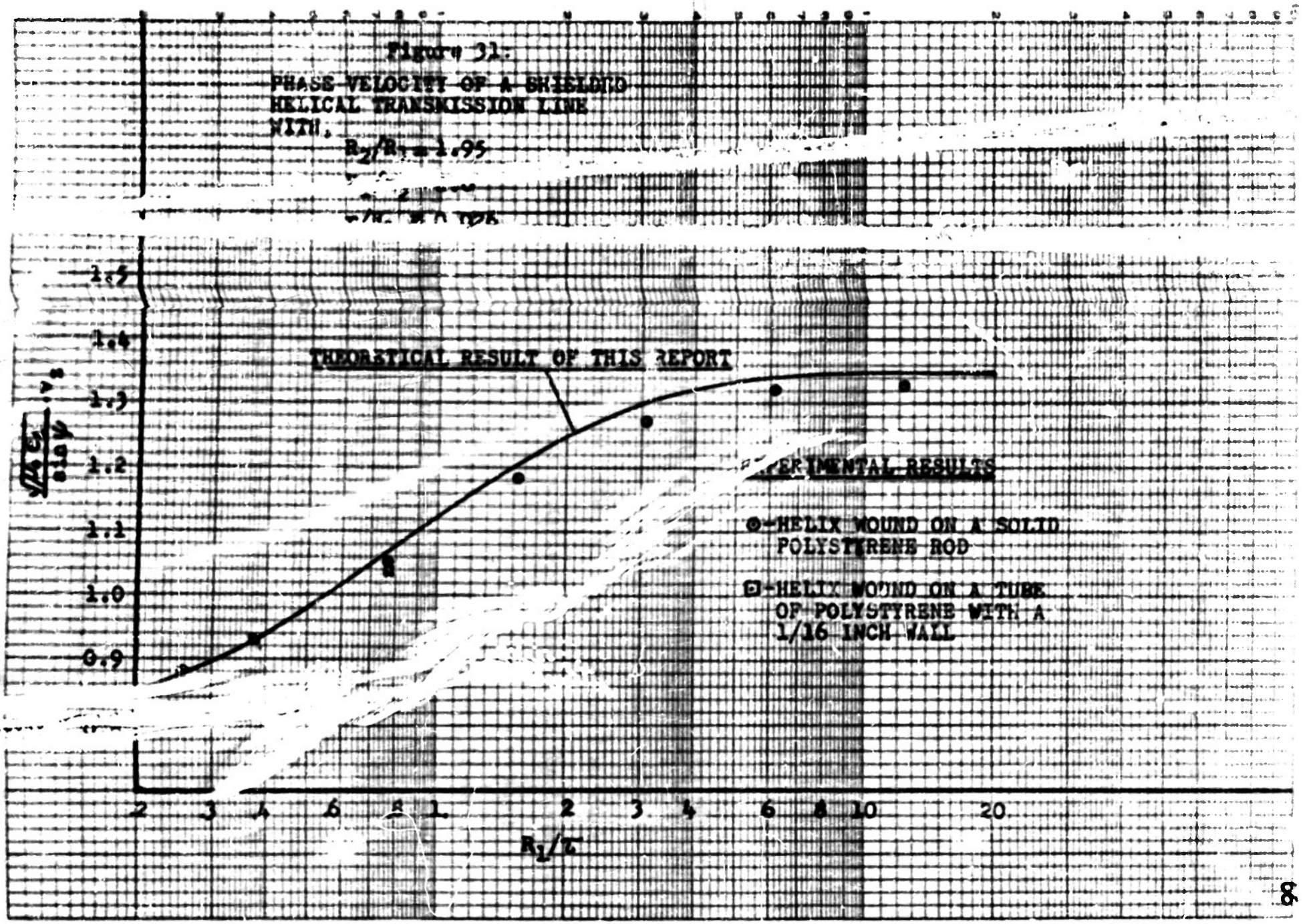

helices is contained in reference (14). In these tests, Keutner considered both wire wound and tape helices. Only his results for wire helices are given here. His method of measuring was to determine the inductance per unit length from a short circuit test and the capacitance per unit length from an open circuit test, both tests being performed at a very low but unspecified frequency. From these measured parameters, he calculated the impedance and phase velocity. The cables he tested had an R_1 of "about" 4.5 mm and an R_2 of "about" 10 mm. The insulation between inner and outer conductors was an air space formed by styroflex insulation. An examination of a photograph of the cable shows that apparently the outer conductor is supported on styrene wafers about 20 mm apart, each wafer being about 3 mm thick. In addition, there appears to be a double helix of insulating cord running over the wire, the pitch being about 55 mm. However, Keutner makes no mention of the insulation between inner and outer conductors, neither with respect to the quantity nor with respect to its disposition. If one considers the effect of styrene wafers 3 mm thick placed 20 mm apart, it is approximately equivalent to increasing the dielectric constant in the air space between the inner and outer conductors to about 1.24. This would have the effect of lowering the characteristic impedance and phase velocity by about 11.5% as compared with these quantities for a pure air dielectric in region 2. The helix itself is wound on a paper core for which the dielectric constant is about 2.0.

No mention is made of the wire diameter used in the tests. However, in Figure 4 of Keutner's report it is obvious that the helix of this photograph is butt wound. This fact, plus the fact that the highest turns density for which he reports any results is 9.7 turns per cm. indicates that the wire diameter used was probably 1.0 mm.

In table 4 are summarized the dimensions and other data which were

probably used in the helices built by Keutner.

Table 4

Dimensions of the Helices Built by Keutner

$R_1 = 4.5$mm	$\tau = 1.03$ to 10mm
$R_2 = 10.0$mm	$K_1 = 2.0$
$r = 0.5$mm	$K_2 = 1.24$

Using the dimensions of Table 4, the characteristic impedance and phase velocity were calculated by the methods outlined in Chapter II of this report. In Table 5, the results of these calculations are compared with the test results obtained by Keutner. These results are also plotted for comparison in Figures 32 and 33.

Table 5

Comparison of Calculated and Test Results

Pitch, mm	$\frac{R_1}{\tau}$	Characteristic Impedance Ohms		$\frac{\sqrt{\mu_0 \epsilon_r}}{\sin} \cdot v_s$	
		Calculated*	Measured	Calculated*	Measured
10.0	0.45	151.5	154	1.037	1.020
4.55	0.99	213.5	217	1.205	1.207
2.50	1.80	338	334	1.280	1.300
1.67	2.70	492	477	1.295	1.304
1.25	3.60	655	626	1.300	1.304
1.03	4.37	798	756	1.295	1.294

* Calculated from the results of Chapter II of this report.

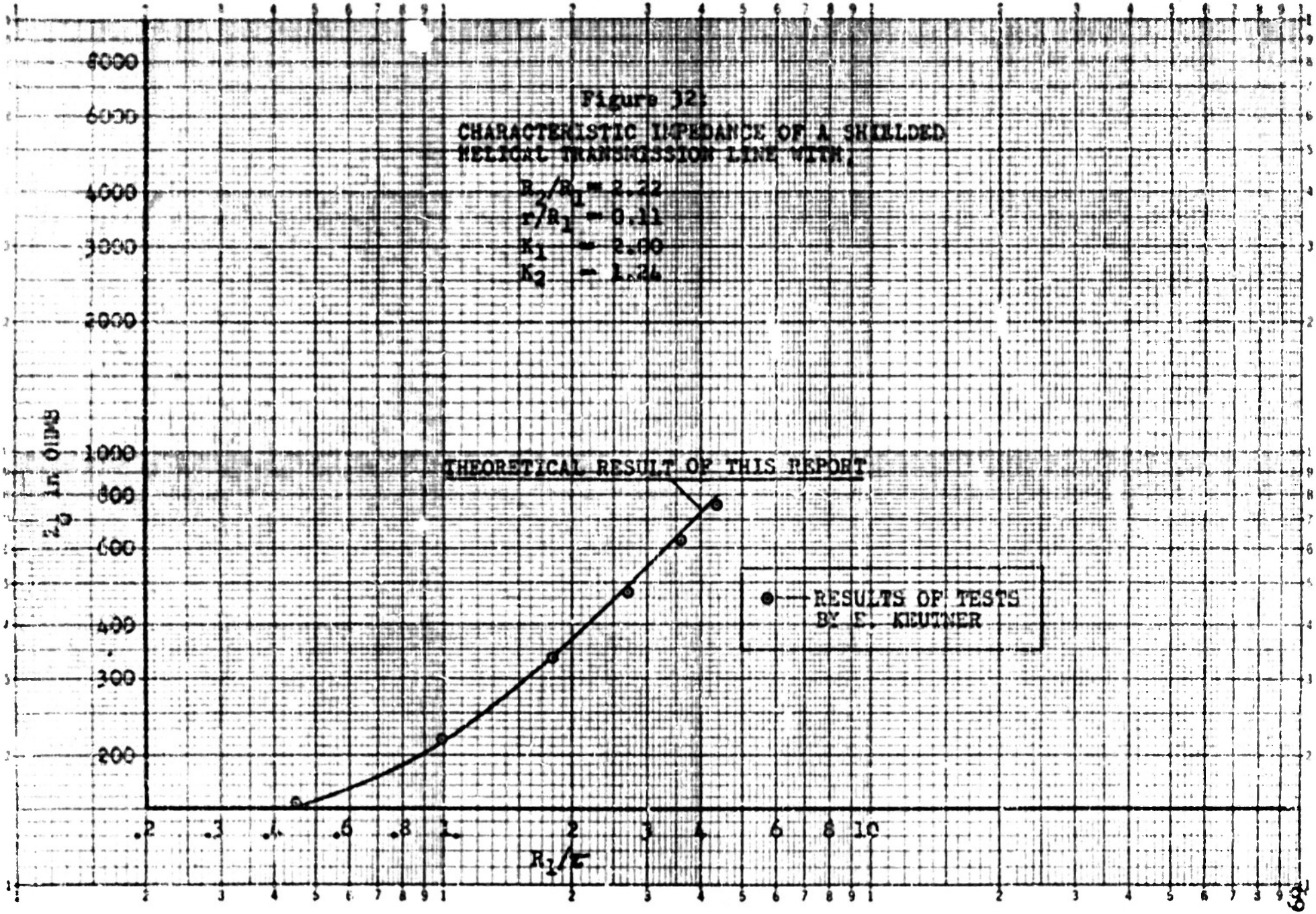
Figure 32
CHARACTERISTIC IMPEDANCE OF A SHIELDED
HELICAL TRANSMISSION LINE WITH
$R_2/R_1 = 2.22$
$r/R_1 = 0.11$
$K_1 = 2.00$
$K_2 = 1.24$
THEORETICAL RESULT OF THIS REPORT
RESULTS OF TESTS BY E. KEUTNER
Z_0 IN OHMS
R_1/r
6000
4000
3000
2000
1000
800
600
400
300
200
.2
.3
.4
.6
.8
1
2
3
4
6
8
10

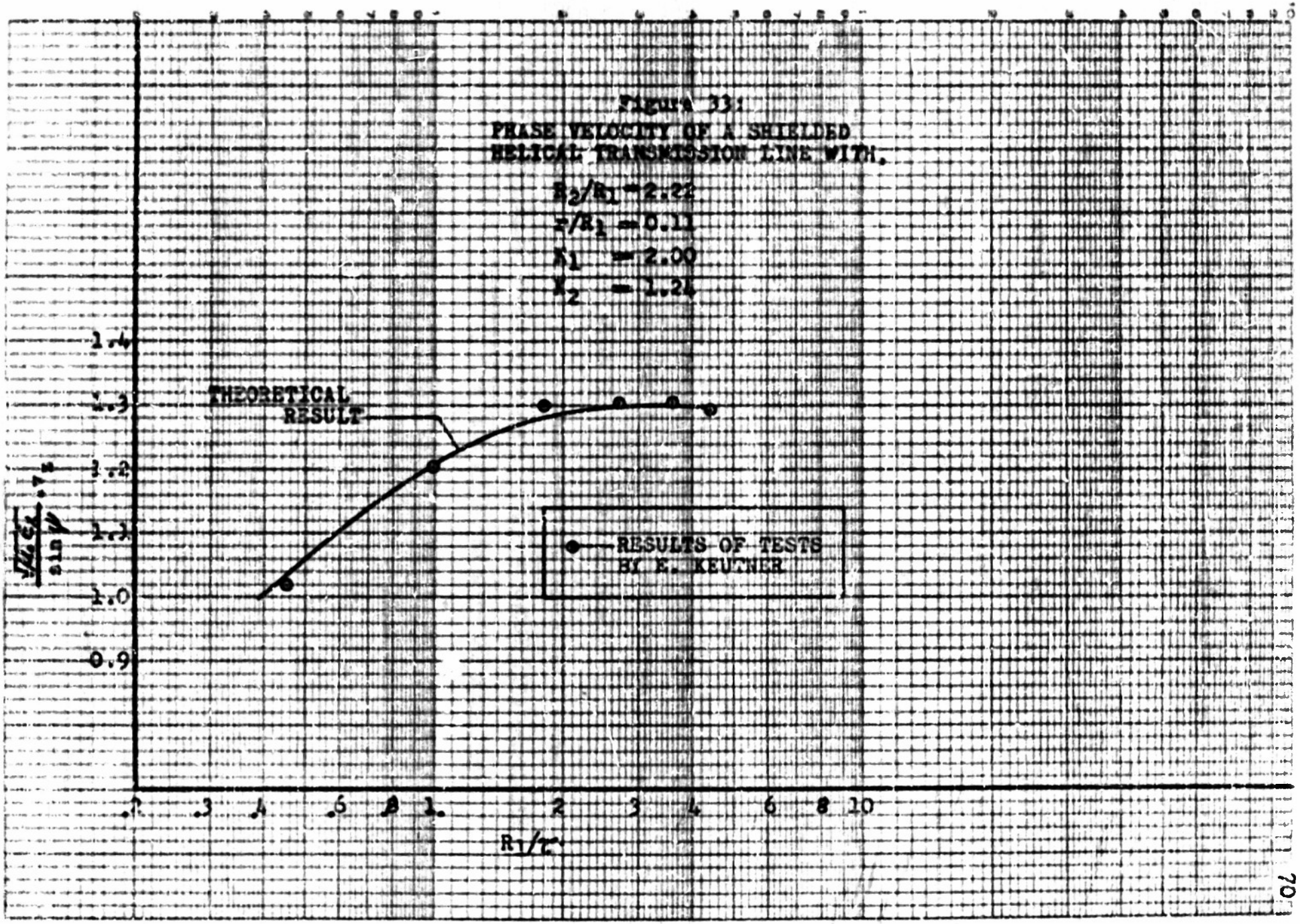
Figure 33:
PHASE VELOCITY OF A SHIELDED HELICAL TRANSMISSION LINE WITH.
R2/R1 = 2.22
r/R1 = 0.11
X1 = 2.00
X2 = 1.24
THEORETICAL RESULT
RESULTS OF TESTS BY E. KEUTNER
1.4
1.3
1.2
1.1
1.0
0.9
.2
.3
.4
.6
.8
1.
2
3
4
6
8
10
R1/λ
70

As can be seen from these results, the agreement between calculations and tests is remarkably good.

(b) The Results of C. Susskind

The report by C. Susskind of the tests on a series of shielded helices is contained in reference 17. This report is deficient in that no mention is made of the method of test. Nor is any mention made of the manner in which the helix is supported, either with regard to the core upon which it is wound or the support between the helix and the shield. No attempt was made to measure the phase velocity, nor was any data given from which phase velocity could be calculated. The helices tested were all quite short, being 11 inches long inside a 12 inch shield. They were all wound with #20 copper wire. These helices were so short that it was felt that end effects would probably have an important effect in lowering the characteristic impedance. For this reason, the helix which was chosen for comparison with the analytic results of Chapter II was one for which $(R_2 - R_1)$ was a minimum.

Figure 34 shows the calculated and test impedances for the case $R_2/R_1 = 3.00$, $R_1 = 0.266$ inches, and $r/R_1 = 0.060$. The calculations assumed a polystyrene winding form upon which the helix was wound, and assumed the presence of no dielectric material in the space between the inner and outer conductors. The test results are 7.3% to 13.4% below the calculated results. In view of the uncertainties regarding end effects and the actual method of supporting the helix, the agreement between test and calculation is good.

(c) Other Miscellaneous Results

Two other helices are here compared with the calculated results. J. Rukel, in reference (20) discusses the measurement of the input impedance of a tapered helical transmission line in which the impedance changes

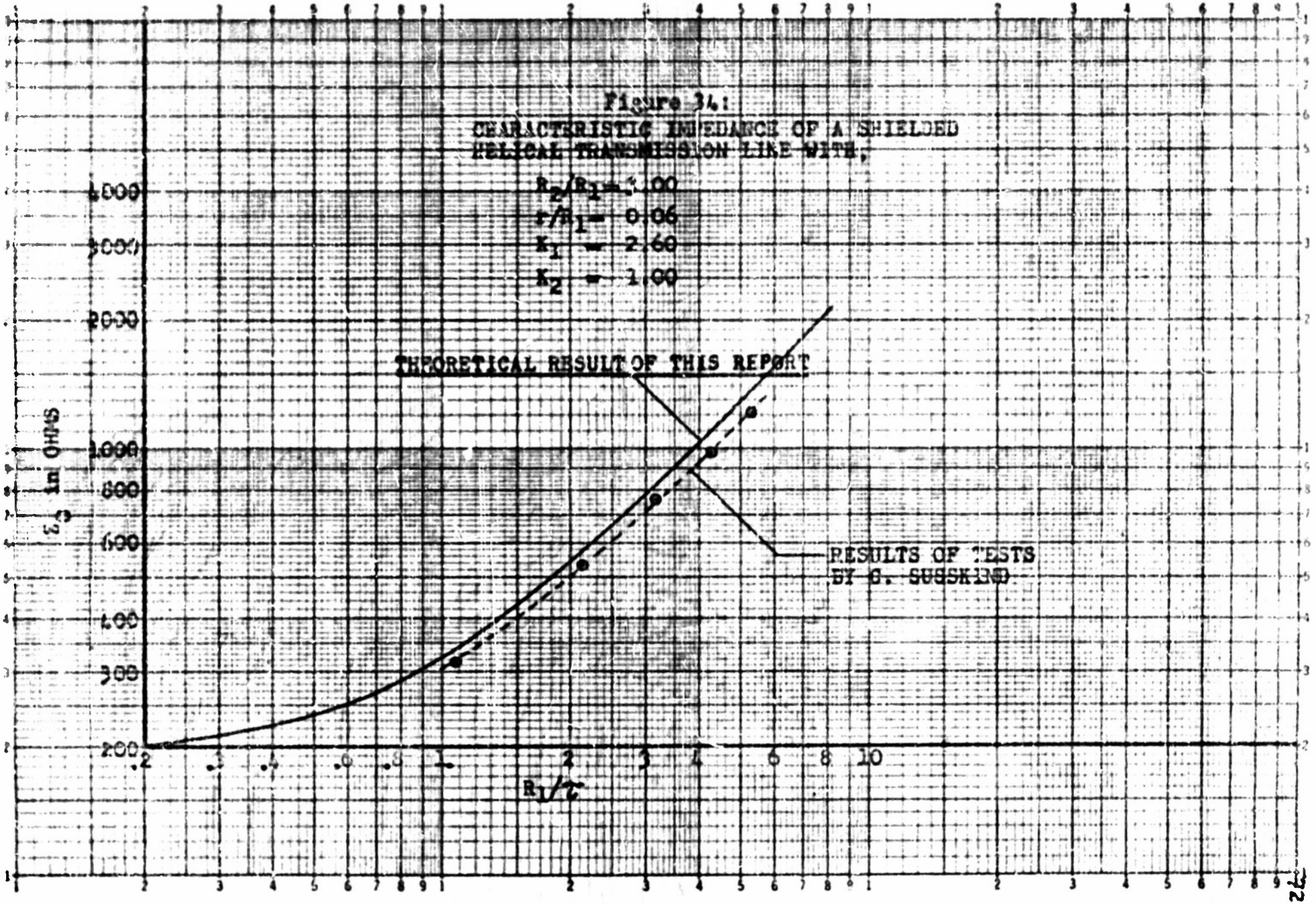
Figure 34:
CHARACTERISTIC IMPEDANCE OF A SHIELDED HELICAL TRANSMISSION LINE WITH,
R_2/R_1 = 1.00
r/R_1 = 0.06
κ_1 = 2.60
κ_2 = 1.00
THEORETICAL RESULT OF THIS REPORT
RESULTS OF TESTS BY G. SUSSKIND
Z_0 in OHMS
R_1/r
4000
3000
2000
1000
800
600
400
300
200
.2
.3
.4
.6
.8
1
2
3
4
6
8
10

approximately 1% per turn. Kukel's helix is wound on Lucite tubing and has the following dimensions: $a_1 = 0.766"$, $R_2 = 1.50"$, $\tau = 1.04$, $K_1 = 3.0$ and $K_2 = 1.0$. The characteristic impedance of this helix was measured by using pulse techniques and observing deflections upon an oscilloscope. His results also depended upon a knowledge of the characteristic impedance of a commercial coaxial cable. Using for this, the manufacturer's nominal value of 52 ohms, he arrived at a value of 290 ohms for his helix as compared with a calculated value of 255 ohms. This agreement is fairly good considering the crude method of measuring the impedance.

As a final comparison, a commercial delay line will be considered. This line is a Federal Telegraph and Radio Corporation RG - 65 - U cable. It has the following dimensions: $R_1 = 0.059$ inches, $R_2 = 0.148$ inches, $\Gamma = 0.004$ inches, $\tau = 0.0089$ inches, and $K_1 = K_2 = 2.4$ to 2.7. The manufacturer specifies for this line that its impedance is 950 ohms and that it has a delay of 0.042 microseconds per foot. Calculations based upon the results of Chapter II yield for the impedance 916 ohms to 972 ohms and for the delay, 0.0463 to 0.0437 microseconds per foot. The first values are for $K_2 = 2.7$ and the second values for $K_2 = 2.4$. The agreement is very good with respect to the impedance, and fairly good with respect to the delay.

(d) Conclusions With Regard to the Experimental Results

The experimental work carried out by this author and others confirms the analytic results set forth in Chapter II. While the author made no attempt to set an upper limit for wire size, the work of Keutner seems to confirm the validity of the analytic results for wire radii up to about 11% of the helix radius. The experimental work of this author seems to show that it is immaterial whether the helix is wound on a tube or a rod.

APPENDIX A.

Modified Bessel Functions

A 1. Differential Equations; Series Expansions

The basic functions with which this appendix is concerned are the independent solutions of the following second order differential equation

$$x^2 \frac{d^2y}{dx^2} + x \frac{dy}{dx} - (x^2 + m^2) y = 0 \tag{1}$$

with real values for x and integral values of m. Whether or not m is an integer, one solution of (1) (following the notation of Watson) is,

$$I_m(x) = \sum_{s=0}^{\infty} \frac{\left(\frac{x}{2}\right)^{m+2s}}{s!\,(m+s)!} = j^{-m} J_m(jx) \tag{2}$$

Except when m is an integer, $I_{-m}(x)$ provides a second solution of (1) which is linearly independent of $I_m(x)$. However for m an integer

$$I_{-m}(x) = I_m(x) \tag{3}$$

and another solution is necessary. The second solution used here for m an integer is,

$$K_m(x) = \frac{\pi}{2} \underset{\epsilon \to 0}{\text{Limit}} \left[\frac{I_{-(m+\epsilon)}(x) - I_{(m+\epsilon)}(x)}{\sin (m+\epsilon)\pi} \right] \tag{4}$$

The function $K_m(x)$ is defined by the following series,

$$K_m(x) = (-1)^{m+1} I_m(x) \log_e \left(\frac{x}{2}\right) + \frac{1}{2} \sum_{s=0}^{\infty} \frac{(-1)^s (m-s-1)!}{s!} \left(\frac{x}{2}\right)^{2s-m}$$

$$+ \frac{(-1)^m}{2} \sum_{s=1}^{\infty} \frac{\left(\frac{x}{2}\right)^{2s+m}}{s!\,(m+s)!} \left\{ \phi(s) + \phi(m+s) - 2\gamma \right\} \tag{5}$$

where γ is Euler's constant (= 0.5772 ...) and where

$$\phi(r) = 1 + \frac{1}{2} + \frac{1}{3} + \cdots + \frac{1}{r} \tag{6}$$

It is evident from the series given by (2) and (5) that $I_m(x)$ and $K_m(x)$ are not regular at x equal to infinity and zero respectively

For x small the following approximations are useful:

$$I_o(x) \cong 1 \tag{7}$$

$$I_m(x) \cong \frac{\left(\frac{x}{2}\right)^m}{m!} \quad , \quad m \neq 0 \tag{8}$$

$$K_0(x) \cong -\left[\gamma + \text{Log}_e\left(\frac{x}{2}\right)\right] \tag{9}$$

$$K_m(x) \cong \frac{(m-1)!}{2}\left(\frac{2}{x}\right)^m \quad , \; m \neq 0 \tag{10}$$

For large values of x where x $>>$ m the following asymptotic series are useful:

$$I_m(x) \cong \frac{e^x}{\sqrt{2\pi x}}\left\{1 - \frac{(4m^2-1)}{1!(8x)} + \frac{(4m^2-1)(4m^2-3^2)}{2!(8x)^2} - \cdots\right\} \tag{11}$$

$$I'_m(x) \cong \frac{e^x}{\sqrt{2\pi x}}\left\{1 - \frac{(4m^2+1\cdot3)}{1!(8x)} + \frac{(4m^2-1)(4m^2+3\cdot5)}{2!(8x)^2} - \cdots\right\} \tag{12}$$

$$K_m(x) \cong \sqrt{\frac{\pi}{2x}} \cdot e^{-x}\left\{1 + \frac{(4m^2-1)}{1!(8x)} + \frac{(4m^2-1)(4m^2-3^2)}{2!(8x)^2} + \cdots\right\} \tag{13}$$

$$K'_m(x) \cong \sqrt{\frac{\pi}{2x}} \cdot e^{-x}\left\{1 + \frac{(4m^2+1\cdot3)}{1!(8x)} + \frac{(4m^2-1)(4m^2+3\cdot5)}{2!(8x)^2} + \cdots\right\} \tag{14}$$

Graphs of these functions are shown on pages 224 and 242 of reference (7). The former page showing $I_m(x)$ for m=0 through 6 and x from 0 to 6, the latter page showing $\frac{2}{\pi} K_0(x)$ and $\frac{2}{\pi} K_1(x)$ for x from 0 to 6. The most complete tables of $I_n(x)$ and $K_n(x)$ are contained in reference (8).

4-2. Recurrence Formulae and Wronskian

The recurrence formulae for the $I_n(x)$ and $K_n(x)$ functions are as follows, where for the sake of simplicity the argument has been omitted:

$$x I'_m = m I_m + x I_{m+1} \quad \text{and} \quad x K'_m = m K_m - x K_{m+1} \tag{15}$$

$$x I'_m = -m I_m + x I_{m-1} \quad \text{and} \quad x K'_m = -m K_m - x K_{m-1} \tag{16}$$

$$2m I_m = x I_{m-1} - x I_{m+1} \quad \text{and} \quad 2m K_m = x K_{m+1} - x K_{m-1} \tag{17}$$

$$2 I'_m = I_{m-1} + I_{m+1} \quad \text{and} \quad 2K'_m = -K_{m-1} - K_{m+1} \tag{18}$$

The Wronskian which gives the relationship between the independent solutions is

$$W(I_m, K_m) = \begin{vmatrix} I_m & K_m \\ I'_m & K'_m \end{vmatrix} = (I_m K'_m - I'_m K_m) = \frac{-1}{x} \tag{19}$$

From this may be obtained the useful relationship,

$$\left(K_{m+1} I_m + K_m I_{m+1}\right) = \frac{1}{x} \tag{20}$$

Many additional useful formulae are given in reference (8) on page xxxiii.

A-3. Products of Modified Bessel Functions

Throughout the analysis in this report, the products $I_m(x)\, K_m(x)$, $I_m'(x)\, K_m'(x)$ and $I_m(x)\, K_m'(x)$ frequently occur. In reference (11), it is shown that these products are given approximately by,

$$I_m(x)\, K_m(x) \cong \frac{1}{2\sqrt{m^2 + x^2}} \tag{21}$$

$$I_m'(x)\, K_m'(x) \cong \frac{-\sqrt{m^2 + x^2}}{2x^2} \tag{22}$$

$$I_m(x)\, K_m'(x) \cong \frac{-1}{2x} \tag{23}$$

Figure 35 shows the function $2\sqrt{m^2 + x^2}\, I_m(x)\, K_m(x)$ plotted as a function of x for m up to 4. This shows the very good agreement between the exact and approximate expressions, especially since use is made of this approximation for values of x in excess of about 3. No calculations were made for m greater than 4, and x greater than 8. However, in view of the character of the separate asymptotic series and the behavior exhibited by the curves of Figure 35, it seems reasonable to expect that the representation

given by (20) is within 2% of the true value for all m greather than 1. Furthermore, it can be shown that (20) holds with increasing accuracy for all m as x increases to infinity.

In Figure 36, there is plotted the function $\frac{-2x^2 I_m'(x) K_m'(x)}{\sqrt{m^2+x^2}}$ for x up to 8 and m up to 4. As in the previous case, there is again remarkably good agreement for x greater than 4. It seems safe to say that the representation given by (21) is within 2% of the true value for all m greater than 1. It can be shown that regardless ofm, this function approaches unity as x approaches infinity.

In Figure 37, there is plotted the function $-2xI_m(x)\,K_m'(x)$ for x up to 8 and m up to 4. Although this plot shows that the approximation given by (22) is not as good as those of (20) and (21), the manner in which this approximation is used obviates the necessity for high accuracy. It appears in an expression of the form,

$$\left\{\frac{\epsilon_1}{\epsilon_2}+\left(\frac{\epsilon_1}{\epsilon_2}-1\right)\left[1-\frac{I_m'(bR_1)K_m(bR_2)}{I_m(bR_2)K_m'(bR_1)}\right](bR_1)I_m(bR_1)K_m'(bR_1)\right\}$$

A typical case would be $\epsilon_1/\epsilon_2 = 2.6$ and $(bR_1) = 3.0$. From Figure 37 for m = 1, $(bR_1)I_m(bR_1)K_m'(bR_1)$ is actually 14% higher than the value given by (22). However, the entire expression in the brackets will be at most only 3% too high. For values of m in excess of unity and values of (bR_1) in excess of 3.0 the agreement is even better. Since this term appears in an infinite series, the sum of the series using the approximation of (22) will be considerably closer to the true sum than the error in the

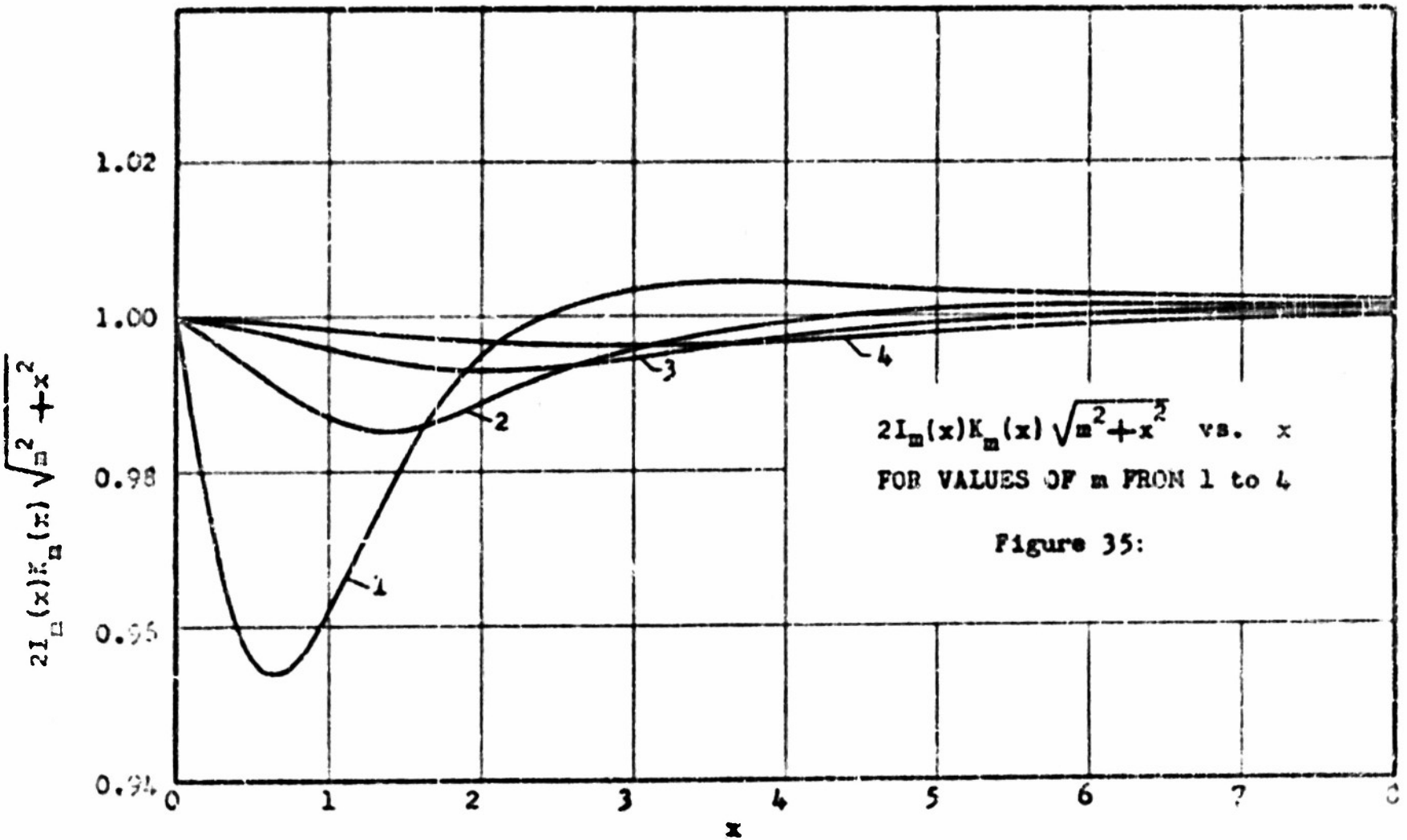

$2I_m(x)K_m(x)\sqrt{m^2+x^2}$ vs. x

FOR VALUES OF m FROM 1 to 4

Figure 35:

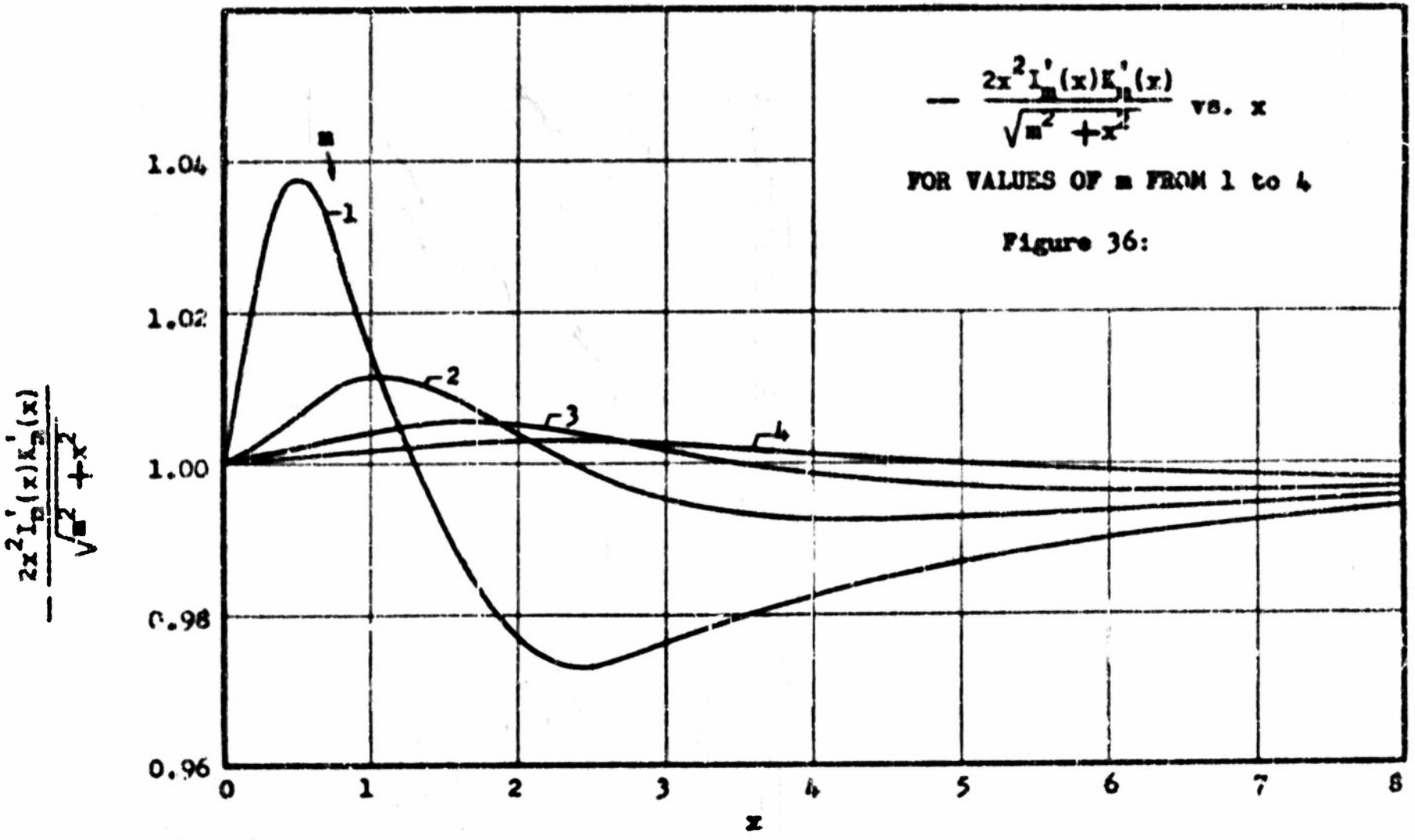
$-\frac{2x^2 I_m'(x) K_m'(x)}{\sqrt{m^2+x^2}}$ vs. x
FOR VALUES OF m FROM 1 to 4
Figure 36:
$-\frac{2x^2 I_n'(x) K_n'(x)}{\sqrt{n^2+x^2}}$
m
1
2
3
4
1.04
1.02
1.00
0.98
0.96
0
1
2
3
4
5
6
7
8
x

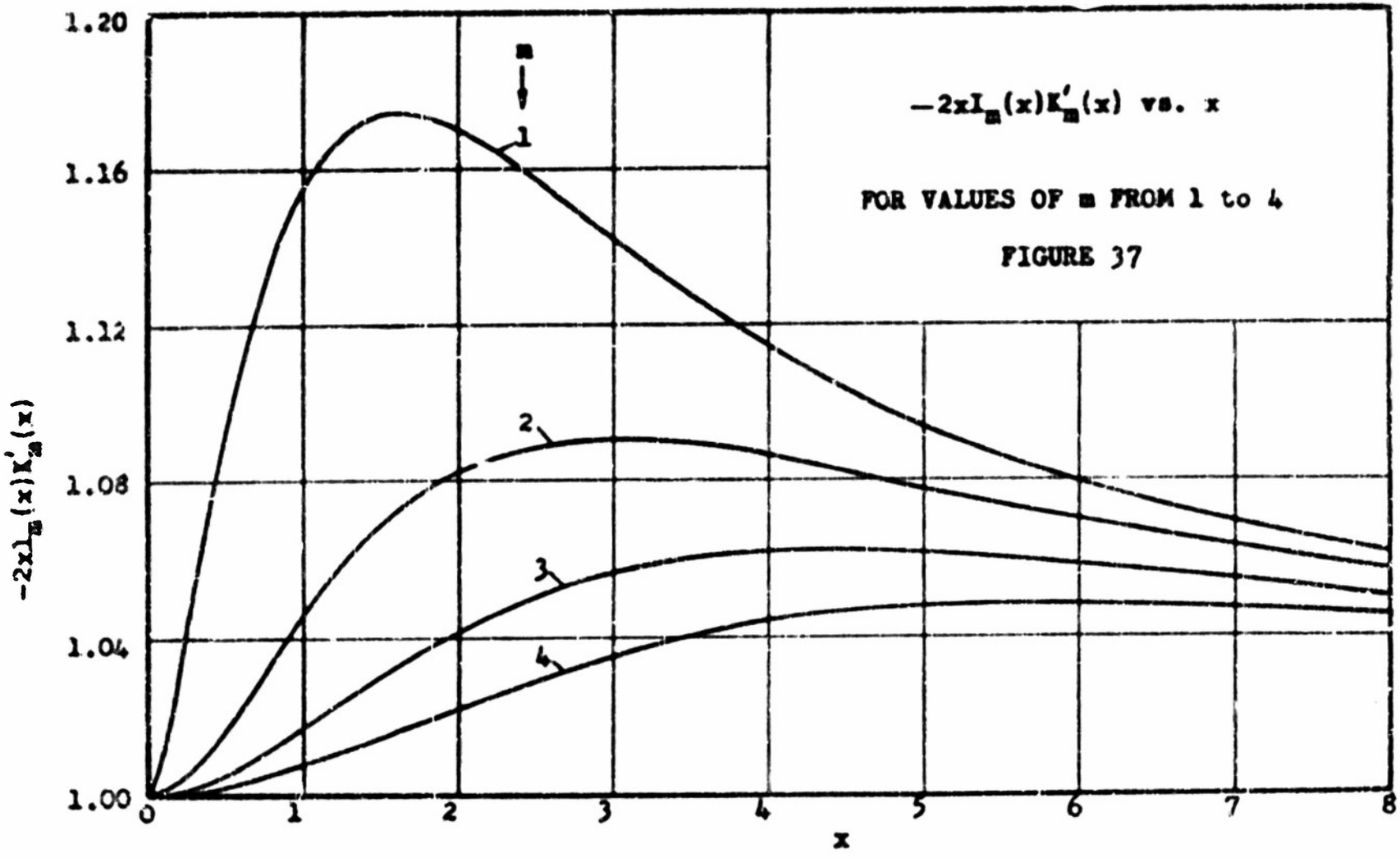
$-2xI_m(x)K'_m(x)$ vs. x
FOR VALUES OF m FROM 1 to 4
FIGURE 37
m
1
2
3
4
1.20
1.16
1.12
1.08
1.04
1.00
$-2xI_m(x)K'_m(x)$
0
1
2
3
4
5
6
7
8
x

first term indicates.

Three other combinations of Bessel functions occur frequently in the foregoing work. They are,

$$\frac{I_m(bR_1)K_m(bR_2)}{I_m(bR_2)K_m(bR_1)} \tag{24}$$

$$\frac{I'_m(bR_1)K'_m(bR_2)}{I'_m(bR_2)K'_m(bR_1)} \tag{25}$$

$$\frac{I'_m(bR_1)K_m(bR_2)}{I_m(bR_1)K'_m(bR_1)} \tag{26}$$

For very small values of b, that is for very large values of pitch τ, all three of these become,

$$\left(\frac{R_1}{R_2}\right)^{2m} \tag{27}$$

Consequently, for large values of m, they become negligible with respect to unity. For large values of b, say $b \gg 3m$, these three become very closely,

$$\epsilon^{-\frac{4m\pi(R_2-R_1)}{\tau}} \tag{28}$$

For example, with $m = 1$, $b = 3$, and $R_2/R_1 = 2$, this is of the order 0.0025 which is certainly negligible with respect to unity.

These approximations are used in the following section.

A-4. Bessel Function Sums.

Series of the form,

$$\sum_{m=1}^{\infty} a_m J_m(mx) \tag{29}$$

are known as Schlömilch series and are discussed in detail in Chapter XIX of reference (5). If in (29), x were replaced by an imaginary argument the series would be one of modified Bessel functions. A typical example from Chapter II would be the expression for the distributed capacitance. This is,

$$\frac{1}{C_g} = \frac{1}{2\pi\epsilon_2}\left\{\log_e\frac{R_2}{R_1} + 2\sum_{m=1}^{\infty}\frac{\left[1-\frac{I_m(bR_1)K_m(bR_2)}{I_m(bR_2)K_m(bR_1)}\right]K_m(bR_1)\cos\left(\frac{br}{\cos\psi}\right)}{\frac{\epsilon_1}{\epsilon_2}+\left(\frac{\epsilon_1}{\epsilon_2}-1\right)\left[1-\frac{I_m'(bR_1)K_m(bR_2)}{I_m(bR_2)K_m'(bR_1)}\right](bR_1)I_m(bR_1)K_m'(bR_1)}\cdot I_m(bR_1)\right\} \tag{30}$$

where,

$$b = \frac{2m\pi}{\tau} \tag{31}$$

The infinite series in (30) is a Schlömilch series and it will be evaluated by making use of the approximations of section A-3. For sufficiently large values of R_1/τ , (30) becomes, using these approximations,

$$\frac{1}{C_2} = \frac{1}{2\pi\epsilon_2}\left\{\log_e\frac{R_2}{R_1} + \frac{2\epsilon_2}{\epsilon_1+\epsilon_2}\sum_{m=1}^{\infty}\frac{\cos\left(\frac{2m\pi r}{\tau\cos\psi}\right)}{m\sqrt{1+\left(\frac{2\pi R_1}{\tau}\right)^2}}\right\} \tag{32}$$

This assumes that R_1/τ is sufficiently large to make the two terms of (30) in the square braces very close to unity. It is the failure of this assumption at small R_1/τ that accounts for the curves of Figure 4.

The infinite sum is of the form,

$$\sum_{m=1}^{\infty}\frac{\cos m\chi}{m} \tag{33}$$

By making use of formula 603.2 of reference (4), this can be expressed in closed form as,

$$\sum_{m=1}^{\infty}\frac{\cos\left(m\frac{2\pi r}{\tau\cos\psi}\right)}{m} = -\log_e\left[2\sin\left(\frac{\pi r}{\tau\cos\psi}\right)\right] \tag{34}$$

and equation (32) becomes,

$$\frac{1}{C_2} = \frac{1}{2\pi\epsilon_2}\left\{\log_e\frac{R_2}{R_1} - \frac{2\epsilon_2}{\epsilon_1+\epsilon_2}\cdot\frac{\log_e\left[2\sin\left(\frac{\pi r}{\tau\cos\psi}\right)\right]}{\sqrt{1+\left(\frac{2\pi R_1}{\tau}\right)^2}}\right\} \tag{35}$$

Since,

$$\sin\psi = \frac{1}{\sqrt{1+\left(\frac{2\pi R_1}{t}\right)^2}} \quad , \tag{36}$$

$$\frac{1}{C_2} = \frac{1}{2\pi\epsilon_2}\left\{\log_e\frac{R_2}{R_1} - \frac{2\epsilon_2\sin\psi}{\epsilon_1+\epsilon_2}\log_e\left[2\sin\left(\frac{\pi r}{t\cos\psi}\right)\right]\right\} \tag{37}$$

By a similar process, the infinite series of Bessel functions which appear in the inductance formula can also be expressed in closed form. This closed form, of course, applies to close wound helices as defined in Figure 4.

Appendix B

The Distributed Capacitance

As has already been noted in Chapter I, one approach to the problem of evaluating the characteristic impedance of a helical transmission line is to determine the distributed capacitance and inductance per unit length. These parameters have meaning only where the wavelength is very long when compared with any of the dimensions of the helix. For the above reason, and because of the simplicity of the derivation, the distributed capacitance is determined for the case of a uniform potential (with respect to time and distance along the line) between the helix and its sheath. Obviously, this corresponds to the case of infinite wavelength. In the ensuing work, the reciprocal of the capacitance per unit length is determined since it lends itself to more convenient manipulation in a later chapter.

B-1. Definitions and Coordinate Systems

In the derivation to follow, use is made of a circular cylindrical coordinate system as shown in Figure 38a. A right handed helix is shown in Figure 38b upon which are shown the significant dimensions of the helix. The helix is shown full where it is in front of the core upon which it is wound.

Throughout this report, the rationalized MKS system is used, and the helix is considered to be immersed in a medium which is characterized by having homogeneous, isotropic and linear properties in each of two regions; one inside the radius R_1 and the other outside the radius R_1 but inside the radius R_2. At the radius R_2 there is a perfectly conducting sheath. The medium in which the helix is immersed is further considered to be lossless and to have a permeability equal to that of free space.

The permittivity of the region ($0 \leq \rho \leq R_1$) is taken to be ϵ_1 and that of the region ($R_1 \leq \rho \leq R_2$) is taken to ϵ_2 . In conformity with

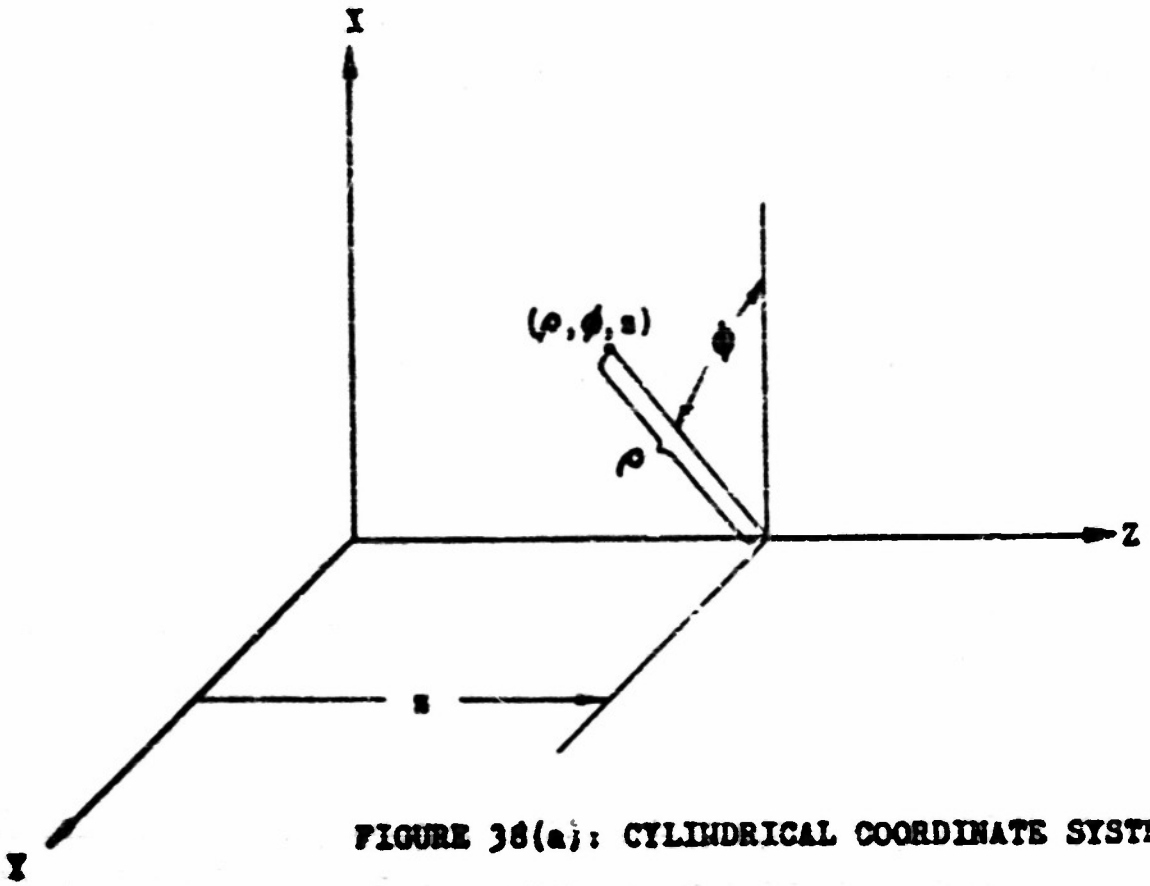

FIGURE 38(a): CYLINDRICAL COORDINATE SYSTEM

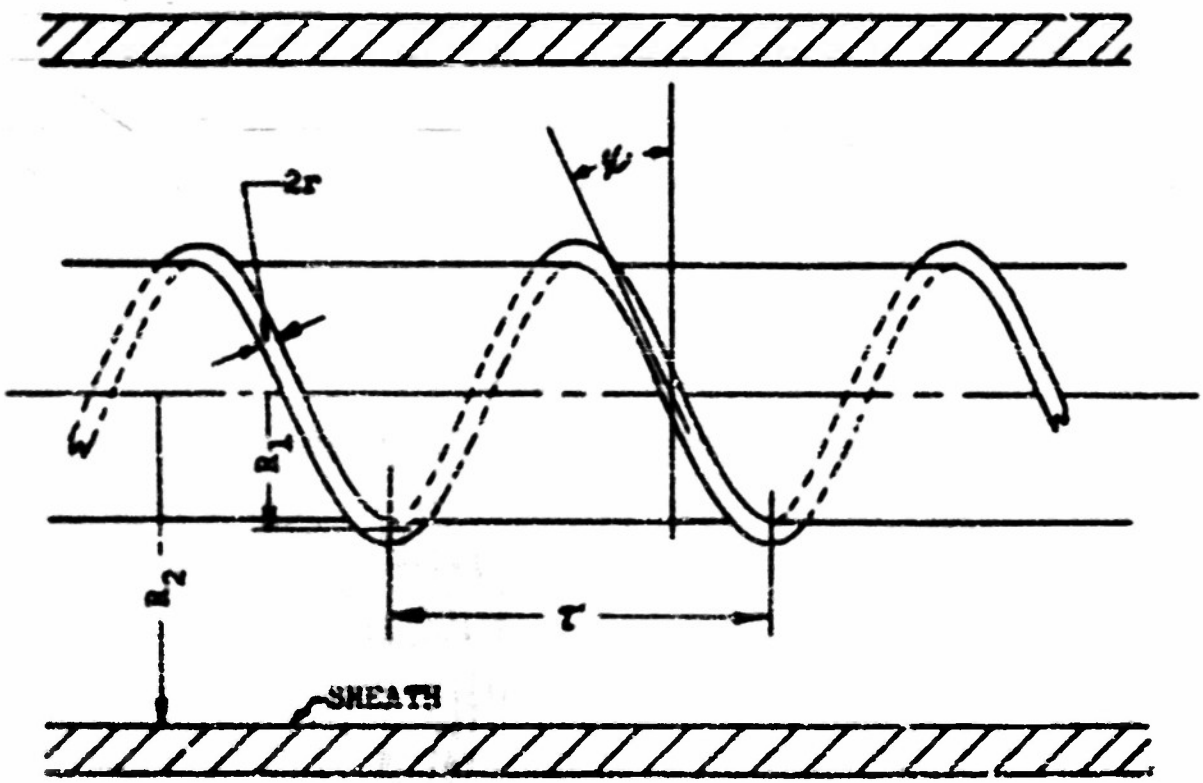

FIGURE 38(b): WIRE HELIX WOUND ON A DIELECTRIC ROD

these choices, these regions will henceforth be designated as regions 1 and 2 respectively.

8-2 Boundary Conditions

In order to determine the capacitance per unit length of a helical wire inside a sheath, it is necessary to first solve Laplace's equation in the coordinate system used, fit the solution to the boundary conditions, and then determine the charge per unit length on the helical conductor. Knowing this charge and potential difference between the helical conductor and the sheath, one can determine the capacitance per unit length.

In this case, the boundary conditions are, that the sheath is at zero potential while the helical conductor is at some potential V_o. However, difficulties are immediately encountered when one tries to represent in cylindrical coordinates the surface of a circular wire wound into the shape of a helix. It is at this surface that the potential is to be kept constant. It is not of much help to use a coordinate system in which the surface of the helical conductor is defined by fixing one coordinate, since as shown in reference (10) such systems are either nonorthogonal or present difficulties when one attempts to solve Laplace's equation.

This dilemma is by-passed by solving for the potential distribution in the case where a wire of infinitesimal cross section has a charge of Q_l coulombs per meter of length. This is a case which can be solved exactly. At this point rather than attempting to employ the actual surface of the wire as an equipotential surface, one of the equipotential surfaces which surrounds the line charge is used to represent the surface of the wire. Whereas the actual wire will intersect the XZ-plane to form an ellipse, the intersection of one of the equipotential surfaces with

the xz plane is not an ellipse. The equipotential surface chosen to represent the wire is made to agree with the wire at the radius $\rho = R_1$ as shown in Figure 39. It can be shown that the agreement between the true and approximate wires approaches perfection as the radius of the wire approaches zero. Hence the solution will be valid only for small wire radii.

B-3. The Solution of Laplace's Equation

In cylindrical coordinates, Laplace's equation is:

$$\frac{1}{\rho}\frac{\partial}{\partial\rho}\left(\rho\frac{\partial V}{\partial\rho}\right)+\frac{1}{\rho^2}\frac{\partial^2 V}{\partial\phi^2}+\frac{\partial^2 V}{\partial z^2}=0 \qquad (1)$$

where V, the potential, is some function of ρ, ϕ and z.
Using the method of separation of variables, we get for V

$$V=\begin{Bmatrix} I_m(b\rho) \\ K_m(b\rho)\end{Bmatrix}\begin{Bmatrix}\cos m\phi \\ \sin m\phi\end{Bmatrix}\begin{Bmatrix}\cos bz \\ \sin bz\end{Bmatrix},\ m\neq 0,\ b\neq 0 \qquad (2)$$

$$V = A + B\,\mathrm{Log}_e\rho\ ,\quad m=b=0 \qquad (3)$$

where for the sake of simplicity, the arbitrary constants have been omitted in (2). The constants m and b are separation constants of which b is to be evaluated later from certain properties of the helix. Since the potential is a single valued function of the angle ϕ the constant m must be confined to real integral values. There is a third possible solution, namely b equal to zero and m not zero. This case is not of interest in this problem, as will become apparent through subsequent developments. The functions I_m and K_m are modified Bessel functions of order m

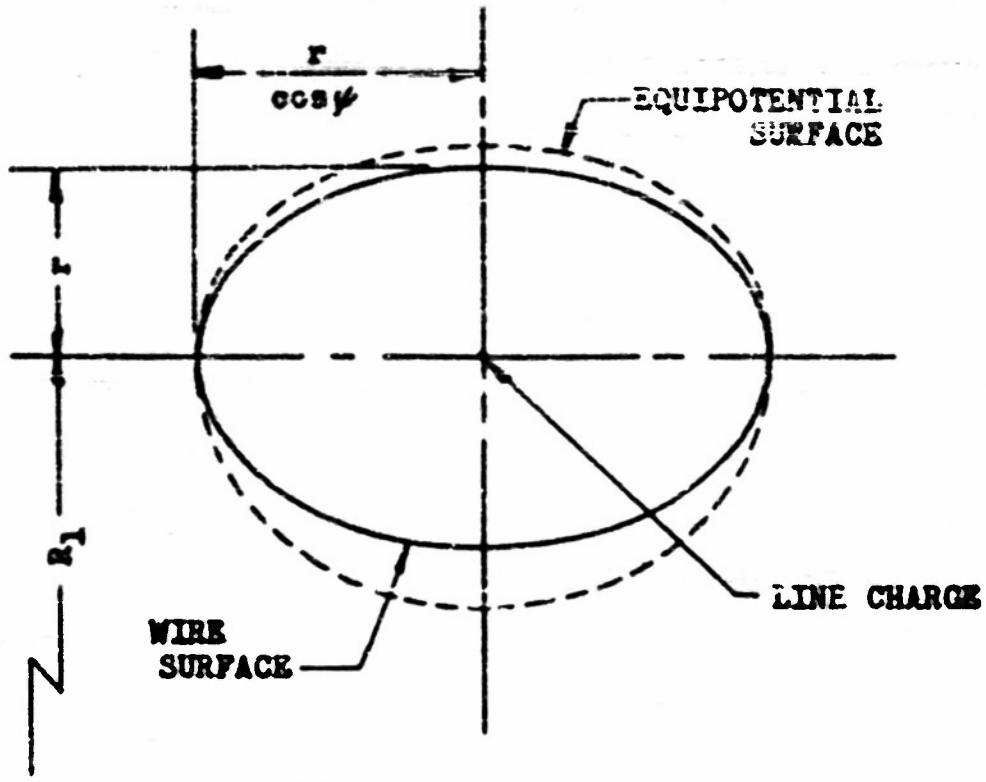

FIGURE 39: A COMPARISON OF WIRE AND EQUIPOTENTIAL SURFACES

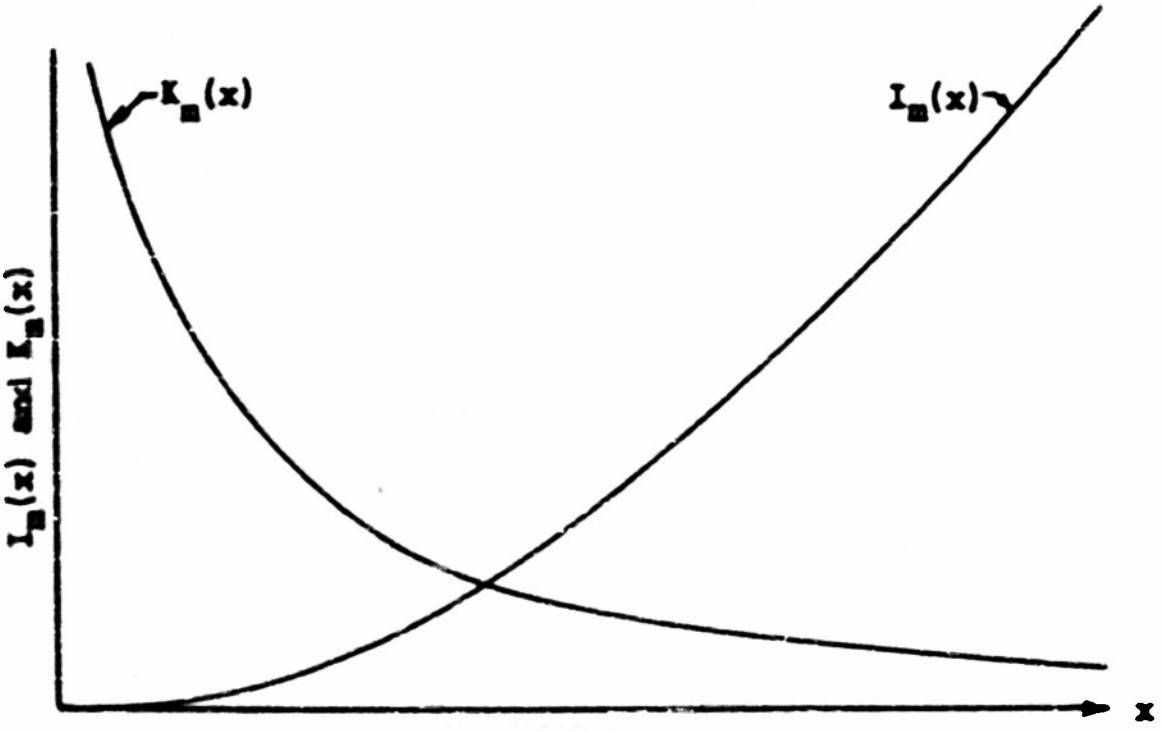

FIGURE 40: THE MODIFIED BESSEL FUNCTIONS OF THE FIRST AND SECOND KINDS

and of the first and second kinds respectively. Although some of their properties are mentioned in Appendix A, note should be taken of the fact that the I_m function has a singular point at infinity while the K_m function has a singular point at zero. The former increases monotonically to infinity as the argument approaches infinity, whereas the latter increases monotonically to infinity as the argument decreases from infinity to zero. Representative behavior is sketched in Figure 40.

The first case ($m = b = 0$) is one which corresponds to the case of the potential difference between two coaxial conducting cylinders. Since this case has been treated by practically every elementary textbook on electrostatic fields, it will not be treated in detail here. Taking the sheath cylinder as being at zero potential and the potential of the cylinder at R_1 as being at some potential V_0, the potentials in regions 1 and 2 are,

$$V_{10} = V_0 \tag{4}$$

$$V_{20} = V_0 \frac{\log_e\left(\frac{\rho}{R_2}\right)}{\log_e\left(\frac{R_1}{R_2}\right)} \tag{5}$$

where V_{10} is the potential in region 1 when the potential is uniform over the cylinder at radius R_1, and V_{20} is the potential in region 2 as a result of a uniform potential at R_1. The charge density at the surface $\rho = R_1$ is of interest and is given by,

$$Q_0 = \epsilon_1 \left[\frac{\partial V_{10}}{\partial \rho}\right]_{\rho=R_1} - \epsilon_2 \left[\frac{\partial V_{20}}{\partial \rho}\right]_{\rho=R_2} \tag{6}$$

where Q_0 is the surface charge density at R_1 as a result of a uniform potential difference between the sheath and the cylinder at R_1. Upon substituting (4) and (5) into (6) there results

$$Q_0 = \frac{\epsilon_2 V_0}{R_1 \text{Log}_e\left(\frac{R_2}{R_1}\right)} \tag{7}$$

This can be solved for V_0 and upon substituting into (4) and (5) the expressions for the potential are obtained for the case of a uniform charge distribution on the inner cylinder.

$$V_{10} = \frac{R_1 Q_0}{\epsilon_2} \text{Log}_e \frac{R_2}{R_1} \tag{8}$$

$$V_{20} = \frac{R_1 Q_0}{\epsilon_2} \text{Log}_e \frac{R_2}{\rho} \tag{9}$$

Now in the more general case where $m \neq 0$ and $b \neq 0$ the potential can be written

$$V_{1m} = \left[A_{1m} I_m(b\rho)\right] \cos(bz - m\phi) \tag{10}$$

$$V_{2m} = \left[A_{2m} I_m(b\rho) + B_{2m} K_m(b\rho)\right] \cos(bz - m\phi) \tag{11}$$

where V_{1m} and V_{2m} are the potentials in regions 1 and 2 respectively each being of space harmonic order m.

In region 1 the origin of ρ is included, hence the function $K_m(b\rho)$ must be omitted from the form of the potential function in this region. In region 2, both $I_m(b\rho)$ and the $K_m(b\rho)$ functions may be present. The constants A_{1m}, A_{2m} and B_{2m} will be determined by the boundary conditions. The reason for combining the z and ϕ variations into a single function is as follows: If an observer were to make observations of the potential at some fixed radius and at the same time confine himself to the helicoidal surface defined by $(z - \frac{\phi}{2\pi}\tau)$ equals a constant, he would detect no change in potential. In other words, on this path he could not detect any change in his orientation with respect to the helix. By fixing the separation constant b at

$$b = \frac{2\pi m}{\tau} \tag{12}$$

this property of the helix will be embodied in (10) and (11). The choice of a cosine variation merely orients the helix so that it passes through the xy plane at the angle $\phi = 0$. No generality is lost by so doing.

At this point two boundary conditions will be introduced, namely, that the potential must be continuous through any boundary and that the potential of the sheath is zero. Expressed analytically, these become

$$\left[V_{2m}\right]_{\rho=R_1} = \left[V_{1m}\right]_{\rho=R_1} \tag{13}$$

$$\left[V_{2m}\right]_{\rho=R_2} = 0 \tag{14}$$

These conditions when applied to (10) and (11) yield

$$A_{2m} I_m(bR_1) + B_{2m} K_m(bR_1) = A_{1m} I_m(bR_1) \tag{15}$$

$$A_{2m} I_m(bR_2) + B_{2m} K_m(bR_2) = 0 \tag{16}$$

from which,

$$A_{2m} = -\frac{I_m(bR_1)\, K_m(bR_2)}{I_m(bR_2) K_m(bR_1)}\, A^*_{1m} \tag{17}$$

$$B_{2m} = \frac{I_m(bR_1)}{K_m(bR_1)} A^*_{1m} \tag{18}$$

$$A_{1m} = \left[1 - \frac{I_m(bR_1)\, K_m(bR_2)}{I_m(bR_2) K_m(bR_1)}\right] A^*_{1m} \tag{19}$$

where the constant A^*_{1m} has been introduced as a matter of convenience. Thus the potential functions in regions 1 and 2 become

$$V_{1m} = A^*_{1m} \left[1 - \frac{I_m(bR_1)\, K_m(bR_2)}{I_m(bR_2) K_m(bR_1)}\right] I_m(b\rho) \cos(bz - m\phi) \tag{20}$$

$$V_{2m} = A^*_{1m} \left[K_m(b\rho) - \frac{K_m(bR_2)}{I_m(bR_2)} I_m(b\rho)\right] \frac{I_m(bR_1)}{K_m(bR_1)} \cos(bz - m\phi) \tag{21}$$

Equation (6) can now be used to determine the surface charge density with, of course, the subscript 0 replaced everywhere by m. By

carrying out the operations indicated in (6) using (20) and (21) there results for Q_m,

$$Q_m = \frac{\epsilon_2 A^*_{im}}{R K_m(bR)} \left\{ \frac{\epsilon_1}{\epsilon_2} + \left(\frac{\epsilon_1}{\epsilon_2} - 1\right) \left[1 - \frac{I'_m(bR) K_m(bR_2)}{I_m(bR_2) K'_m(bR_1)} \right] (bR_1) I_m(bR_1) K'_m(bR_1) \right\} \cos(bz - m\phi) \quad (22)$$

where the primes on the I'_m and K'_m functions denote differentiation with respect to the argument ($b\rho$). This can be written in the form,

$$Q_m = Q_{mm} \cos(bz - m\phi) \quad (23)$$

where,

$$Q_{mm} = \frac{\epsilon_2 A^*_{im}}{R_1 K_m(bR_1)} \left\{ \frac{\epsilon_1}{\epsilon_2} + \left(\frac{\epsilon_1}{\epsilon_2} - 1\right) \left[1 - \frac{I'_m(bR_1) K_m(bR_2)}{I_m(bR_2) K'_m(bR_1)} \right] (bR_1) I_m(bR_1) K'_m(bR_1) \right\} \quad (24)$$

The quantity Q_{mm} is the maximum value of the surface charge density having harmonic variation of order m in both the z and ϕ directions.

From (24) the quantity A^*_{im} can be determined in terms of Q_{mm} and by substituting this value of A^*_{im} into (20) and (21) the potential in terms of the surface charge density at R_1 is determined. This procedure yields,

$$V_{1m} = \frac{R_1 Q_{mn} K_m(bR_1)\left[1 - \frac{I_m(bR_2)K_m(bR_1)}{I_m(bR_2)K_m(bR_1)}\right] I_m(b\rho)\cos(bz - m\phi)}{\epsilon_2\left\{\frac{\epsilon_1}{\epsilon_2} + \left(\frac{\epsilon_1}{\epsilon_2} - 1\right)\left[1 - \frac{I_m'(bR_1)K_m(bR_2)}{I_m(bR_2)K_m'(bR_1)}\right] I_m(bR_1)K_m'(bR_1)\right.} \tag{25}$$

$$V_{2m} = \frac{R_1 Q_{mn} I_m(bR_1)\left[K_m(b\rho) - \frac{K_m(bR_2)}{I_m(bR_2)} I_m(b\rho)\right]\cos(bz - m\phi)}{\epsilon_2\left\{\frac{\epsilon_1}{\epsilon_2} + \left(\frac{\epsilon_1}{\epsilon_2} - 1\right)\left[1 - \frac{I_m'(bR_2)K_m(bR_2)}{I_m(bR_2)K_m'(bR_2)}\right] I_m(bR_1)K_m'(bR_1)\right.} \tag{26}$$

As will now be shown, the charge on an infinitesimally thin helical wire can be represented as a Fourier series of terms of the form of equation (23). This fact will permit an evaluation of the C_{mn} in terms of the linear charge density on a "thin wire" helix and lead to a subsequent evaluation of the potential due to such a line charge.

Figure 41 shows a helix which consists of an infinitesimally thin tape of width 2a, measured perpendicular to the edge of the tape. If this helix were slit by the yz plane at integral values of the pitch τ, and then developed in the plane $y = R_1$, the developed helix would appear as shown in Figure 42. Let this helical tape be charged uniformly with a linear charge density in the helix direction of Q_1 Coulombs per meter. Then, since the tape is 2a meters wide, the surface charge density at the tape is $Q_1/2a$ Coulombs per square meter. This is shown in Figure 43. It will be noted that at any given angle ϕ, the surface charge density is a periodic function of the axial distance z and at any given z the surface charge density is a periodic function of ϕ, the periods being τ and 2π respectively. At

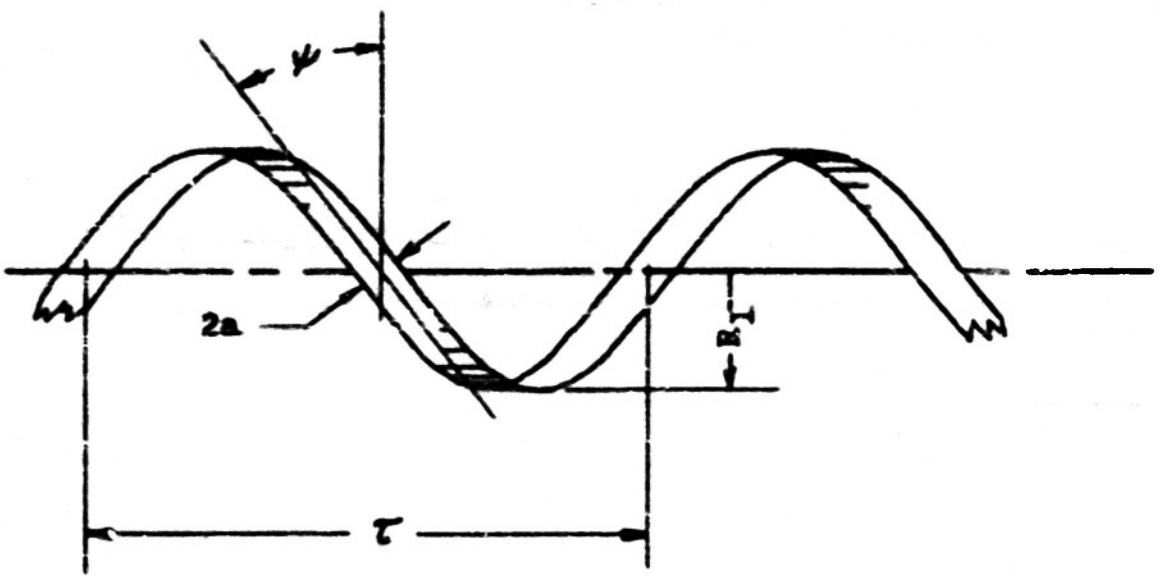

FIGURE 41: NARROW TAPE HELIX

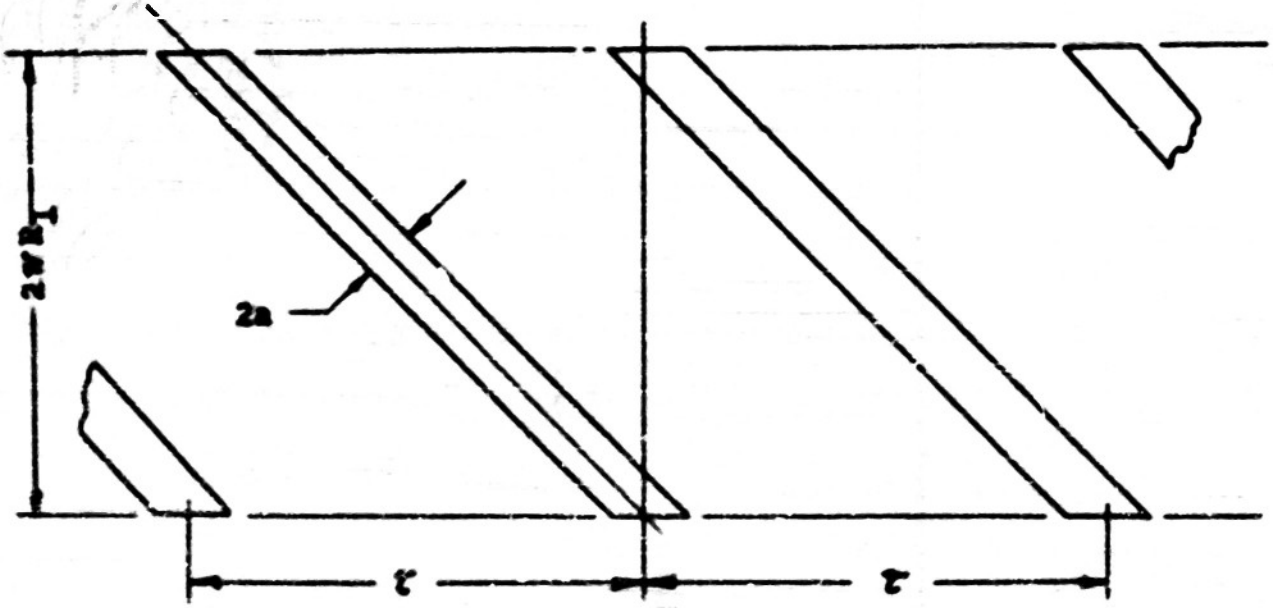

FIGURE 42: DEVELOPED NARROW TAPE HELIX

FIGURE 43:

SURFACE CHARGE DENSITY AT, $\rho = R_1$ and $\phi = 0$, FOR A TAPE HELIX

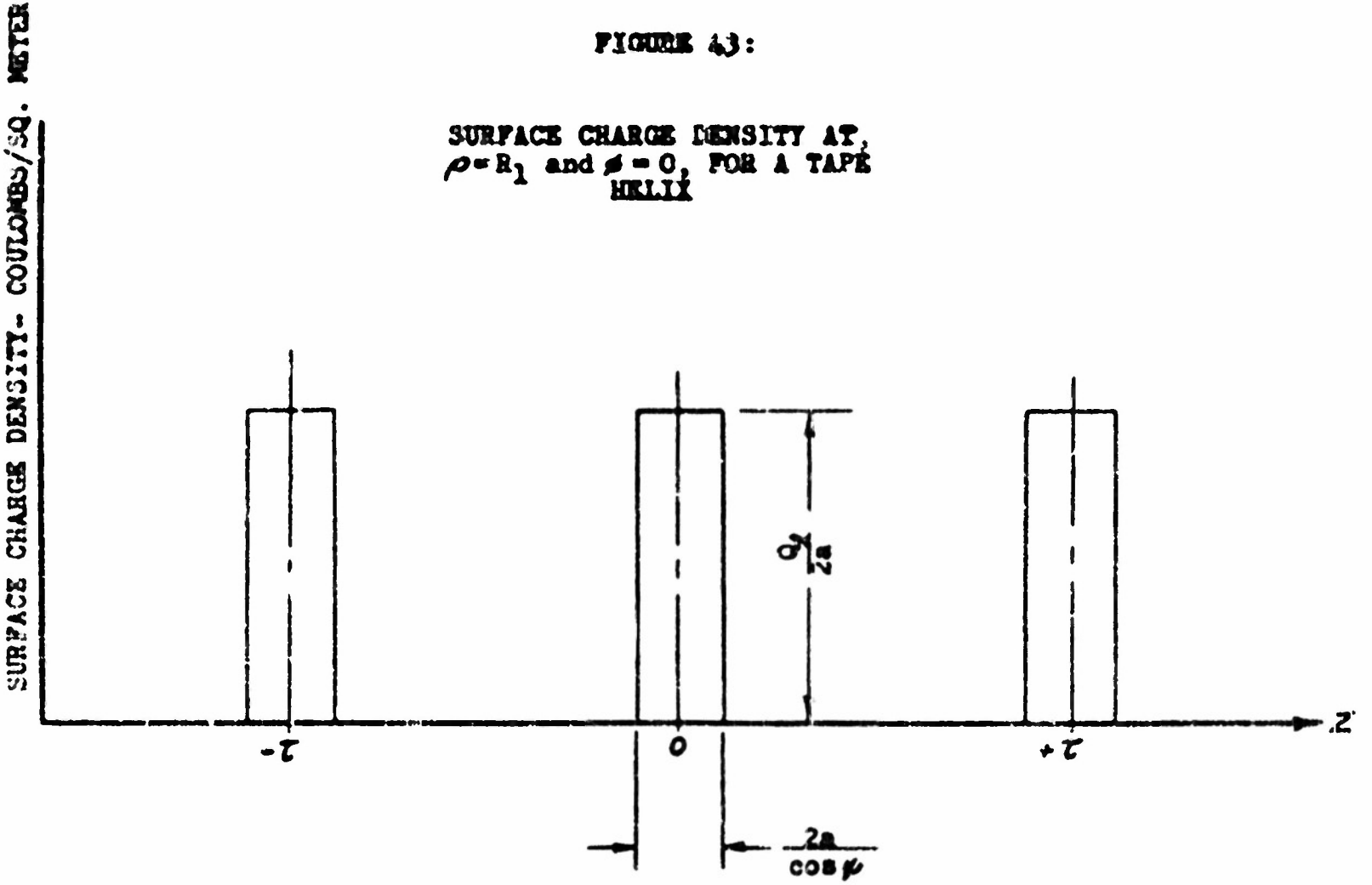

ϕ equal to zero, the Fourier series for the charge density function shown in Figure 43 is,

$$Q = \frac{Q_1}{\tau \cos\psi} + \sum_{m=1}^{\infty} A_m \cos bz \tag{27}$$

where,

$$A_m = \frac{2 Q_1}{\tau \cos\psi}\left[\frac{\sin\left(\frac{ba}{\cos\psi}\right)}{\left(\frac{ba}{\cos\psi}\right)}\right] \tag{28}$$

The tape helix becomes a "thin wire" helix if the width a is allowed to approach zero. It will still have a linear charge density of Q_1 Coulombs per meter. Allowing a to approach zero, the surface charge density at R_1 becomes in general

$$Q = \frac{Q_1}{\tau \cos\psi}\left[1 + 2\sum_{m=1}^{\infty} \cos(bz - m\phi)\right] \tag{29}$$

The ϕ variation has been introduced in this manner since the surface charge density function would be shifted in the positive z direction by a distance $\frac{\phi}{2\pi}\tau$ for any general angle ϕ. Hence in (27), which is the series for the charge density at $\phi = 0$, z may be replaced by $(z - \frac{\phi}{2\pi}\tau)$. Thus it is seen that the charge on a "thin wire" helix can be represented by a term similar to that of equation (7) plus an infinite sum of terms similar to the term given by equation (23).

Therefore we can write,

$$Q_0 = \frac{Q_s}{\tau \cos\psi} \tag{30}$$

$$Q_{mn} = \frac{2 Q_s}{\tau \cos\psi} \tag{31}$$

If these are substituted into (8) and (9), and into (25) and (26) respectively, and summed for all m, the potential about a charged helical line in a coaxial sheath is found, the result being,

$$V_1' = \frac{R_1 Q_s}{\epsilon_2 \tau \cos\psi} \left\{ \log_e \frac{R_2}{R_1} + 2 \sum_{m=1}^{\infty} \frac{\left[1 - \frac{I_m(bR_1) K_m(bR_2)}{I_m(bR_2) K_m(bR_1)}\right] K_m(b\rho) I_m(b\rho) \cos(bz - m\phi)}{\frac{\epsilon_1}{\epsilon_2} + \left(\frac{\epsilon_1}{\epsilon_2} - 1\right)\left[1 - \frac{I_m'(bR_1) K_m(bR_2)}{I_m(bR_1) K_m'(bR_1)}\right](bR_1) I_m(bR_1) K_m'(bR_1)} \right\} \tag{32}$$

$$V_2 = \frac{R_1 Q_s}{\epsilon_2 \tau \cos\psi} \left\{ \log_e \frac{R_2}{\rho} + 2 \sum_{m=1}^{\infty} \frac{\left[K_m(b\rho) - \frac{K_m(bR_2)}{I_m(bR_2)} I_m(b\rho)\right] I_m(bR_1) \cos(bz - m\phi)}{\frac{\epsilon_1}{\epsilon_2} + \left(\frac{\epsilon_1}{\epsilon_2} - 1\right)\left[1 - \frac{I_m'(bR_1) K_m(bR_2)}{I_m(bR_2) K_m'(bR_2)}\right](bR_1) I_m(bR_1) K_m'(bR_1)} \right\} \tag{33}$$

These equations were used to prepare Figure 44 which shows the equipotential lines in the yz plane for a helix having the dimensions shown in Table 6.

Table 6

Dimensions of Helix Used to Calculate Equipotential Lines

$$\frac{R_2}{R_1} = 2.0$$

$$\psi = 45^\circ$$

$$\epsilon_1 = \epsilon_2$$

The numbers shown on each curve give the relative potential. These curves were prepared by calculating the potential along the lines $Z = 0$ and $\rho = R_1$, both at $\phi = 0$. These calculations established four points on each curve, the remainder of the curve being sketched in. It should be noted that these equipotential lines are quite close to the "thin wire", the potential = 5 curve being at most only 6.2% of R_1 away from the wire. An ellipse having a major to minor axis ratio of $\sqrt{2}$ is also shown, its major axis being the same as that of the potential = 5 curve.

In spite of the fact that the helical wire is curved and is in the vicinity of other charge carrying conductors, the potential distribution close to the wire will be very close to that for a straight conductor carrying charge. As the distance between an observer and the helical line becomes very small, the radius of curvature of the line becomes large compared with this distance and the wire appears to be essentially straight. The equipotential surfaces surrounding a straight wire are right circular cylinders. These cylinders would form elliptical equipotential lines, if they intersected a plane at some angle ψ from the perpendicular. In particular, if the angle $\psi = 45^\circ$ these ellipses would have a major to minor axis ratio of $\sqrt{2}$. It should be expected, therefore, that (32) and

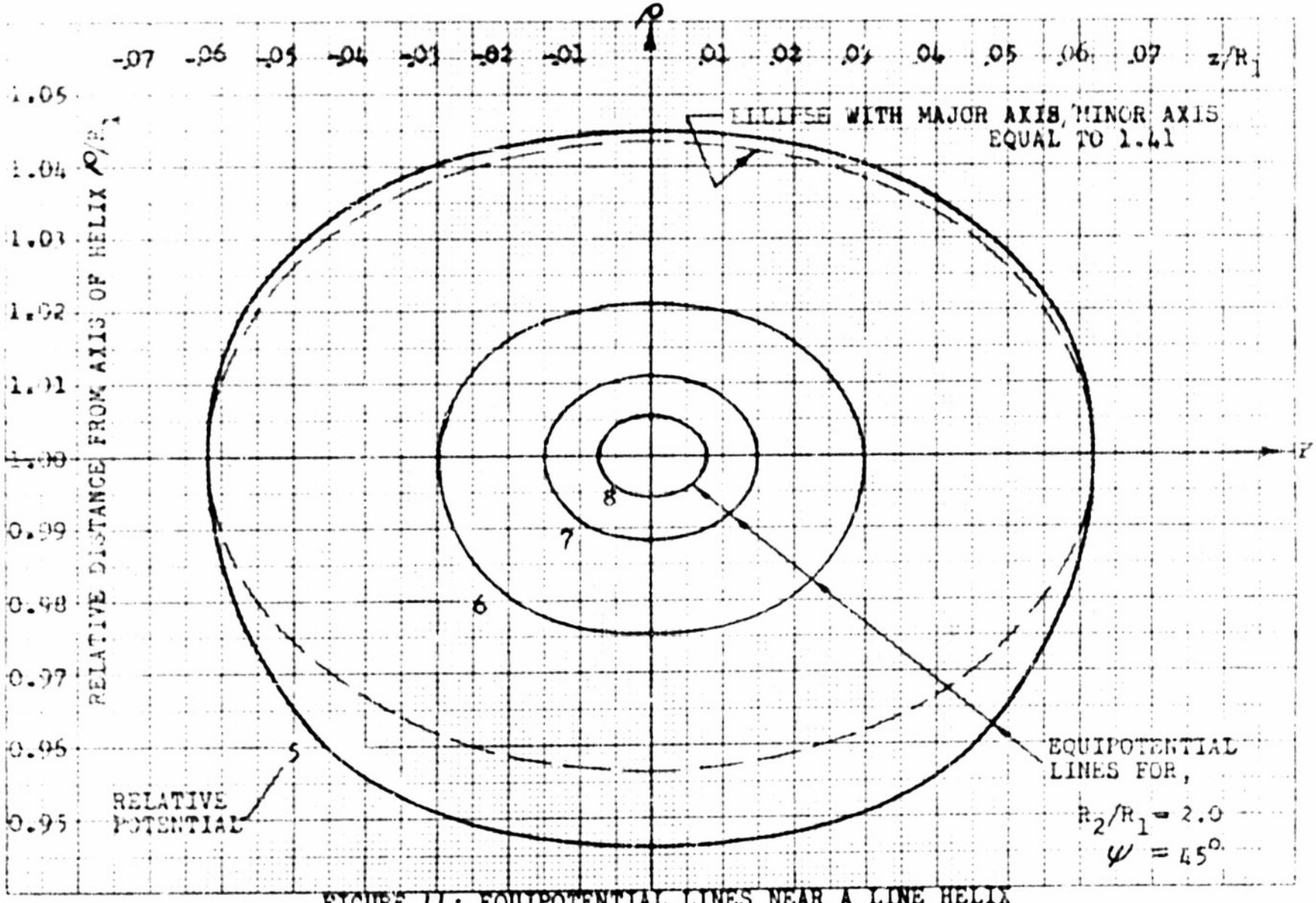

FIGURE 44: EQUIPOTENTIAL LINES NEAR A LINE HELIX

(33) would yield equipotential lines which are very close to ellipses as we approach the wire. This fact is borne out in Figure 44.

The presence of dielectric material in region 1 does not alter the above statements since the equipotential surfaces surrounding a thin line of charge, the line being placed at the plane boundary between two different dielectric media, are still circular cylinders coaxial with the line.

The problem now is to choose that one of the equipotential surfaces given by (32) and (33) which will most nearly approximate a wire of given radius. If only very small wire radii are considered, it seems reasonable to choose as the equipotential surface to represent a given wire, that surface which intersects the cylinder $\rho = R_1$ along the same line as does the actual wire. The actual wire intersects the cylinder $\rho = R_1$ along the lines

$$\left\{ \begin{array}{c} \left(z - \frac{\phi}{2\pi}\tau\right) = \pm \frac{r}{\cos\psi} \\ \\ \rho = R_1 \end{array} \right\} \tag{34}$$

where r is the wire radius. If this is substituted into either (32) or (33) at $\rho = R_1$, the potential of this surface is found to be

$$V_1 = \frac{R_1 Q_L}{\epsilon_2 \tau \cos\psi} \left\{ \ln \frac{R_2}{R_1} + 2 \sum_{m=1}^{\infty} \frac{\left[-\frac{I_m(bR_1)K_m(bR_2)}{I_m(bR_2)K_m(bR_1)} \right] I_m(bR_1)K_m(bR_1) \cos\left(\frac{br}{\cos\psi}\right)}{\frac{\epsilon_1}{\epsilon_2} + \left(\frac{\epsilon_1}{\epsilon_2} - 1\right)\left[-\frac{I'_m(bR_1)K_m(bR_2)}{I_m(bR_2)K'_m(bR_1)} \right] bR_1 I_m(bR_1)K'_m(bR_1)} \right\} \tag{35}$$

The potential (35) divided by Q_1 will give the reciprocal of the distributed capacitance in farads per meter. Thus,

$$\frac{V_1}{Q_1} = \frac{1}{C}$$

$$= \frac{R_1}{\epsilon_2 \tau \cos\psi}\left\{\log_e \frac{R_2}{R_1} + 2\sum_{m=1}^{\infty} \frac{\left[1 - \frac{I_m(bR_1)K_m(bR_2)}{I_m(bR_2)K_m(bR_1)}\right] I_m(bR_1)K_m(bR_1)\cos\left(\frac{br}{\cos\psi}\right)}{\frac{\epsilon_1}{\epsilon_2} + \left(\frac{\epsilon_1}{\epsilon_2} - 1\right)\left[1 - \frac{I_m'(bR_1)K_m(bR_2)}{I_m(bR_2)K_m'(bR_1)}\right] bR_1 I_m(bR_1)K_m'(bR_1)}\right\} \tag{36}$$

A special case of this would be where $\epsilon_1 = \epsilon_2$, resulting in the denominator under the summation sign becoming unity. Hence for a helix immersed in a medium of uniform permittivity.

$$\frac{1}{C} = \frac{R_1}{\epsilon_2 \tau \cos\psi}\left\{\log_e \frac{R_2}{R_1} + 2\sum_{m=1}^{\infty}\left[1 - \frac{I_m(bR_1)K_m(bR_2)}{I_m(bR_2)K_m(bR_1)}\right] I_m(bR_1)K_m(bR_1)\cos\left(\frac{br}{\cos\psi}\right)\right\} \tag{37}$$

There are two points about the above expression which must be mentioned. The first of these is that if the the pitch τ is such that it is comparable to the wire diameter, the equipotentials do not closely approximate ellipses; they appear more football shaped, as sketched in Figure 45. If we still confine ourselves to small wire radii, as compared to R_1, then the helix in which the wires are close together is one which might be designated as a close wound helix. For such a helix, the term under the summation sign in (36) becomes negligible with respect to the first term in the brackets. Since this first term is independent of the shape of the wire, it may be concluded that for close wound small wire helices, the distributed capacitance is practically independent of the wire shape. As an

example of this fact, three capacitances are presented below in Table 7. The first of these is for a tape helix in which the tape width is 5% of the radius R_1 and the pitch is such that the turns butt against each other. The second helix is a wire helix with wire diameter 5% of R_1 and wound with the same pitch as the tape helix. Its capacitance is calculated from (37). The third helix is wound with square wire having a cross section of $0.05R_1 \times 0.05R_1$ and wound with the same pitch as the first two. All three of these helices are butt helices in that their turns touch each other. In all three cases, the sheath is taken at a distance $2R_1$ from the axis of the helix. These are illustrated in Figure 46. It is obvious that the capacitance to the sheath of the round wire helix should be somewhere between that for the tape helix and that for the square wire helix. Equation (37) used for the round wire helix does give such a capacitance. Whereas it might not be the exact capacitance, it certainly cannot be in error by more than 2.6%, and is probably in error by much less than 2.6%.

Table 7

Capacitances of Three Helices Having Different Wire Cross Sections

Tape Helix	100%	Capacitance per unit length
Round Wire Helix	101%	" " " "
Square Wire Helix	103.6%	" " " "

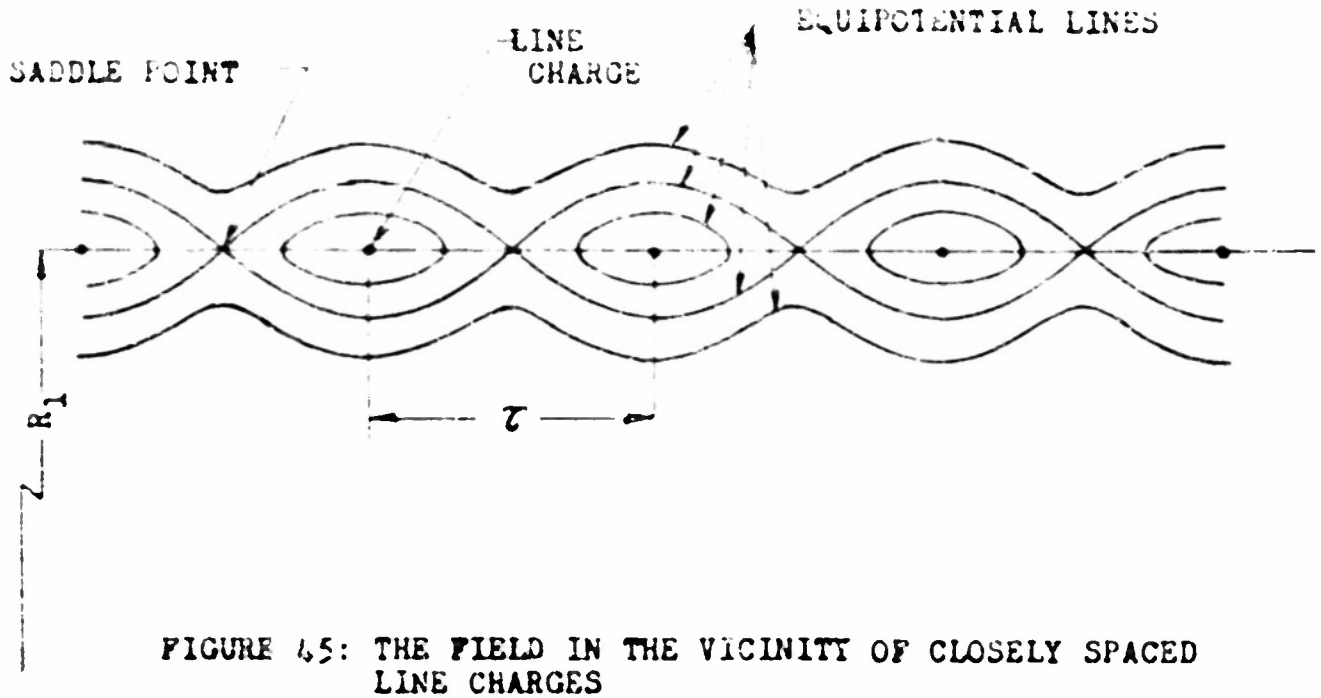

FIGURE 45: THE FIELD IN THE VICINITY OF CLOSELY SPACED LINE CHARGES

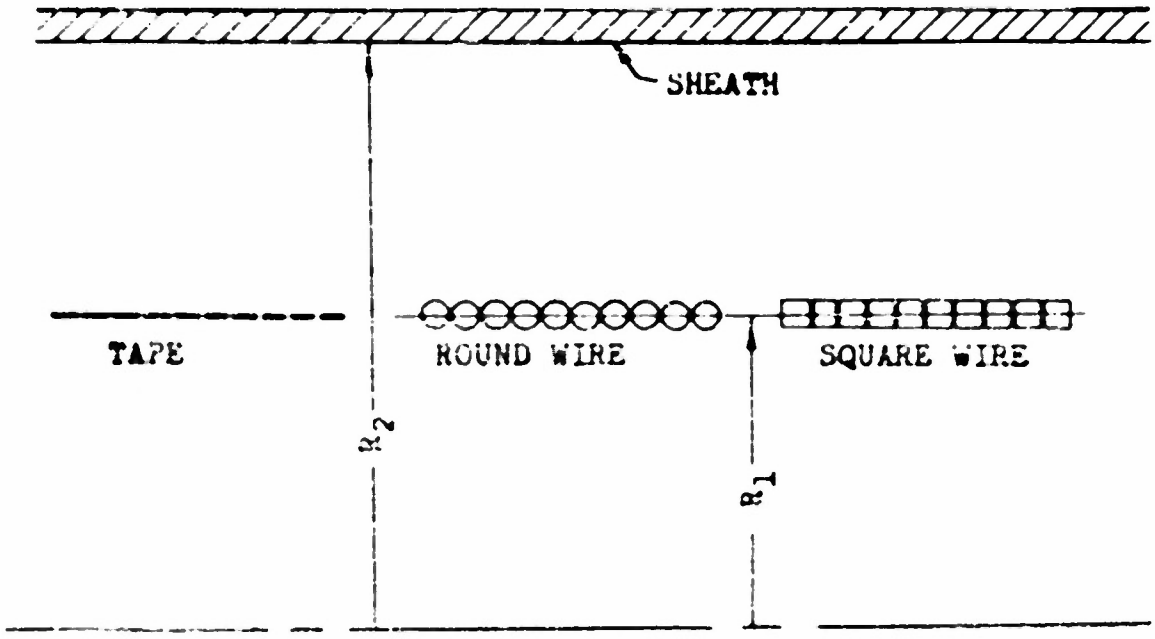

FIGURE 46: BUTT WOUND HELICES WITH VARIOUS WIRE CROSS SECTIONS

The second point is, that it is implicit in the derivation that the round wire of which the helix is wound is semi-imbedded in the dielectric material in region 1. This is so because the assumption was made that the dielectric material of region 1 extends out to a radius R_1, which radius is also the radius out to the center of the round wire. Such a helix could be built by cutting, with an appropriately shaped tool, a helical thread into the surface of the dielectric rod. Into this thread the round wire could be laid, the depth of the cut being such as to leave half the wire exposed and half of it buried in the dielectric material. However, in a practical case, it would be simpler to wind the helix of round wire upon the surface of a smooth dielectric rod. If R_1 is taken as the distance from the axis of the helix to the center of the round wire, then the dielectric material will not entirely fill region 1. It will have a diameter less than the requisite diameter by an amount equal to the diameter of the wire. The error introduced by this type of construction would not be serious since this analysis is limited to wire diameters which are much smaller than $2R_1$. Furthermore, the effect of the dielectric rod is small since in any helix of reasonable pitch ($\tau \leq 2R_1$), region 1 is practically at a uniform potential. Being at almost constant potential means that very little electrostatic energy is stored in region 1 as compared with region 2. For this reason, the presence of dielectric material in region 1 has very little effect on close wound helices. A study of Figures 6 to 13 will bear this out.

B-4 Approximate Expression for Close Wound Helices

The infinite series in (37) is discussed briefly in Appendix A. In Appendix A, it is shown that the term in the square bracket immediately after the summation sign in (37) is different from unity by a negligibly small value for values of (R_1/τ) which are sufficiently large. Also shown in Appendix A is the fact that $I_m(bR_1)\, K_m(bR_1)$ is given to satisfactory accuracy by,

$$I_m(bR_1)K_m(bR_1) \cong \frac{1}{2\sqrt{m^2+(bR_1)^2}} \tag{38}$$

where $\cong$ denotes "is approximately equal to". By making use of (12), this can be written

$$I_m(bR_1)K_m(bR_1) \cong \frac{1}{2m\sqrt{1+\left(\frac{2\pi R_1}{\tau}\right)^2}} \tag{39}$$

or,

$$I_m(bR_1)K_m(bR_1) \cong \frac{\sin\psi}{2m} \tag{40}$$

Therefore, for τ sufficiently small, (37) becomes

$$\frac{1}{C} = \frac{R_1}{\epsilon_2 \tau \cos\psi}\left\{\log_e\frac{R_2}{R_1} + \sin\psi\sum_{m=1}^{\infty}\frac{\cos\left(\frac{2\pi m r}{\tau\cos\psi}\right)}{m}\right\} \tag{41}$$

The infinite sum in this expression can be expressed in closed form as,

$$\sum_{m=1}^{\infty} \frac{\cos mx}{m} = -\log_e\left[2\sin\left(\frac{x}{2}\right)\right] \tag{42}$$

Substituting this into (41),

$$\frac{1}{C} = \frac{R_1}{\epsilon_2 \tau \cos\psi}\left\{\log_e\frac{R_2}{R_1} - \sin\psi\cdot\log_e\left[2\sin\left(\frac{\pi r}{\tau\cos\psi}\right)\right]\right\} \tag{43}$$

The capacitance C in (43) is the capacitance per meter in the helix direction. If we let C_z denote the capacitance per meter in the axial direction, (43) becomes,

$$\frac{1}{C_z} = \frac{1}{2\pi\epsilon_2}\left\{\log_e\frac{R_2}{R_1} - \sin\psi\cdot\log_e\left[2\sin\left(\frac{\pi r}{\tau\cos\psi}\right)\right]\right\} \tag{44}$$

If now, the helix is wound so that $\tau = 2r$ and r is allowed to approach zero, the helix degenerates into a cylindrical sheet at a radius of R_1 from the axis. The angle ψ becomes zero and (44) becomes,

$$\frac{1}{C_z} = \frac{1}{2\pi\epsilon_2}\log_e\frac{R_2}{R_1} \tag{45}$$

which is recognizable as the capacitance per meter between two coaxial cylinders of infinite length.

The more general case in which there is dielectric material inside

the helix radius can be treated in a similar manner. In (36) the denominator approaches a constant value, independent of the index of summation, as (R_1/τ) becomes sufficiently large. Thus,

$$\underset{(\frac{R_1}{\tau})\to\infty}{\text{Limit}} \left\{ \frac{\epsilon_1}{\epsilon_2} + \left(\frac{\epsilon_1}{\epsilon_2} - 1\right)\left[1 - \frac{I_m'(bR_1)K_m(bR_1)}{I_m(bR_2)K_m'(bR_2)}\right](bR_1)I_m(bR_1)K_m'(bR_1) \right\}$$

$$= \frac{\epsilon_1 + \epsilon_2}{2\epsilon_2} \tag{46}$$

Therefore, for very large (R_1/τ), (36) becomes

$$\frac{1}{C_2} = \frac{1}{2\pi\epsilon_2}\left\{ \text{Log}_e \frac{R_2}{R_1} - \frac{2\epsilon_2}{\epsilon_1 + \epsilon_2} \sin\psi \cdot \text{Log}_e\left[2\sin\left(\frac{\pi r}{\tau\cos\psi}\right)\right] \right\} \tag{47}$$

B-5 Approximate Expression for Coarse Helices

This section will deal with the capacitance per unit length for the case of very large pitch. This type of helix, which will be referred to as a coarse helix, will degenerate into a parallel wire transmission line in which the center conductor is displaced from the axis by a distance R_1. This line will have dielectric material inside the radius R_1.

The limit of (36) as the pitch τ is allowed to approach infinity will be found by examining each of the parts of (36) separately.

$$\lim_{\tau \to \infty} \left[1 - \frac{I_m(bR_1) K_m(bR_2)}{I_m(bR_2) K_m(bR_1)} \right] = \left[1 - \left(\frac{R}{R_2} \right)^{2m} \right] \tag{48}$$

$$\lim_{\tau \to \infty} \left[I_m(bR_1) K_m(bR) \right] = \frac{1}{2m} \tag{49}$$

$$\lim_{\tau \to \infty} \left[\cos\left(\frac{br}{\cos\alpha} \right) \right] = \cos\left(\frac{mr}{R} \right) \tag{50}$$

$$\lim_{\tau \to \infty} \left[1 - \frac{I_m'(bR_1) K_m(bR_2)}{I_m(bR_2) K_m'(bR_1)} \right] = \left[1 - \left(\frac{R_1}{R_2} \right)^{2m} \right] \tag{51}$$

$$\lim_{\tau \to \infty} \left[(bR_1) I_m(bR_1) K_m'(bR_1) \right] = -\frac{1}{2} \tag{52}$$

When these are substituted into (36), the capacitance for infinite pitch becomes,

$$\frac{1}{C_2} = \frac{1}{2\pi\epsilon_2} \left\{ \log_e \frac{R_2}{R_1} + \frac{2\epsilon_2}{\epsilon_1 + \epsilon_2} \sum_{m=1}^{\infty} \frac{\left[1 - \left(\frac{R_1}{R_2} \right)^{2m} \right] \cos\left(\frac{mr}{R_1} \right)}{m \left[1 - \left(\frac{\epsilon_1 - \epsilon_2}{\epsilon_1 + \epsilon_2} \right) \left(\frac{R_1}{R_2} \right)^{2m} \right]} \right\} \tag{53}$$

and for $\epsilon_1 = \epsilon_2$ equation (53) be comes,

$$\frac{1}{C_2} = \frac{1}{2\pi\epsilon_2}\left\{\log_e \frac{R_2}{R_1} + \sum_{m=1}^{\infty}\left[1-\left(\frac{R_1}{R_2}\right)^{2m}\right]\frac{\cos\left(\frac{mr}{R_1}\right)}{m}\right\} \tag{54}$$

This can be expressed in closed form by making use of formula 418, page 85 of reference (4). Upon doing this and recognizing that (r/R_1) is very small,

$$\frac{1}{C_2} = \frac{1}{2\pi\epsilon_2}\left\{\log_e\left[\frac{R_2}{r}\left(1-\frac{R_1^2}{R_2^2}\right)\right]\right\} \tag{55}$$

Appendix C

The Distributed Inductance

As has already been noted in Chapter I, one approach to the problem of evaluating the characteristic impedance of a helical transmission line is to determine the distributed capacitance and inductance per unit length. These parameters L and C are those corresponding to infinite wave length or static excitation of the line. In practice, the impedance determined from L and C is useful so long as the wavelength is much greater than the significant dimensions of the helical transmission line. A complete solution of the problem involves a solution of the wave equation. This is attempted in Appendix D, but at this point, the inductance will be determined for infinite wavelength.

C-1 The Effect of the Sheath

In an infinitely long coaxial transmission line with a helical inner conductor which is carrying a current at some frequency f, there will be induced on the sheath, current and charge distributions of such a nature as to greatly reduce the fields outside the sheath. The extent to which the sheath succeeds in shielding the inner conductor depends upon the frequency f and the sheath conductivity σ. These determine the depth or penetration of the electric and magnetic fields into the sheath. The fields decay exponentially as a function of the distance into the material of the sheath. For this reason, a skin depth is defined as that depth at which the field is $1/\epsilon$ of the field at the surface of the sheath. If the sheath thickness is say less than four times the skin depth, there may be appreciable fields outside the sheath. The skin depth is given by,

$$\delta = \sqrt{\frac{2}{\omega \mu \sigma}} \qquad (1)$$

where δ is the skin depth, ω is the angular frequency $2\pi f$, μ is the permeability of the medium and σ is the conductivity. For copper this becomes,

$$\delta = \frac{6.62}{\sqrt{f}} \text{ cm.} \qquad (2)$$

The following table shows the behavior of skin depth in copper as a function of frequency.

Table 8

Skin Depth in Copper For Different Frequencies

Frequency cycles/sec.	Skin Depth cm.
100	0.662
10^4	0.0662
10^6	0.0066

Since the transmission lines considered in this report will be operated in the megacycle range, the assumption will be made in the derivation that the skin depth is zero. From (1), it will be noticed that

the skin depth is zero for all frequencies greater than zero if the conductivity is assumed to be infinite. At zero frequency, the skin depth for infinite conductivity is not defined. However, since the frequency can be made as close to zero as desired and still have zero skin depth, it will be assumed that at zero frequency the skin depth is still zero for infinite conductivity. Based upon this assumption the inductance will be calculated with direct current flowing in the inner conductor and with the shield currents of such a nature as to reduce the magnetic field outside the sheath to zero. In addition the current in the helical wire will be confined to the surface of the wire. Therefore, the internal inductance will be zero and the only inductance of interest will be that due to the external flux.

C-2 Definitions and Coordinate Systems

In the derivation to follow, use is made of a circular cylindrical coordinate system as shown in Figure 37. A right handed helix is shown in Figure 38 upon which are shown the significant dimensions of the helix.

Throughout this report the rationalized MKS system of units is used. The helix is considered to be immersed in a medium which is characterized by having homogeneous, istotropic, linear properties in each of three regions. One of these regions, region 1 is inside the radius R_1. Another region which is designated as region 2 is outside the radius R_1 but inside the radius R_2. A third region, region 3 is outside the radius R_2. All of these regions are considered to have permeability equal to that of free space.

C-3 Boundary Conditions

The inductance is best arrived at by determining the vector potential of the electric current. As will be shown in a later section, the inductance can be expressed directly in terms of this vector potential. The

vector potential which is designated as A must satisfy a pair of differential equations which are presented in section C-4, and in addition it must satisfy certain boundary conditions. These are, that the magnetic field outside the sheath be zero and that the surface of the round wire be a surface of constant vector potential. This latter requirement is approximate, in that it is based upon the fact that the surface of an infinitely long round wire carrying direct or alternating current is an equi-vector-potential surface. This requirement restricts the following analysis to those wires where the wire radius is small compared to the radius of curvature of the wire.

As in the case of the capacitances, the vector potential of current can be found for the case of an infinitesimally thin wire carrying a direct current, I. amperes. In the immediate vicinity of this infinitesimally thin wire the equi-vector-potential surfaces are very nearly circular cylinders surrounding the helical line. One of these surfaces is taken as the surface of the wire. As a result, the inductance is evaluated for a wire that is not quite round, but very close to round.

C-4 The Solution of the Curl Curl Equation and the Satisfying of Certain of the Boundary Conditions

In a region in which there is no current flowing, the vector potential of electric current must satisfy (3) and (4) for a static field. This is completely discussed in reference (1), Chapter IV .

$$\nabla \times \nabla \times \underline{A} = 0 \tag{3}$$

$$\nabla \cdot \underline{A} = 0 \tag{4}$$

where $\underline{A}$ is a vector such that,

$$\nabla \times \underline{A} = \underline{H} \quad \text{the magnetic field intensity} \tag{5}$$

Equations (3) and (4) when written in cylindrical coordinates are,

$$[\nabla \times \nabla \times \underline{A}]_\rho = \frac{1}{\rho}\frac{\partial^2 A_\phi}{\partial \phi \partial \rho} + \frac{1}{\rho^2}\frac{\partial A_\phi}{\partial \phi} - \frac{1}{\rho^2}\frac{\partial^2 A_\rho}{\partial \phi^2} - \frac{\partial^2 A_\rho}{\partial z^2} + \frac{\partial^2 A_z}{\partial z \partial \rho} = 0 \tag{6}$$

$$[\nabla \times \nabla \cdot \underline{A}]_\phi = \frac{1}{\rho}\frac{\partial^2 A_z}{\partial z \partial \phi} - \frac{\partial^2 A_z}{\partial z^2} - \frac{\partial^2 A_\phi}{\partial z^2} - \frac{\partial^2 A_\phi}{\partial \rho^2} - \frac{1}{\rho}\frac{\partial A_\phi}{\partial \rho} + \frac{1}{\rho^2} A_\phi + \frac{1}{\rho}\frac{\partial^2 A_\rho}{\partial \rho \partial \phi} - \frac{1}{\rho^2}\frac{\partial A_\rho}{\partial \phi} = 0 \tag{7}$$

$$[\nabla \times \nabla \cdot \underline{A}]_z = \frac{\partial^2 A_\rho}{\partial \rho \partial z} + \frac{1}{\rho}\frac{\partial A_\rho}{\partial z} - \frac{\partial^2 A_z}{\partial \rho^2} - \frac{1}{\rho}\frac{\partial A_z}{\partial \rho} - \frac{1}{\rho^2}\frac{\partial^2 A_\rho}{\partial \phi^2} + \frac{1}{\rho}\frac{\partial^2 A_\phi}{\partial \phi \partial z} = 0 \tag{8}$$

$$[\nabla \cdot \underline{A}] = \frac{\partial A_\rho}{\partial \rho} + \frac{1}{\rho} A_\rho + \frac{1}{\rho}\frac{\partial A_\phi}{\partial \phi} + \frac{\partial A_z}{\partial z} = 0 \tag{9}$$

where A_ρ , A_ϕ and A_z are the ρ , ϕ and z components of the vector potential respectively. These are each scalar functions of the coordinates ρ , ϕ , and z . Equations (10), (11) and (12) which follow are obtained by the following processes: Equation (6) is subtracted from the derivative with respect to ρ of equation (9) to yield (10). Equation (7) is subtracted from $\frac{1}{\rho}\frac{\partial}{\partial z}$ (9) to yield (11). Equation (8) is subtracted from $\frac{\partial}{\partial z}$ (9) to yield (12).

$$\frac{\partial^2 A_\rho}{\partial \rho^2} + \frac{1}{\rho}\frac{\partial A_\rho}{\partial \rho} - \frac{1}{\rho^2}A_\rho + \frac{1}{\rho^2}\frac{\partial^2 A_\rho}{\partial \phi^2} + \frac{\partial^2 A_\rho}{\partial z^2} = \frac{2}{\rho^2}\frac{\partial A_\phi}{\partial \phi} \tag{10}$$

$$\frac{\partial^2 A_\phi}{\partial \rho^2} + \frac{1}{\rho}\frac{\partial A_\phi}{\partial \rho} - \frac{1}{\rho^2}A_\phi + \frac{1}{\rho^2}\frac{\partial^2 A_\phi}{\partial \phi^2} + \frac{\partial^2 A_\phi}{\partial z^2} = -\frac{2}{\rho^2}\frac{\partial A_\rho}{\partial \phi} \tag{11}$$

$$\frac{\partial^2 A_z}{\partial \rho^2} + \frac{1}{\rho}\frac{\partial A_z}{\partial \rho} + \frac{1}{\rho^2}\frac{\partial^2 A_z}{\partial \phi^2} + \frac{\partial^2 A_z}{\partial z^2} = 0 \tag{12}$$

Thus the A_z has been separated from the other two functions A_ρ and A_ϕ . This function A_z can be found by the usual method of separating variables. The functions A_ρ and A_ϕ are present in a pair of simultaneous second order partial differential equations. By proper differentiations and additions, it would be possible to eliminate one of these functions between (10) and (11) to obtain a fourth order partial differential equation in the remaining function. This procedure leads to an equation which is very difficult to solve and furthermore results in solutions which are far more general than are needed in this problem. For the needs of this problem,

(10) and (11) can be solved more simply by making use of the periodic nature of the helix and its fields. An observer placed at a constant radius from the z axis will observe no change in the magnetic field if he is confined to the surface of a helicoid defined by $\left(z - \frac{\phi}{2\pi} \tau \right)$ = constant. This means that the ϕ and z variations of the vector potential must appear as (or be capable of assuming the form of) a function of $\left(\frac{2\pi}{\tau} z - \phi \right)$. Furthermore, an observer at constant radius moving in a plane defined by ϕ = constant, will detect a periodic variation of the field with period τ. In the plane z = constant he will, at constant radius, observe a periodic variation in the field with period 2π. The periodic variations are not necessarily sinusoidal, suggesting the possibility of representing the field as a Fourier series in both the ϕ and z directions.

Hence, let

$$A_{\rho m} = R_{\rho m} \cdot \sin(bz - m\phi) \tag{13}$$

be the form of the ρ component of vector potential having harmonic order m. In this expression $R_{\rho m}$ is a function of ρ alone and $b = \frac{2\pi m}{\tau}$. The choice of the sine function alone, merely orients the helix with respect to the coordinate system so that it is at z = 0 when ϕ = 0. No generality is lost by so doing. An examination of (10) or (11) will reveal that if $A_{\rho m}$ varies as the sine of the argument, the $A_{\phi m}$ will have to vary as the cosine of the argument. Thus,

$$A_{\phi m} = R_{\phi m} \cdot \cos(bz - m\phi) \tag{14}$$

where $A_{\phi m}$ is the ϕ component of the vector potential having harmonic order m. In this expression $R_{\phi m}$ is a function of ρ alone. If (13) and (14) are substituted into (10) and (11), they become,

$$\left[\frac{d^2}{d\rho^2} + \frac{1}{\rho}\frac{d}{d\rho} - \left(\frac{1+m^2}{\rho^2} + b^2\right)\right] R_{\rho m} = \frac{2m}{\rho^2} R_{\phi m} \tag{15}$$

$$\left[\frac{d^2}{d\rho^2} + \frac{1}{\rho}\frac{d}{d\rho} - \left(\frac{1+m^2}{\rho^2} + b^2\right)\right] R_{\phi m} = \frac{2m}{\rho^2} R_{\rho m} \tag{16}$$

If these are both added and subtracted from each other, there results

$$\left[\frac{d^2}{d\rho^2} + \frac{1}{\rho}\frac{d}{d\rho} - \left(b^2 + \frac{m^2+2m+1}{\rho^2}\right)\right](R_{\rho m} + R_{\phi m}) \tag{17}$$

$$\left[\frac{d^2}{d\rho^2} + \frac{1}{\rho}\frac{d}{d\rho} - \left(b^2 + \frac{m^2-2m+1}{\rho^2}\right)\right](R_{\rho m} - R_{\phi m}) \tag{18}$$

These equations are recognizable as the Bessel equations of order $(m+1)$ and $(m-1)$ respectively which lead to solutions which are the so called modified Bessel functions. The solutions of (17) and (18) are

$$(R_{\rho m} + R_{\phi m}) = 2A'_m I_{m+1}(b\rho) + 2B'_m K_{m+1}(b\rho) \tag{19}$$

$$(R_{\rho m} - R_{\phi m}) = 2C'_m I_{m-1}(b\rho) + 2D'_m K_{m-1}(b\rho) \tag{20}$$

where $A'_m \ldots D'_m$ are arbitrary constants and the I_n and K_n are

modified Bessel functions of order n ($= m \pm 1$) and of the first and second kinds respectively. In what follows, wherever the arguments of the Bessel functions are omitted, the argument ($b\rho$) is to be understood.

Solving (19) and (20) for $R_{\rho m}$ and $R_{\phi m}$ yields

$$R_{\rho m} = \left[A'_m I_{m+1} + B'_m K_{m+1} + C'_m I_{m-1} + D'_m K_{m-1} \right] \tag{21}$$

$$R_{\phi m} = \left[A'_m I_{m+1} + B'_m K_{m+1} - C'_m I_{m-1} - D'_m K_{m-1} \right] \tag{22}$$

Equation (12) of this chapter is the same as equation (1) of Appendix B and may be solved in exactly the same way. Considerations of single valuedness for variations of the ϕ coordinate and periodicity in both the ϕ and z directions will restrict the solution of (12) to,

$$A_{zm} = \left[E'_m I_m + F'_m K_m \right] \cdot \left[\cos(bz - m\phi) + G'_m \sin(bz - m\phi) \right] \tag{23}$$

where the E'_m . . . G'_m are arbitrary constants and the other symbols have their usual significance. In order to satisfy that $\nabla \cdot \underline{A} = 0$ it can be shown that G'_m must be identically zero. Hence,

$$A_{zm} = \left[E'_m I_m + F'_m K_m \right] \cos(bz - m\phi) \tag{24}$$

The ρ and ϕ components of the vector potential are as follows:

$$A_{\rho m} = \left[A'_m I_{m+1} + B'_m K_{m+1} + C'_m I_{m-1} + D'_m K_{m-1}\right] \sin(bz - m\phi) \tag{25}$$

$$A_{\phi m} = \left[A'_m I_{m+1} + B'_m K_{m+1} - C'_m I_{m-1} + D'_m K_{m-1}\right] \cos(bz - m\phi) \tag{26}$$

These expressions, (24), (25) and (26) for the components of the vector potential satisfy equation (3) and can be made to satisfy (4) by an appropriate set of relationships among the constants A'_m to F_m. These equations also are in accordance with the periodic nature of the helix and its fields. They are valid however, for $m \neq 0$.

Next the components of the vector potential will be found for $m = b = 0$. The case of $m = b = 0$ would correspond to no variations in the fields in either the z or ϕ directions. Physically, this would require the presence of current systems of the following types. First, there might be a current density in the z direction with no variation of this current density with either z or ϕ. Such a current density would produce only a z component of vector potential and a ϕ component of magnetic field. In the second place, there might be a current density in the ϕ direction with no variation of this current density with either z or ϕ. This would produce only a ϕ component of vector potential with an attendant z component of magnetic field. Hence, since for $m = b = 0$, A_ρ, A_ϕ and A_z can have no variation with either ϕ or z, equations (6), (7), (8) and (9) become

$$\left[\nabla \times \nabla \times \underline{A}\right]_\phi \equiv 0 \tag{27}$$

$$[\nabla\times\nabla\times\underline{A}]_\phi = -\frac{\partial^2 A_\phi}{\partial\rho^2} - \frac{1}{\rho}\frac{\partial A_\phi}{\partial\rho} - \frac{1}{\rho^2}A_\phi = 0 \tag{28}$$

$$[\nabla\times\nabla\times\underline{A}]_z = -\frac{\partial^2 A_z}{\partial\rho^2} - \frac{1}{\rho}\frac{\partial A_z}{\partial\rho} = 0 \tag{29}$$

$$[\nabla\cdot\underline{A}] = \frac{\partial A_\rho}{\partial\rho} + \frac{1}{\rho}A_\rho = 0 \tag{30}$$

These have solutions,

$$A_{\rho 0} = \frac{E_0}{\rho} \tag{31}$$

$$A_{\phi 0} = C_0\rho + \frac{D_0}{\rho} \tag{32}$$

$$A_{z0} = A_0 + B_0 \operatorname{Log}_e \rho \tag{33}$$

where the subscript zero denotes that there is no variation of these quantities with either ϕ or z. The constants A_0 to E_0 are arbitrary constants to be determined by boundary conditions. The origin of ρ is included in the region for which the solution is to hold, hence the constant E_0 in (31) must be zero, since the vector potential is not infinity at $\rho = 0$, and it must be continuous at all boundaries.

Equations (24), (25), (26), (32) and (33) constitute a set of functional relationships from which shall be built up a solution satisfying certain boundary conditions. The boundary conditions will be stated below. Some of them are satisfied in this section and the remainder in the section to follow. Before doing this, however, the expression $\nabla\cdot\underline{A} = 0$ will be

used to establish certain relationships among the constants A'_m . . . P'_m. By using the recurrence formulae listed in Appendix A, (21) and (22) can be rewritten,

$$R_{\rho m} = \left[A_m I'_m - \frac{m}{b\rho} B_m I_m - C_m K'_m - \frac{m}{b\rho} D_m K_m\right] \tag{34}$$

$$R_{\phi m} = \left[B_m I'_m - \frac{m}{b\rho} A_m I_m + D_m K'_m - \frac{m}{b\rho} C_m K_m\right] \tag{35}$$

where, $A_m = (A'_m + C'_m)$

$B_m = (A'_m - C'_m)$

$C_m = -(B'_m + D'_m)$

$D_m = -(B'_m - D'_m)$

The primes on the Bessel functions denote differentiation with respect to the argument ($b\rho$).

Now from $\nabla \cdot \underline{A} = 0$ follows,

$$\frac{\partial R_{\rho m}}{\partial \rho} + \frac{1}{\rho} R_{\rho m} + \frac{m}{\rho} R_{\phi m} - b R_{zm} = 0 \tag{36}$$

If (24), (34) and (35) are substituted in (36) there follows,

$$\left[A_m I_m'' + \frac{1}{\rho} A_m I_m' - \left(E_m' + \frac{m^2}{b^2\rho^2} A_m\right) I_m\right]$$

$$-\left[C_m K_m'' + \frac{1}{b\rho} C_m K_m' - \left(F_m' + \frac{m^2}{b^2\rho^2} C_m\right) K_m\right] = 0 \qquad (37)$$

from which it can be deduced that $E_m' = A_m$ and $F_m' = C_m$. Making use of these relations, there results,

$$A_{\rho m} = \left[A_m I_m' - \frac{m}{b\rho} B_m I_m + C_m K_m' - \frac{m}{b\rho} D_m K_m\right] \sin(bz - m\phi) \qquad (38)$$

$$A_{\phi m} = \left[B_m I_m' - \frac{m}{b\rho} A_m I_m + D_m K_m' - \frac{m}{b\rho} C_m K_m\right] \cos(bz - m\phi) \qquad (39)$$

$$A_{zm} = \left[A_m I_m + C_m K_m\right] \cos(bz - m\phi) \qquad (40)$$

The four constants Am to Dm are dependent upon the boundary conditions and will subsequently be determined from them. In this section only some of the boundary conditions will be applied, the result being that all the arbitrary constants will be determined in terms of one of them. In the next section, it will be shown how this one remaining arbitrary constant is related to the current sheet at R_1. The boundary conditions dealt with in this section are that $\underline{A}$ is continuous through any of the boundaries dealt with in this report (see reference (1), page 245), and that $\underline{H}$ must vanish for all $\rho > R_2$. In this analysis $\underline{H}$ is the magnetic field intensity in amperes per meter and is related to the vector potential by

The following equation,

$$\underline{H} = \nabla \times \underline{A} \tag{41}$$

Let the field be divided into four regions as tabulated in Table 9. From these definitions, it is apparent that

$$\underline{A}_1 = \underline{A}_a + \underline{A}_c \tag{42}$$

$$\underline{A}_2 = \underline{A}_b + \underline{A}_c \tag{43}$$

$$A_3 = \underline{A}_b + \underline{A}_d \tag{44}$$

Table 9

Four Regions Into Which Field Is Divided

Region	Definition	Symbol for Vector-Potential	Current Which is Seat of Vector-Potential
a	$0 \leq \rho \leq R_1$	$\underline{A}_a$	Helix current at R_1
b	$R_1 \leq \rho < \infty$	$\underline{A}_b$	" " " "
c	$0 \leq \rho \leq R_2$	$\underline{A}_c$	Sheath current at R_2
d	$R_2 \leq \rho \leq \infty$	$\underline{A}_d$	" " " "

Because of the irregularity of the I_m and K_m functions at $\rho = 0$, they must be excluded from the expressions for $\underline{A_a}$ and $\underline{A_c}$. Because of the irregularity of the I_m and I_m' functions at infinity they must be excluded from the expressions for $\underline{A_b}$ and $\underline{A_c}$. Thus,

In region a:

$$A_{\rho ma} = \left[A_{ma} I_m' - \frac{m}{c\rho} B_{ma} I_m\right] \sin(bz - m\phi) \tag{45}$$

$$A_{\phi ma} = \left[B_{ma} I_m' - \frac{m}{c\rho} A_{ma} I_m\right] \cos(bz - m\phi) \tag{46}$$

$$A_{zma} = \left[A_{ma} I_m\right] \cos(bz - m\phi) \tag{47}$$

In region b:

$$A_{\rho mb} = \left[C_{mb} K_m' - \frac{m}{b\rho} D_{mb} K_m\right] \sin(bz - m\phi) \tag{48}$$

$$A_{\phi mb} = \left[D_{mb} K_m' - \frac{m}{b\rho} C_{mb} K_m\right] \cos(bz - m\phi) \tag{49}$$

$$A_{zmb} = \left[C_{mb} K_m\right] \cos(bz - m\phi) \tag{50}$$

In region c:

$$A_{\rho mc} = \left[A_{mc} I_m' - \frac{m}{b\rho} B_{mc} I_m\right] \sin(bz - m\phi) \tag{51}$$

$$A_{\phi mc} = \left[B_{mc} I_m' - \frac{m}{b\rho} A_{mc} I_m\right] \cos(bz - m\phi) \tag{52}$$

$$A_{zmc} = \left[A_{mc} I_m\right] \cos(bz - m\phi) \tag{53}$$

In region d:

$$A_{\rho md} = \left[C_{md} K_m' - \frac{m}{b\rho} D_{md} K_m\right] \sin(bz - m\phi) \tag{54}$$

$$A_{\phi md} = \left[D_{md} K_m' - \frac{m}{b\rho} C_{md} K_m\right] \cos(bz - m\phi) \tag{55}$$

$$A_{zmd} = \left[C_{md} K_m\right] \cos(bz - m\phi) \tag{56}$$

Since the vector potential must be continuous across any boundary, $\underline{A_a}$ must equal $\underline{A_b}$ at $\rho = R_1$ and $\underline{A_c}$ must equal $\underline{A_d}$ at $\rho = R_2$. These conditions yield the following set of relations among the coefficients,

$$B_{ma} = -\frac{bR_1}{m} \frac{K_m'(bR_1)}{K_m(bR_1)} A_{ma} \tag{57}$$

$$C_{mb} = \frac{I_m(bR_1)}{K_m(bR_1)} A_{ma} \tag{58}$$

$$D_{mb} = -\frac{bR_1}{m} \frac{I_m'(bR_1)}{K_m(bR_1)} A_{ma} \tag{59}$$

$$B_{mc} = -\frac{bR_2}{m} \frac{K_m'(bR_2)}{K_m(bR_2)} A_{mc} \tag{60}$$

$$C_{md} = \frac{I_m(bR_2)}{K_m(bR_2)} A_{mc} \tag{61}$$

$$D_{md} = -\frac{bR_2}{m}\frac{I'_m(bR_2)}{K_m(bR_2)} A_{mc} \tag{62}$$

Thus the continuity of $\underline{A}$ has established six of the eight constants in terms of the remaining two. The fact that the magnetic field $\underline{H}$ must vanish for $\rho > R_2$ will establish a relationship between Ama and Amc. From equation (44), the components of the vector potential in region 3 are

$$A_{\rho m3} = \left[(C_{mb}+C_{md})K'_m - \frac{m}{b\rho}(D_{mb}+D_{md})K_m\right]\sin(bz-m\phi) \tag{63}$$

$$A_{\phi m3} = \left[(D_{mb}+D_{md})K'_m - \frac{m}{b\rho}(C_{mb}+C_{md})K_m\right]\cos(bz-m\phi) \tag{64}$$

$$A_{zm3} = \left[(C_{mb}+C_{md})K_m\right]\cos(bz-m\phi) \tag{65}$$

From $\underline{H}_3 = \nabla \times \underline{A}_3$ follows the components of the magnetic field in region 3,

$$H_{\rho m3} = \left[b(D_{mb}+D_{md})K'_m\right]\sin(bz-m\phi) \tag{66}$$

$$H_{\phi m3} = -\left[\frac{m}{\rho}(D_{mb}+D_{md})K_m\right]\cos(bz-m\phi) \tag{67}$$

$$H_{zm3} = \left[b(D_{mb}+D_{md})K_m\right]\cos(bz-m\phi) \tag{68}$$

Hence in order that $\underline{H}$ vanish for all $\rho > R_2$, (Dmb + Dmd) must be zero.

By using this fact along with (59) and (62), we get,

$$A_{mc} = -\frac{R_1}{R_2}\frac{I'_m(bR_1)K_m(bR_2)}{I'_m(bR_2)K_m(bR_1)}A_{ma} \tag{69}$$

and equations (60), (61) and (62) become,

$$B_{mc} = \frac{bR_1}{m}\frac{I'_m(bR_1)K'_m(bR_2)}{I'_m(bR_2)K_m(bR_1)}A_{mo}. \tag{70}$$

$$C_{md} = -\frac{R_1}{R_2}\frac{I'_m(bR_1)I_m(bR_2)}{I'_m(bR_2)K_m(bR_1)}A_{ma} \tag{71}$$

$$D_{md} = \frac{bR_1}{m}\frac{I'_m(bR_1)}{K_m(bR_1)}A_{ma} \tag{72}$$

Since the introduction of these constants in terms of Ama will make the expressions for the vector potention cumbersome, they will not be used until later. From (42) and (43) follows,

$$A_{\rho m_1} = \left[(A_{ma}+A_{mc})I'_m - \frac{m}{b\rho}(B_{ma}+B_{mc})I_m\right]\sin(bz-m\phi) \tag{73}$$

$$A_{\phi m_1} = \left[(B_{ma}+B_{mc})I'_m - \frac{m}{b\rho}(A_{ma}+A_{mc})I_m\right]\cos(bz-m\phi) \tag{74}$$

$$A_{zm} = \left[(A_{ma}+A_{mc})I_m\right]\cos(bz-m\phi) \tag{75}$$

$$A_{\rho mz} = \left[A_{mc}I'_m - \frac{m}{bc}B_{mc}I_m + C_{mb}K'_m - \frac{m}{bc}D_{mb}K_m\right]\sin(bz-m\phi) \tag{76}$$

$$A_{\phi mz} = \left[B_{mc}I'_m - \frac{m}{bc}A_{mc}I_m + D_{mb}K'_m - \frac{m}{bc}C_{mb}K_m\right]\cos(bz-m\phi) \tag{77}$$

$$A_{zmz} = \left[A_{mc}I_m + C_{mb}K_m\right]\cos(bz-m\phi) \tag{78}$$

From (73) to (78) and $\underline{H} = \nabla \times \underline{A}$ the components of magnetic field in regions 1 and 2 follow,

$$H_{\rho m_1} = b\left[(B_{ma}+B_{mc})I'_m\right]\sin(bz-m\phi) \tag{79}$$

$$H_{\phi m_1} = -\frac{m}{\rho}\left[(B_{ma}+B_{mc})I_m\right]\cos(bz-m\phi) \tag{80}$$

$$H_{zm_1} = b\left[(B_{ma}+B_{mc})I_m\right]\cos(bz-m\phi) \tag{81}$$

$$H_{\rho mz} = b\left[B_{mb}K'_m + B_{mc}I'_m\right]\sin(bz-m\phi) \tag{82}$$

$$H_{\phi mz} = -\frac{m}{\rho}\left[B_{mb}K_m + B_{mc}I_m\right]\cos(bz-m\phi) \tag{83}$$

$$H_{zm2} = b\left[B_{mt}I'_m + B_{mc}I_m\right]\cos(cz - m\phi) \tag{84}$$

As will be shown in the next section, the current flowing in a tape helix of very narrow width can be represented as a pair of Fourier series of surface current density sheets in both the ϕ and z directions. A knowledge of the coefficients of these series will enable us to determine the remaining constant A_{ma} which up to the present is unknown. In preparation for this process, (79) to (84) will be used to determine the current density vectors at the radius $\rho = R_1$. Let us denote the ϕ and z components of surface current density as $j\phi m$ and jzm respectively. Then,

$$j_{\phi m} = \left[H_{zm1} - H_{zm2}\right]_{\rho=R_1} \tag{85}$$

$$j_{zm} = \left[H_{\phi m2} - H_{\phi m1}\right]_{\rho=R_1} \tag{86}$$

Upon substituting (81) and (84) into (85) and (80) and (83) into (86) there results,

$$j_{\phi m} = \frac{b}{m}\,\frac{A_{ma}}{K_m(bR_1)}\cos(bz - mz) \tag{87}$$

$$j_{zm} = \frac{1}{R_1}\,\frac{A_{ma}}{K_m(bR_1)}\cos(bz - mz) \tag{88}$$

In arriving at (87) and (88) use must be made of the Wronskian relationship mentioned in Appendix A-1.

It is interesting to note that, since the current in the helical conductor is confined to flow in the helix direction, which makes an angle ψ with a circumferencial line drawn on the cylinder of radius R_1, any current density sheets derived from the line current by a Fourier analysis must also have its direction of maximum current density in the helix direction. Therefore the ratio ($j_{zm}/j_{\phi m}$) must equal $\tan\psi$. This is borne out by (87) and (88) which give,

$$\frac{j_{zm}}{j_{\phi m}} = \frac{m}{bR_1} = \frac{\tau}{2\pi R_1} = \tan\psi \qquad (89)$$

Before proceeding to the next section where the current in a thin helical conductor will be represented by two Fourier series of current density sheets, the case of $m = b = 0$ will be discussed.

Again consider the regions (a, b, c, and d) tabulated in Table 9 above.

In region a,

$$A_{z0a} = C_{0a}\rho \qquad (90)$$

$$A_{z0a} = A_{0a} + B_{0a}\log_e \rho \qquad (91)$$

In region b,

$$A_{z0b} = \frac{D_{0b}}{\rho} \tag{92}$$

$$A_{z0b} = A_{0b} + B_{0b} \log_e \rho \tag{93}$$

In region c,

$$A_{0oc} = C_{oc} \rho \tag{94}$$

$$A_{z0c} = A_{0c} + B_{0c} \log_e \rho \tag{95}$$

In region d,

$$A_{\phi 0d} = \frac{D_{0d}}{\rho} \tag{96}$$

$$A_{z0d} = A_{0d} + B_{0d} \log_e \rho \tag{97}$$

The continuity of the vector potential at R_1 and R_2 requires

$$D_{0b} = R_1^2 C_{0a} \tag{98}$$

$$D_{0d} = R_2^2 C_{0c} \tag{99}$$

$$(A_{0a} - A_{0b}) = (B_{0b} - B_{0a}) \log_e R_1 \tag{100}$$

$$(A_{0c} - A_{0d}) = (B_{0d} - B_{0c}) \log_e R_2 \tag{101}$$

In addition to the continuity of $\underline{A}_0$ there are several conditions on $\underline{A}_0$ and $\underline{H}_0$ which must be satisfied. These are that $\underline{H}_0 = 0$ for $\rho > R_2$, $H_{\phi 0} = 0$ for $\rho < R_1$, and $\underline{A}_0$ must approach zero as ρ approaches infinity.

The application of these conditions requires in turn that,

$$(B_{ob} + B_{od}) = 0 \tag{102}$$

$$(B_{oa} + B_{oc}) = 0 \tag{103}$$

$$(A_{ob} + A_{od}) = 0 \tag{104}$$

Using these results, the vector potential in regions 1 and 2 are,

$$A_{\phi o1} = (C_{oa} + C_{oc})\cdot\rho \tag{105}$$

$$A_{zo1} = (A_{oa} + A_{oc}) \tag{106}$$

$$A_{\phi o2} = \frac{D_{ob}}{\rho} + C_{oc}\,\rho \tag{107}$$

$$A_{zo2} = (A_{ob} + A_{oc}) + (B_{ob} + B_{oc}) \log_e \rho \tag{108}$$

From $\underline{H}_o = \nabla \times \underline{A}_o$ comes,

$$H_{ro1} = 0 \tag{109}$$

$$H_{\phi o1} = 0 \tag{110}$$

$$H_{zo1} = 2(C_{oa} + C_{oc}) \tag{111}$$

$$H_{ro2} = 0 \tag{112}$$

$$H_{\phi 02} = -\frac{(B_{0b}+B_{0c})}{\rho} \tag{113}$$

$$H_{z02} = 2C_{0c} \tag{114}$$

Now in region 2, the line integral of $H\phi_2$ on a circle of radius ρ $(> R_1)$ must equal the total current enclosed. Hence,

$$(B_{0b}+B_{0c}) = -R_1 j_{z0} \tag{115}$$

where j_{z0} is the surface current density at radius R_1 flowing in the z direction. This current density is independent of ϕ and z.

Also since the sheath has perfect conductivity, the total magnetic flux in the z direction must be zero. Hence,

$$2(C_{0a}+C_{0c})\pi R_1^2 + 2C_{0c}\pi(R_2^2-R_1^2) = 0 \tag{116}$$

from which,

$$C_{0c} = -\frac{R_1^2}{R_2^2} C_{0a} \tag{117}$$

The constant C_{0a} can be determined from the surface current density in the ϕ direction as follows. If equation (85) is applied with the subscript m replaced everywhere by 0, we get,

$$C_{oo} = \frac{1}{2} j_{\phi o} \tag{118}$$

where $j_{\phi o}$, the surface current density in the ϕ direction, is independent of ϕ and z. The results from (98) to (118) yield,

$$A_{\phi o1} = \frac{1}{2} j_{\phi o} \left(1 - \frac{R_1^2}{R_2^2}\right) \rho \tag{119}$$

$$A_{zo1} = R_1 j_{zo} \log_e \frac{R_2}{R_1} \tag{120}$$

$$A_{\phi o2} = \frac{1}{2} j_{\phi o} \left(\frac{R_1^2}{\rho^2} - \frac{R_1^2}{R_2^2}\right) \rho \tag{121}$$

$$A_{zo2} = R_1 j_{zo} \log_e \frac{R_2}{\rho} \tag{122}$$

In summary, equations (73) to (78) and (119) to (122) constitute a set of vector potentials which can be used to represent the vector potential caused by a helical line of current shielded by a perfectly conducting sheath.

C-5 The Fourier Series Representation of the Helical Current

The Fourier series representation of the current in a fine wire helix will now be developed with the aid of Figures 47 to 49. Figure 47 shows a tape helix of width 2a carrying a total current of I Amperes in the helix direction. The surface current density at the tape is (I)/2a amperes per meter in the helix direction. This current density can be broken up

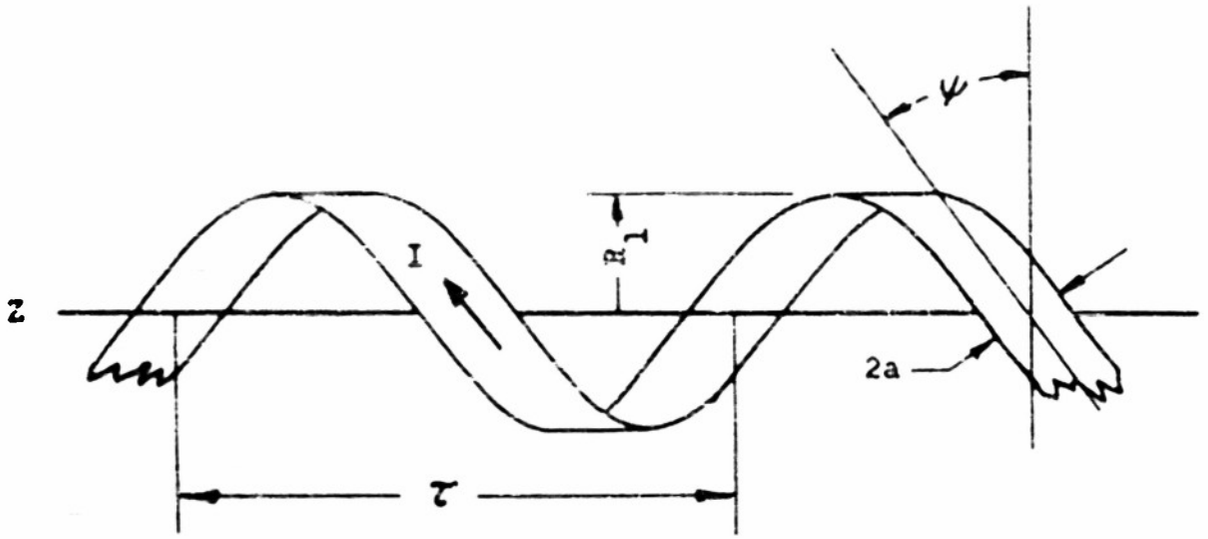

FIGURE 47: A NARROW TAPE HELIX CARRYING A CURRENT OF I AMPERES

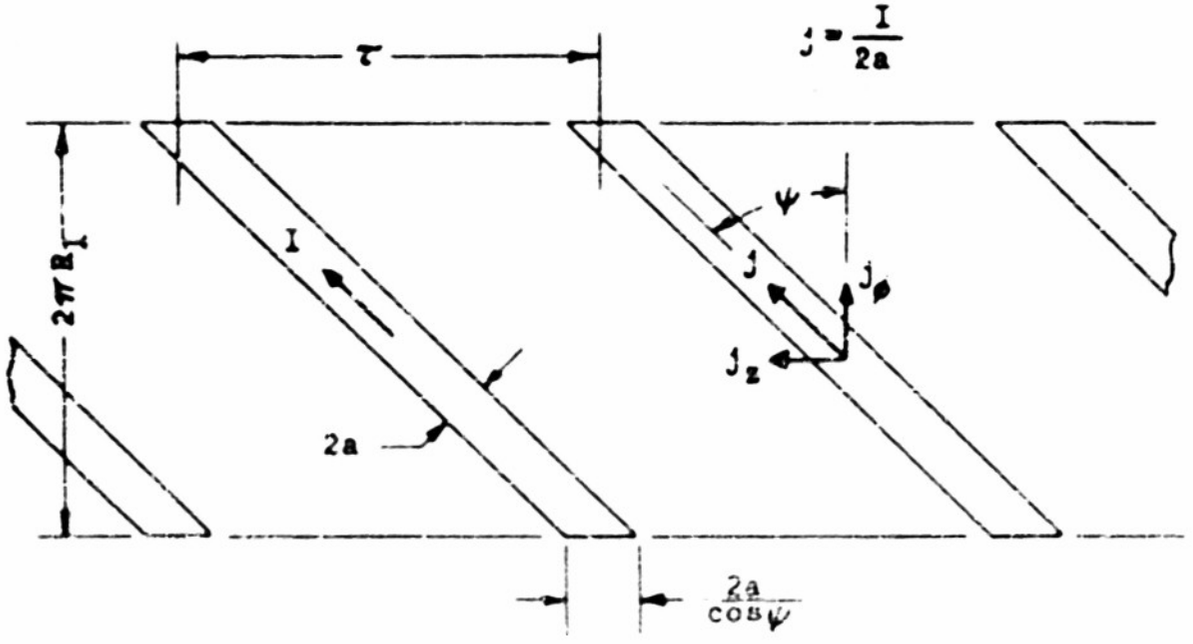

FIGURE 48: DEVELOPED NARROW TAPE HELIX

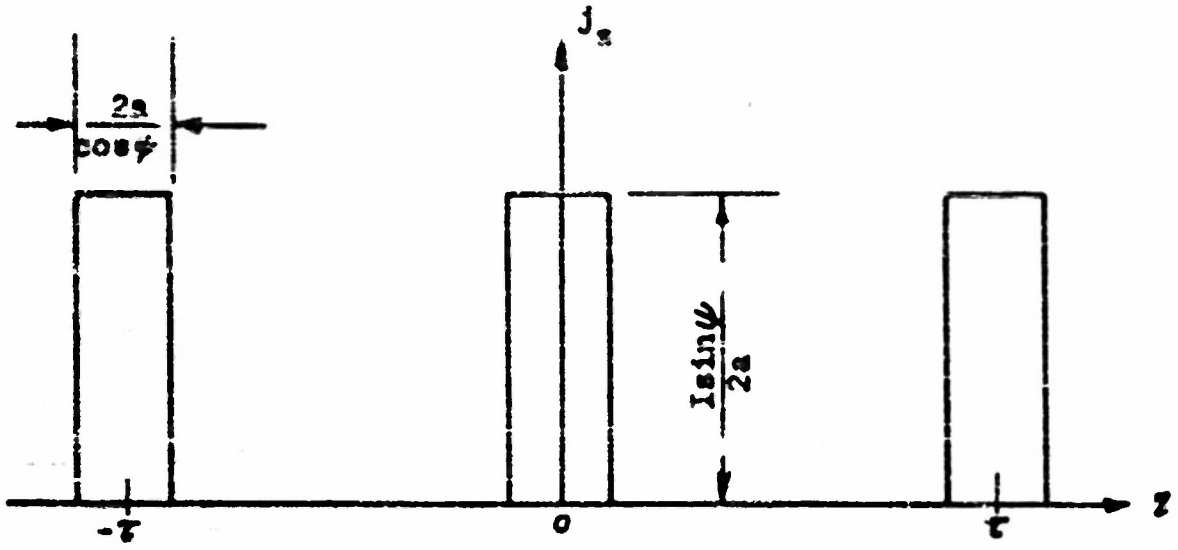

FIGURE 49(a): AXIAL COMPONENT OF SURFACE CURRENT DENSITY AT $\rho = R_1$ and $\phi = 0$.

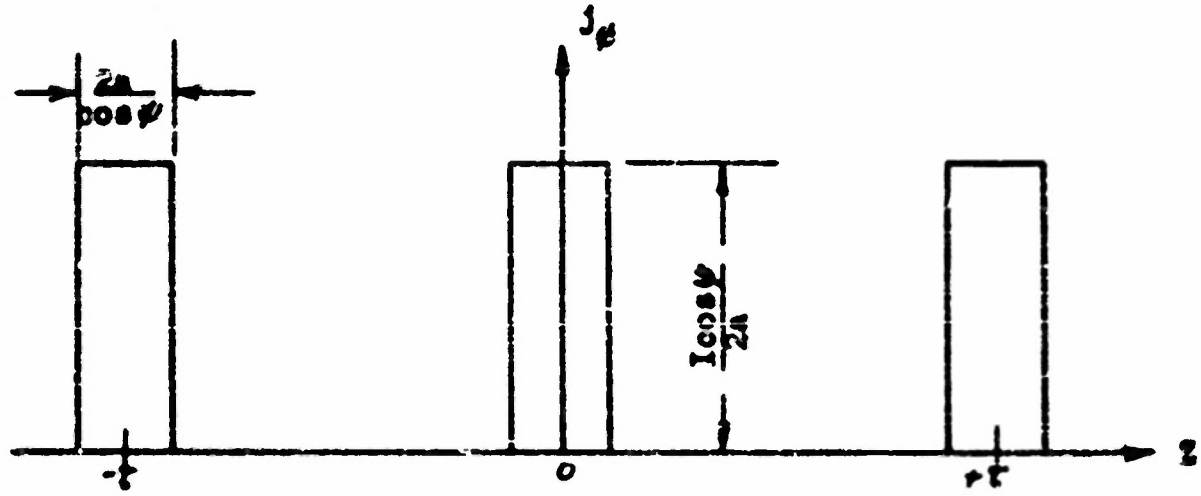

FIGURE 49(b); CIRCUMFERENCIAL COMPONENT OF SURFACE CURRENT DENSITY AT $\rho = R_1$ and $\phi = 0$.

into two components, one axial and one circumferential. The axial component j_z has a magnitude at the tape of $\frac{I}{2a}\sin\psi$. It is plotted in Figure 49(a) as a function of z at the particular value $\phi = 0$. The circumferencial component j_ϕ has a magnitude at the tape of $\frac{I}{2a}\cos\psi$. It is plotted in Figure 49(b) as a function of z at the value $\phi = 0$. As can be seen from Figure 49, these current densities are periodic functions of z with period τ . They can be represented by the Fourier series below,

$$j_\phi = \frac{I}{\tau}\left\{1 + 2\sum_{m=1}^{\infty}\left[\frac{\sin\left(\frac{ba}{\cos\psi}\right)}{\left(\frac{ba}{\cos\psi}\right)}\right]\cos bz\right\} \tag{123}$$

$$j_z = \frac{I\tan\psi}{\tau}\left\{1 + 2\sum_{m=1}^{\infty}\left[\frac{\sin\left(\frac{ba}{\cos\psi}\right)}{\left(\frac{ba}{\cos\psi}\right)}\right]\cos bz\right\} \tag{124}$$

where $b = \frac{2\pi m}{\tau}$

If the dimension, a, is allowed to approach zero, the tape approaches an infinitesimally thin wire. If this is done and at the same time recognizing that z can be replaced everywhere by $\left(z - \frac{\phi}{2\pi}\tau\right)$ there results

$$j_\phi = \frac{I}{\tau}\left\{1 + 2\sum_{m=1}^{\infty}\cos(bz - m\phi)\right\} \tag{125}$$

$$j_z = \frac{I\tan\psi}{\tau}\left\{1 + 2\sum_{m=1}^{\infty}\cos(bz - m\phi)\right\} \tag{126}$$

From equations (87), (88), (125) and (126) the constant A_{ma} can be obtained. It is,

$$A_{ma} = \frac{I}{\pi} K_m(bR_1) \tag{127}$$

where $m \neq 0$. It can also be recognized that the $j_{\phi o}$ and j_{zo} of equations (119) to (122) are

$$j_{\phi o} = \frac{I}{\tau} \tag{128}$$

$$j_{zo} = \frac{I \tan\psi}{\tau} \tag{129}$$

from which,

$$A_{\phi o1} = \frac{\rho I}{2\tau}\left(1 - \frac{R_1^2}{R_2^2}\right) \tag{130}$$

$$A_{zo1} = \frac{I}{2\pi} \operatorname{Log}_e \frac{R_2}{R_1} \tag{131}$$

$$A_{\phi o2} = \frac{\rho I}{2\tau}\left(\frac{R_1^2}{\rho^2} - \frac{R_1^2}{R_2^2}\right) \tag{132}$$

$$A_{zo2} = \frac{I}{2\pi} \operatorname{Log}_e \frac{R_2}{\rho} \tag{133}$$

Below are listed the complete equations for the vector potential about an infinitesimally thin wire helix carrying direct current, the helix shielded by a perfectly conducting sheath. These expressions are obtained by using (130) to (133) above plus an infinite sum of terms like those in (75) to (78). Each of these terms in the infinite series corresponds to

a current sheet of harmonic order m as obtained in (125) and (126). In obtaining the following equations, use is also made of (57), (58), (59), (70), (71) and (72).

$$A_{\rho 1} = \frac{I}{\pi}\sum_{m=1}^{\infty}\left\{\left[1-F_m\right]K_m(bR_1)I_m' + \frac{R_1}{\rho}\left[1-G_m'\right]K_m'(bR_1)I_m\right\}\sin(bz-m\phi) \tag{134}$$

$$A_{\phi 1} = \frac{\rho I}{2\pi}\left[1-\frac{R_1^2}{R_2^2}\right] - \frac{I}{\pi}\sum_{m=1}^{\infty}\left\{\cot\psi\left[1-G_m'\right]K_m'(bR_1)I_m' + \frac{R_1}{\rho}\tan\psi\left[1-F_m\right]K_m(bR_1)I_m\right\}\cos(bz-m\phi) \tag{135}$$

$$A_{z1} = \frac{I}{2\pi}\log_e\frac{R_2}{R_1} + \frac{I}{\pi}\sum_{m=1}^{\infty}\left\{\left[1-F_m\right]K_m(bR_1)I_m\right\}\cos(bz-m\phi) \tag{136}$$

$$A_{\rho 2} = \frac{I}{\pi}\sum_{m=1}^{\infty}\left\{I_m(bR_1)K_m' - F_mK_m(bR_1)I_m' + \frac{F_1}{\rho}I_m'(bR_1)K_m - \frac{R_1}{\rho}G_m'K_m'(bR_1)I_m\right\}\sin(bz-m\phi) \tag{137}$$

$$A_{\phi 2} = \frac{\rho I}{2\pi}\left[\frac{R_1^2}{\rho^2}-\frac{R_1^2}{R_2^2}\right] - \frac{I}{\pi}\sum_{m=1}^{\infty}\left\{\cot\psi\left[I_m'(bR_1)K_m' - G_m'K_m'(bR_1)I_m'\right] + \frac{R_1}{\rho}\tan\psi\left[I_m(bR_1)K_m - F_mK_m(bR_1)I_m\right]\right\}\cos(bz-m\phi) \tag{138}$$

$$A_{z2} = \frac{I}{2\pi}\log_e\frac{R_2}{\rho} + \frac{I}{\pi}\sum_{m=1}^{\infty}\left\{I_m(bR_1)K_m - F_mK_m(bR_1)I_m\right\}\cos(bz-m\phi) \tag{139}$$

where,

$$F_m = \frac{R_1}{R_2} \frac{I'_m(bR_1)K_m(bR_2)}{I'_m(bR_2)K_m(bR_1)} \tag{140}$$

$$G'_m = \frac{I'_m(bR_1)K'_m(bR_2)}{I'_m(bR_2)K'_m(bR_1)} \tag{141}$$

Using these components of the vector potential, the magnetic field can be found from $\underline{H} = \nabla \times \underline{A}$

$$H_{\rho 1} = -\frac{2I}{\tau} \sum_{m=1}^{\infty} \left\{ bR_1 \left[1 - G'_m\right] K'_m(bR_1) I'_m \right\} \sin(bz - m\phi) \tag{142}$$

$$H_{\phi 1} = \frac{I}{\pi\rho} \sum_{m=1}^{\infty} \left\{ bR_1 \left[1 - G'_m\right] K'_m(bR_1) I_m \right\} \cos(bz - m\phi) \tag{143}$$

$$H_{z1} = \frac{I}{\tau}\left(1 - \frac{R_1^2}{R_2^2}\right) - \frac{2I}{\tau} \sum_{m=1}^{\infty} \left\{ bR_1 \left[1 - G'_m\right] K'_m(bR_1) I_m \right\} \cos(bz - m\phi) \tag{144}$$

$$H_{\rho 2} = -\frac{2I}{\tau} \sum_{m=1}^{\infty} \left\{ bR_1 \left[I'_m(bR_1) K'_m - G'_m K'_m(bR_1) I'_m \right] \right\} \cos(bz - m\phi) \tag{145}$$

$$H_{\phi 2} = \frac{I}{2\pi\rho} + \frac{I}{\pi\rho} \sum_{m=1}^{\infty} \left\{ bR \left[I'_m(bR) K_m - G'_m K'_m(bR_1) I_m \right] \right\} \cos(bz - m\phi) \tag{146}$$

$$H_{z2} = -\frac{I}{\tau}\frac{R_1^2}{R_2^2} - \frac{2I}{\tau} \sum_{m=1}^{\infty} \left\{ bR_1 \left[I'_m(bR_1) K_m - G'_m K'_m(bR_1) I_m \right] \right\} \cos(bz - m\phi) \tag{147}$$

The inductance per unit length can be calculated from the vector potential above. The magnetic fields given in (142) to (147) are presented only as a matter of interest. Some of these, notably (146) and (147) might be used to calculate the losses in a sheath with finite conductivity. This is discussed in Chapter II, Section 5.

C-6 The Inductance Per Unit Length

Consider any surface S enclosed by a simple closed curve C as in Figure 50. Let it be assumed that this curve C is situated in a region where there is a magnetic field $\underline{H}$. Then linking this closed curve C will be a magnetic flux given by,

$$\Phi = \mu_0 \iint_S \underline{n} \cdot \underline{H} \, ds \tag{148}$$

where μ_0 is the permeability of the medium (free space in this case). If the field $\underline{H}$ is caused by a current I flowing close to the path C, this field will be proportional to I in a region characterized by linear properties. Consequently the total flux Φ which passes through the surface S will also be proportional to the current I. This constant of proportionality between the total flux Φ and the current which causes it is generally called the external inductance of the path. The total flux Φ in (148) can be written in terms of the vector potential. By a well known theorem from vector calculus,

$$\iint_S (\nabla \times \underline{G}) \cdot \underline{n} \, ds = \oint \underline{G} \cdot \underline{dl} \tag{149}$$

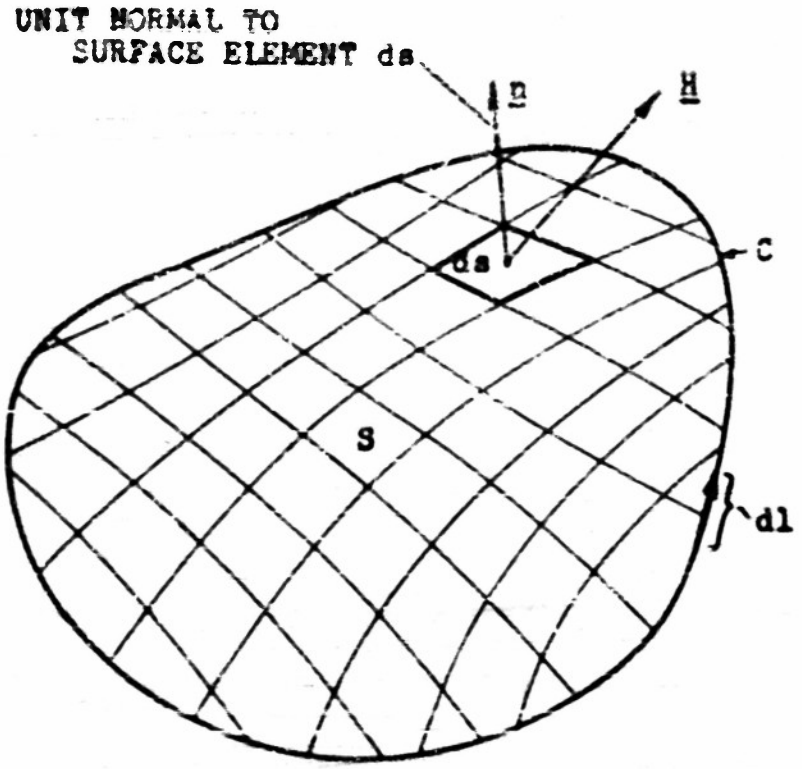

FIGURE 50: A SURFACE THREADED BY MAGNETIC FLUX

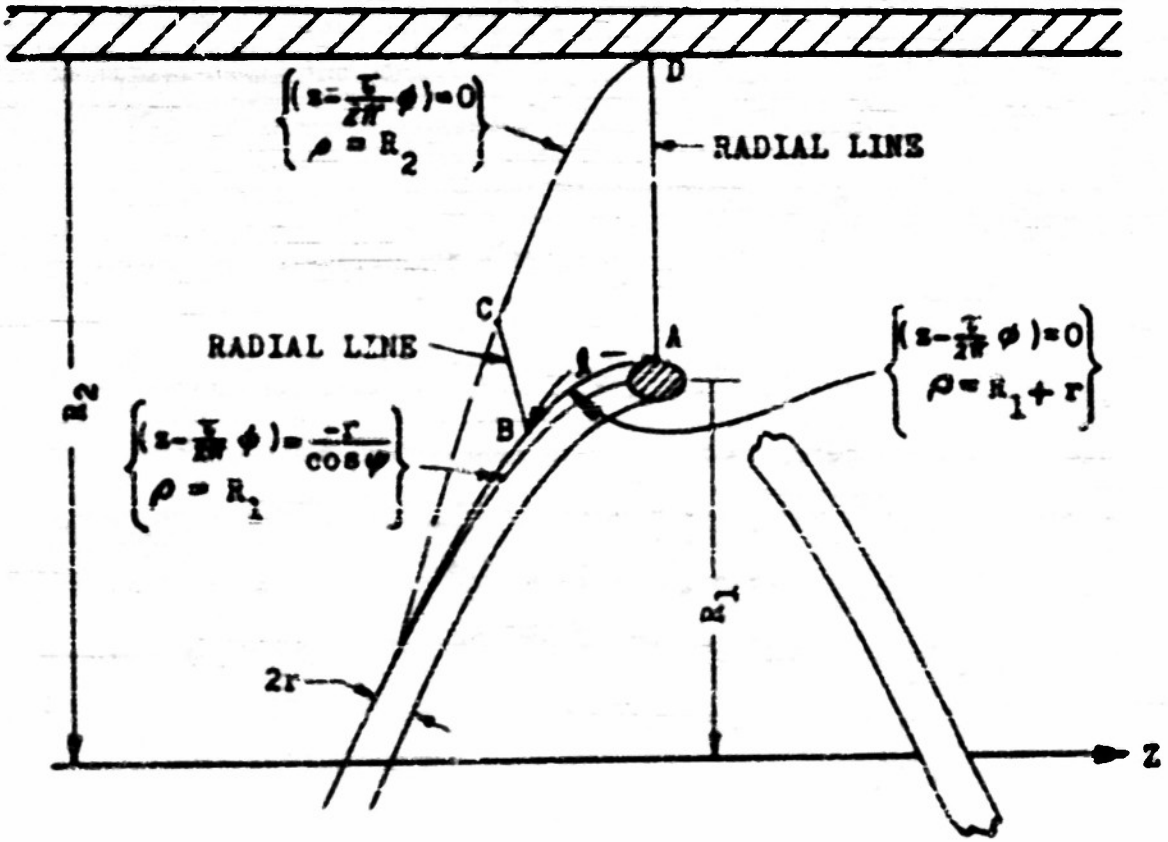

FIGURE 51: PATH OF INTEGRATION USED TO DETERMINE THE INDUCTANCE

where $\underline{C}$ is any vector, $\underline{n}$ is the unit normal to the element of surface ds and $d\underline{l}$ is a vector element of length taken on the path C. Since $\underline{H} = \nabla \times \underline{A}$, applying (149) to (148) yields,

$$\Phi = \mu_0 \oint \underline{A} \cdot d\underline{l} \tag{150}$$

This result can be applied to determine the total flux linking a path which is formed by the intersection of the helicoidal surface $(z - \frac{\phi}{2\pi}\tau) = 0$ with both the sheath and the wire. Figure 51 shows a portion of the wire and sheath, showing the path around which the integration of (150) can be performed. As in the case of the capacitance which was discussed in Appendix B, the surfaces of equi-vector-potential are very nearly the same as the surface of the wire for very small wire radii. Hence the vector potential along the line $\left\{ \begin{array}{c} (z - \frac{\phi}{2\pi}\tau) = 0 \\ \rho = R_1 + r \end{array} \right\}$ is very nearly equal to the vector potential along the lines $\left\{ \begin{array}{c} (z - \frac{\phi}{2\pi}\tau) = \pm \frac{r}{\cos\psi} \\ \rho = R_1 \end{array} \right\}$

These latter lines are formed by the intersection of the wire with the cylinder $\rho = R_1$. The use of this latter path of integration will lead to slightly simpler results. In performing the integration around the path in Figure 51, the contributions to the integral along the two radial lines BC and DA will cancel each other. This is so because $A_{\rho z}$ is the same along either of these paths, and since the integration is performed in both directions, they cancel.

Before proceeding to the evaluation of the inductance, it will

be shown that the component of vector potential at the sheath along the line CD is zero. Let ψ_2 be the helix angle at the sheath. This is the angle between the line CD and a circumferencial line drawn on the cylinder at radius R_2. Consequently,

$$\tan \psi_2 = \frac{\tau}{2\pi R_2} \tag{151}$$

The vector potential A_{ψ_2} in the helix direction at the sheath is given by,

$$A_{\psi 2} = \left[A_{\phi 2} \cos \psi_2 + A_{z2} \sin \psi_2\right]_{\rho = R_2} \tag{152}$$

Upon substituting (138) and (139) into (152) one obtains

$$A_{\psi 2} = \frac{I}{\pi} \sum_{m=1}^{\infty} \left\{ \cos \psi_2 \left[\tan \psi_2 - \frac{R_1}{R_2} \tan \psi\right] \left[I_m(bR) K_m(bR_2) - F_m K_m(bR_1) I_m(bR_2)\right] \right\} \cos(bz - m\phi) \tag{153}$$

However, since $\tan \psi_2 = \frac{\tau}{2\pi R_2}$ the term in the first pair of brackets is zero, and the vector potential at the sheath in the helix direction is identically zero.

Thus the inductance of a length of the wire ℓ meters long is given by the integral (at the surface of the wire) of the vector potential in the direction of the wire along this length ℓ. Therefore, the

inductance per meter in the helix direction is given by,

$$L = \frac{\mu_0}{I}\left[A_{01}\cos\psi + A_{21}\sin\psi\right]\Big\{_{\left(z-\frac{\phi}{2\pi}\tau\right)=\frac{r}{\cos\psi}}^{\rho=R_1} \tag{154}$$

Upon substituting (135) and (136) into (154) one obtains,

$$L = \frac{\mu_0 R_1 \cos\psi}{\tau}\left\{\frac{1}{2}\left(1-\frac{R_1^2}{R_2^2}\right)+\tan^2\psi\cdot\log_e\frac{R_2}{R_1} - 2\sum_{m=1}^{\infty}\left[1-G_m'\right]K_m'(bR_1)I_m'(bR_1)\cos\left(\frac{br}{\cos\psi}\right)\right\} \tag{155}$$

If μ_0 is the permeability of free space expressed in the units of the rationalized MKS system, the inductance given by (155) is henries per meter in the helix direction.

C-7 Approximate Expressions for Close Wound Helices

For the case where $R_2/R_1 > 1.25$ and $R_1/\tau > 1$ the helix may be defined as being close wound. This definition is not based upon physical appearance, but upon the fact that under these conditions the expression (155) can be written in closed form. Thus, for τ small, the expression under the summation sign becomes, very closely,

$$\left\{\left[1-G_m'\right]I_m'(bR_1)K_m'(bR_1)\right\} \equiv -\frac{\tan^2\psi}{2m\sin\psi} \tag{156}$$

When this is substituted into (155) and use made of formula 603.2 on page 132 of reference (4),

$$L = \frac{\mu_0 R_1 \cos\psi}{2}\left\{\frac{1}{2}\left(1-\frac{R_1^2}{R_2^2}\right)+\tan^2\psi\left[\log_e\frac{R_2}{R_1}-\frac{1}{\sin\psi}\log_e\left(2\sin\left(\frac{\pi r}{\tau\cos\psi}\right)\right)\right]\right\} \tag{157}$$

This is the inductance per meter in the helix direction. If the inductance per meter in the axial direction is desired, the above expression must be divided by $\sin\psi$. Denoting the inductance per unit length in the axial direction by L_z , there follows that,

$$L_z = 2\pi\mu_0\left(\frac{R_1}{\tau}\right)^2\left\{\frac{1}{2}\left(1-\frac{R_1^2}{R_2^2}\right)+\tan^2\psi\left[\log_e\frac{R_2}{R_1}-\frac{1}{\sin\psi}\log_e\left(2\sin\left(\frac{\pi r}{\tau\cos\psi}\right)\right)\right]\right\} \tag{158}$$

C-8 Approximate Expression for Coarse Helices

As the pitch of the helix becomes very large, it degenerates into a transmission line in which the inner conductor is parallel to the axis of the sheath and distant from it by R_1. Upon allowing τ to approach infinity, (155) becomes,

$$L_z = \frac{\mu_0}{2\pi}\left\{\log_e\frac{R_2}{R_1}+\sum_{m=1}^{\infty}\left[1-\left(\frac{R_1}{R_2}\right)^{2m}\right]\frac{\cos\left(\frac{mr}{R_1}\right)}{m}\right\} \tag{159}$$

This can be expressed in closed form by applying formula 418 on page 85 of reference (4). Upon doing this and also recognizing that r/R_1 is very small,

$$L_2 = \frac{\mu_0}{2\pi} \left\{ \log_e \frac{R_2}{r} \left(1 - \frac{R_1^2}{R_2^2} \right) \right\} \qquad (160)$$

Appendix D

The Wave Equation

In this appendix, a tape helix is considered in an attempt to solve the wave equation. In particular, if the helix is assumed to be wound of a very thin tape, exact expressions for the fields can be obtained in terms of the surface current density. An exact formal solution is obtained for the tape helix, but the completion of this solution requires the solving for the roots of a determinantal equation in the form of an infinite determinant. By assuming that the tape is so wide as to result in a butt helix, this determinant reduces to a 1x1 determinant and the propagation constant can be found. It is shown further that such a helix is dispersive and as a consequence one might expect a close wound wire helix to also be dispersive.

D-1 Maxwell's Equation and the Vector Potentials

In the nonconducting, charge free medium surrounding the tape helix, the electric and magnetic fields with harmonic variation must satisfy the Maxwell equations,

$$\nabla \times \underline{E} = -j\omega\mu \underline{H} \tag{1}$$

$$\nabla \times \underline{H} = j\omega\epsilon \underline{E} \tag{2}$$

$$\nabla \cdot (\mu \underline{H}) = 0 \tag{3}$$

$$\nabla \cdot (\epsilon \underline{E}) = 0 \tag{4}$$

where $\underline{E}$ and $\underline{H}$ are, respectively, the electric and magnetic field intensities. The medium which is nonconducting homogeneous, isotropic and linear is characterized by the permeability μ and permittivity ϵ.

From (1) and (2) the wave equations follow,

$$\nabla \times \nabla \times \underline{H} - \beta_0^2 \underline{H} = 0 \tag{5}$$

$$\nabla \times \nabla \times \underline{E} - \beta_0^2 \underline{E} = 0 \tag{6}$$

where,

$$\beta_0^2 = \omega^2 \mu \epsilon \tag{7}$$

These are most conveniently solved in terms of two vector potential functions such that

$$\underline{H} = \nabla \times \underline{A} \tag{8}$$

$$\underline{E} = \nabla \times \underline{F} \tag{9}$$

In (8) and (9), $\underline{A}$ and $\underline{F}$ are vector potential functions from which may be derived the electric and magnetic fields. For harmonically varying fields, these vector potentials are related to the Herztian vectors by a simple factor of proportionality. Equation (8) will be solved in the circular cylindrical coordinate system as defined in Appendix B. The solution to (9) will be similar. In both (8) and (9), it will be assumed that only the z component of the vector potentials exists, since it has been shown that any wave may be synthesized from the two solutions based upon this assumption. (See reference 1, page 351).

Substituting (8) into (5) there results,

$$\nabla \times \left\{ \nabla \times \nabla \times \underline{A} - \beta_0^2 \underline{A} \right\} = 0$$

from which,

$$\nabla \times \nabla \times \underline{A} - \beta_0^2 \underline{A} = \nabla \Phi$$

where Φ is any arbitrary scalar function of ρ, ϕ and z. Now if it is assumed that $A_\rho = A_\phi = 0$, the following may be used, since A_z is a rectangular component of the vector

$$\left[\nabla \times \nabla \times \underline{A} \right]_z = \left[\nabla (\nabla \cdot \underline{A}) \right]_z - \nabla^2 A_z$$

and consequently,

$$\left[\nabla (\nabla \cdot \underline{A}) \right]_z - \nabla^2 A_z - \beta^2 A_z = \left[\nabla \Phi \right]_z$$

If the arbitrary scalar function Φ is defined as,

$$\Phi = \nabla \cdot \underline{A}$$

(15)

and has as its

(16)

of simplicity.

(17)

valued function
zero. The I_m
irst and
lied to a
lic properties
fields are
fields experi-
clear since,
, it coin-
w by only
form of a

$$\epsilon^{-j\beta z} \cdot \epsilon^{-j\frac{2n\pi}{\tau}z} = \epsilon^{-j\delta_n z} \tag{18}$$

where δ_n is given by

$$\delta_n = \beta + \frac{2n\pi}{\tau} \tag{19}$$

An additional requirement due to the periodicity of the helix is that if one moves at a fixed radius on the surface of a helicoid defined by $\left(\frac{2\pi z}{\tau} - \phi\right)$ = constant, the fields are multiplied by only some complex constant. Thus the n of (18) and (19) must equal the m of (16) which can now be written in the form,

$$A_z = \begin{Bmatrix} I_m(\gamma_m \rho) \\ K_m(\gamma_m \rho) \end{Bmatrix} \epsilon^{-j\beta z} \epsilon^{-j\left(\frac{2m\pi}{\tau}z - m\phi\right)} \tag{20}$$

Further, since the complete set of functions must be used to satisfy the boundary conditions and since the field equations are linear so that elementary solutions can be added, the representation for A_z becomes,

$$A_z = \epsilon^{-j\beta z} \sum_{m=1} \left[A_m I_m(\gamma_m \rho) + B_m K_m(\gamma_m \rho)\right] \epsilon^{-j\left(\frac{2m\pi}{\tau}z - m\phi\right)} \tag{21}$$

where the constants A_m and B_m are determined by boundary conditions. In exactly the same manner, the vector potential F_z can be written

$$F_z = \epsilon^{-j\beta z} \sum_m \left[C_m I_m(\gamma_m \rho) + D_m K_m(\gamma_m \rho) \right] \epsilon^{-j\left(\frac{2m\pi}{\phi} z - m\phi\right)} \tag{22}$$

From (21) a set of $\underline{E}$ and $\underline{H}$ vectors can be derived, which set is defined as a transverse magnetic mode. From (22) a set of $\underline{E}$ and $\underline{H}$ vectors can be derived; in this case, the set defining what is called a transverse electric mode. The electromagnetic field obtained by superposing the transverse magnetic and transverse electric fields is of such generality that one can satisfy a prescribed set of boundary conditions on any cylindrical surface whose generating elements are parallel to the z axis.

Let regions 1, 2 and 3 be defined as follows:

region 1 corresponds to $0 \leq \rho \leq R_1$ (23)

region 2 corresponds to $R_1 \leq \rho \leq R_2$ (24)

region 3 corresponds to $R_2 \leq \rho < \infty$ (25)

Then, because of the known singularities of the Bessel functions, the vector potentials in these regions are,

$$A_{z1} = \epsilon^{-j\beta z} \sum_m \left[A_m I_m(\gamma_m \rho) \right] \epsilon^{-j(bz - m\phi)} \tag{26}$$

$$F_{z1} = \epsilon^{-j\beta z} \sum_m \left[C_m I_m(\gamma_m \rho) \right] \epsilon^{-j(bz - m\phi)} \tag{27}$$

$$A_{z2} = \epsilon^{-j\beta z} \sum_m \left[A_{m2} I_m(\gamma_m \rho) + B_{m2} K_m(\gamma_m \rho) \right] \epsilon^{-j(bz - m\phi)} \tag{28}$$

$$F_{z2} = \epsilon^{-j\beta z} \sum_m \left[C_{m2} I_m(\gamma_m \rho) + D_{m2} K_m(\gamma_m \rho) \right] \epsilon^{-j(bz - m\phi)} \tag{29}$$

$$A_{z3} = \epsilon^{-j\beta z} \sum_m \left[B_{m3} K_m(\gamma_m \rho) \right] \epsilon^{-j(bz - m\phi)} \tag{30}$$

$$F_{z3} = \epsilon^{-j\beta z} \sum_m \left[D_{m3} K_m(\gamma_m \rho) \right] \epsilon^{-j(bz - m\phi)} \tag{31}$$

where,

$$b = \frac{2m\pi}{\tau} \tag{32}$$

Now, from (1), (2) and (11), the total electric and magnetic fields are,

$$H_\rho = \frac{1}{\rho} \frac{\partial A_z}{\partial \phi} - \frac{1}{j\omega\mu} \frac{\partial^2 F_z}{\partial \rho \partial z} \tag{33}$$

$$H_z = -\frac{\partial A_z}{\partial \rho} - \frac{1}{j\omega\mu} \frac{1}{\rho} \frac{\partial^2 F_z}{\partial \phi \partial z} \tag{34}$$

$$H_z = \frac{\gamma_m^2}{j\omega\mu} F_z \tag{35}$$

$$E_\rho = \frac{1}{\rho}\frac{\partial F_z}{\partial \phi} + \frac{1}{j\omega\epsilon}\frac{\partial^2 A_z}{\partial \rho\, \partial z} \tag{36}$$

$$E_\phi = -\frac{\partial F_z}{\partial \rho} + \frac{1}{j\omega\epsilon}\cdot\frac{1}{\rho}\frac{\partial^2 A_z}{\partial \phi\, \partial z} \tag{37}$$

$$E_z = -\frac{\gamma_m^2}{j\omega\epsilon} A_z \tag{38}$$

Equations (26) to (38) define the electromagnetic fields in regions (1), (2) and (3) in terms of the constants A_m to D_m. These constants must be found from the boundary conditions.

D-2. The Boundary Conditions

There are two boundaries at which the electric and magnetic fields must satisfy certain boundary conditions. These are at the surface of the shield defined by $\rho = R_2$ and at the surface of the tape defined by,

$$\left\{ \begin{array}{c} \rho = R_1 \\ -\frac{a}{\cos\psi} < \left(z - \frac{\phi}{2\pi}\tau\right) < \frac{a}{\cos\psi} \end{array} \right\} \tag{39}$$

where the tape width perpendicular to its edge is 2a and the helix angle is ψ. The center line of the helix is assumed to pass through z = 0

when $\phi = 0$. No generality is lost by so assuming.

At the shield, since it is assumed to be perfectly conducting, the tangential component of electric field must vanish everywhere. When this is satisfied, the normal component of magnetic field will automatically satisfy the condition that it vanish. This follows immediately from (1).

For all ρ greater than R_2, both the electric and magnetic fields must vanish since the shield is assumed to be perfectly conducting. At the radius R_1 the tangential component of electric field must be continuous everywhere, and the discontinuity of the tangential component of the magnetic field must equal the total surface current density. That is,

$$E_z = H_z = 0 \; ; \; \rho > R_2 \tag{40}$$

$$E_{\phi 2} = E_{z2} = 0 \; ; \; \rho = R_2 \tag{41}$$

$$E_{\phi 1} = E_{\phi 2} \; ; \; \rho = R_1 \tag{42}$$

$$E_{z1} = E_{z2} \; ; \; \rho = R_1 \tag{43}$$

$$(H_{z1} - H_{z2}) = J_\phi \; ; \; \rho = R_1 \tag{44}$$

$$(H_{\phi 2} - H_{\phi 1}) = J_z \; ; \; \rho = R_1 \tag{45}$$

where J_ϕ and J_z are the total surface current densities in the ϕ and z directions respectively. It is natural to expect that these current densities would have the same form as the vector potentials, consequently we may write,

$$J_\phi = \epsilon^{-j\beta z} \sum_m J_{\phi m} \epsilon^{-j(bz - m\phi)} \tag{46}$$

$$J_z = \epsilon^{-j\beta z} \sum_m J_{zm} \epsilon^{-j(bz-m\phi)} \tag{47}$$

where $J_{\phi m}$ and J_{zm} are the Fourier coefficients of the current density distribution. Before making use of conditions (40) to (47), it is desirable to have the electric and magnetic fields in regions (1) and (2) written explicitly. These are,

$$H_{\rho 1} = j\epsilon^{-j\beta z} \sum_m \left[\frac{m}{\rho} A_{m1} I_m(\gamma_m \rho) + \frac{\gamma_m \delta_m}{j\omega\mu} C_{m1} I_m'(\gamma_m \rho) \right] \epsilon^{-j(bz-m\phi)} \tag{48}$$

$$H_{\phi 1} = -j\epsilon^{-j\beta z} \sum_m \left[\gamma_m A_{m1} I_m'(\gamma_m \rho) + \frac{m}{\rho} \frac{\delta_m}{j\omega\mu} C_{m1} I_m(\gamma_m \rho) \right] \epsilon^{-j(bz-m\phi)} \tag{49}$$

$$H_{z1} = \epsilon^{-j\beta z} \sum_m \left[\frac{\gamma_m^2}{j\omega\mu} C_{m1} I_m(\gamma_m \rho) \right] \epsilon^{-j(bz-m\phi)} \tag{50}$$

$$E_{\rho 1} = j\epsilon^{-j\beta z} \sum_m \left[\frac{m}{\rho} C_{m1} I_m(\gamma_m \rho) - \frac{\gamma_m \delta_m}{j\omega\epsilon} A_{m1} I_m'(\gamma_m \rho) \right] \epsilon^{-j(bz-m\phi)} \tag{51}$$

$$E_{\phi 1} = -\epsilon^{-j\beta z} \sum_m \left[\gamma_m C_{m1} I_m'(\gamma_m \rho) - \frac{m}{\rho} \frac{\delta_m}{j\omega\epsilon} A_{m1} I_m(\gamma_m \rho) \right] \epsilon^{-j(bz-m\phi)} \tag{52}$$

$$E_{z1} = -\epsilon^{-j\beta z} \sum_m \left[\frac{\gamma_m^2}{j\omega\epsilon} A_{m1} I_m(\gamma_m \rho) \right] \epsilon^{-j(bz-m\phi)} \tag{53}$$

$$H_{\rho 2}=\frac{1}{\rho}\epsilon^{-j\beta z}\sum_m\left\{\frac{m}{\rho}\left[A_{m2}I_m(\gamma_m\rho)+B_{m2}K_m(\gamma_m\rho)\right]+\frac{\gamma_m\delta_m}{j\omega\mu}\left[C_{m2}I_m'(\gamma_m\rho)+D_{m2}K_m'(\gamma_m\rho)\right]\right\}\epsilon^{-j(bz-m\phi)} \tag{54}$$

$$H_{\phi 2}=-j\epsilon^{-j\beta z}\sum_m\left\{\gamma_m\left[A_{m2}I_m'(\gamma_m\rho)+B_{m2}K_m'(\gamma_m\rho)\right]+\frac{m}{\rho}\frac{\delta_m}{j\omega\mu}\left[C_{m2}I_m(\gamma_m\rho)+D_{m2}K_m(\gamma_m\rho)\right]\right\}\epsilon^{-j(bz-m\phi)} \tag{55}$$

$$H_{z2}=\epsilon^{-j\beta z}\sum_m\left\{\frac{\gamma_m^2}{j\omega\mu}\left[C_{m2}I_m(\gamma_m\rho)+D_{m2}K_m(\gamma_m\rho)\right]\right\}\epsilon^{-j(bz-m\phi)} \tag{56}$$

$$E_{\rho 2}=j\epsilon^{-j\beta z}\sum_m\left\{\frac{m}{\rho}\left[C_{m2}I_m(\gamma_m\rho)+D_{m2}K_m(\gamma_m\rho)\right]-\frac{\gamma_m\delta_m}{j\omega\epsilon}\left[A_{m2}I_m'(\gamma_m\rho)+B_{m2}K_m'(\gamma_m\rho)\right]\right\}\epsilon^{-j(bz-m\phi)} \tag{57}$$

$$E_{\phi 2}=-\epsilon^{-j\beta z}\sum_m\left\{\gamma_m\left[C_{m2}I_m'(\gamma_m\rho)+D_{m2}K_m'(\gamma_m\rho)\right]-\frac{m}{\rho}\frac{\delta_m}{j\omega\epsilon}\left[A_{m2}I_m(\gamma_m\rho)+B_{m2}K_m(\gamma_m\rho)\right]\right\}\epsilon^{-j(bz-m\phi)} \tag{58}$$

$$E_{z2}=-\epsilon^{-j\beta z}\sum_m\left\{\frac{\gamma_m^2}{j\omega\epsilon}\left[A_{m2}I_m(\gamma_m\rho)+B_{m2}K_m(\gamma_m\rho)\right]\right\}\epsilon^{-j(bz-m\phi)} \tag{59}$$

From (35), (38) and (40), there follows immediately that B_{m3} and D_{m3} of (30) and (31) are identically zero. From (41), (42) and (43), there follows,

$$A_{m1}=\left[1-\frac{I_m(\gamma_m R)K_m(\gamma_m R_1)}{I_m(\gamma_m R_1)K_m(\gamma_m R)}\right]A_{m3}^e=\left[1-G_m\right]A_{m2}^e \tag{}$$

$$A_{m2} = -\frac{I_m(\gamma_m R_1) K_m(\gamma_m R_1)}{I_m(\gamma_m R_2) K_m(\gamma_m R_1)} A^*_{m2} = -G_m A^*_{m2} \tag{61}$$

$$B_{m2} = \frac{I_m(\gamma_m R_1)}{K_m(\gamma_m R_1)} A^*_{m2} \tag{62}$$

$$C_{m1} = \left[1 - \frac{I'_m(\gamma_m R) K'_m(\gamma_m R_2)}{I_m(\gamma_m R_1) K'_m(\gamma_m R_1)}\right] C^*_{m2} = \left[1 - G'_m\right] C^*_{m2} \tag{63}$$

$$C_{m2} = -\frac{I'_m(\gamma_m R_1) K'_m(\gamma_m R_2)}{I'_m(\gamma_m R_2) K'_m(\gamma_m R_1)} C^*_{m2} = -G'_m C^*_{m2} \tag{64}$$

$$D_{m2} = \frac{I'_m(\gamma_m R_1)}{K'_m(\gamma_m R_1)} C^*_{m2} \tag{65}$$

where A^*_{m2} and C^*_{m2} have been introduced as a matter of convenience. The definitions of the G_m and G'_m functions are obvious from (60) and (63). From (44), (45), (46) and (47), the constants A^*_{m2} and $C_{m2}{}^*$ can be evaluated in terms of the Fourier coefficients $J_{\phi m}$ and $J_{\xi m}$. Use is made of the orthogonality of the space harmonics for $-\pi \leq \phi \leq \pi$ and $\frac{-\tau}{2} \leq z \leq \frac{\tau}{2}$. These two constants are,

$$A^*_{m2} = R_1 K_m(\gamma_m R_1)\left[J_{\xi m} - \frac{m \delta_m}{R_1 \gamma_m^2} J_{\phi m}\right] \tag{66a}$$

$$C^*_{m2} = -\frac{j\omega\mu}{\gamma_m} R_1 K'_m(\gamma_m R_1) J_{\phi m} \tag{66b}$$

Using (59) to (66), the electric and magnetic fields in regions (1) and (2) become

$$H_{\rho 1} = \; j\epsilon^{-j\beta z}\sum_m \left\{ \frac{mR_1}{\rho}\left[\frac{1}{\epsilon_1}-G_m\right]\left[J_{zm}-\frac{m\delta_m}{R_1\gamma_m^2}J_{\phi m}\right]K_m(\gamma_m R_1)I_m \right.$$
$$\left. -\delta_m R\left[\frac{1}{\epsilon_1}-G_m\right]K_m'(\gamma_m R_1)I_m' J_{\phi m} \right\}\epsilon^{-j(bz-m\phi)} \qquad (67)$$

$$H_{\phi 1} = \; -\epsilon^{-j\beta z}\sum_m \left\{ \gamma_m R_1\left[\frac{1}{\epsilon_1}-G_m\right]\left[J_{zm}-\frac{m\delta_m}{R_1\gamma_m^2}J_{\phi m}\right]K_m(\gamma_m R_1)I_m' \right.$$
$$\left. -\frac{mR_1}{\rho}\cdot\frac{\delta_m}{\gamma_m}\left[\frac{1}{\epsilon_1}-G_m'\right]J_{\phi m}K_m'(\gamma_m R_1)I_m \right\}\epsilon^{-j(bz-m\phi)} \qquad (68)$$

$$H_{z1} = \; -\epsilon^{-j\beta z}\sum_m \left\{ \gamma_m R_1\left[\frac{1}{\epsilon_1}-G_m'\right]J_{\phi m}K_m'(\gamma_m R_1)I_m \right\}\epsilon^{-j(bz-m\phi)} \qquad (69)$$

$$E_{\rho 1} = \sqrt{\frac{\mu}{\epsilon}}\,\epsilon^{-j\beta z}\sum_m \left\{ \frac{mR_1}{\rho}\frac{\beta_0}{\gamma_m}\left[\frac{1}{\epsilon_1}-G_m'\right]J_{\phi m}K_m(\gamma_m R_1)I_m \right.$$
$$\left. -\delta_m R_1\frac{\gamma_m}{\beta_0}\left[\frac{1}{\epsilon_1}-G_m\right]\left[J_{zm}-\frac{m\delta_m}{R_1\gamma_m^2}J_{\phi m}\right]K_m(\gamma_m R_1)I_m' \right\}\epsilon^{-j(bz-m\phi)} \qquad (70)$$

$$E_{\phi 1} = j\sqrt{\frac{\mu}{\epsilon}}\,\epsilon^{-j\beta z}\sum_m \left\{ \beta R_1\left[\frac{1}{\epsilon_1}-G_m'\right]J_{\phi m}K_m'(\gamma_m R_1)I_m' \right.$$
$$\left. -m\frac{\delta_m R_1}{\rho_0\rho}\left[\frac{1}{\epsilon_1}-G_m\right]\left[J_{zm}-\frac{m\delta_m}{R_1\gamma_m^2}J_{\phi m}\right]K_m(\gamma_m R_1)I_m \right\}\epsilon^{-j(bz-m\phi)} \qquad (71)$$

$$E_{z1} = j\sqrt{\frac{\mu}{\epsilon}}\,\epsilon^{-j\beta z}\sum_m \left\{ \frac{\gamma_m^2 R_1}{\beta_0}\left[\frac{1}{\epsilon_1}-G_m\right]\left[J_{zm}-\frac{m\delta_m}{R_1\gamma_m^2}J_{\phi m}\right]K_m(\gamma_m R_1)I_m \right\}\epsilon^{-j(bz-m\phi)} \qquad (72)$$

$$H_{\rho 2} = \; j\epsilon^{-j\beta z}\sum_m \left\{ \frac{mR_1}{\rho}\left[K_m-\frac{K_m(\gamma_m R_1)}{I_m(\gamma_m R_1)}I_m\right]\left[J_{zm}-\frac{m\delta_m}{R_1\gamma_m^2}J_{\phi m}\right]I_m(\gamma_m R_1) \right.$$
$$\left. -\delta_m R_1\left[K_m'-\frac{K_m'(\gamma_m R_1)}{I_m'(\gamma_m R_1)}I_m'\right]J_{\phi m}I_m'(\gamma_m R) \right\}\epsilon^{-j(bz-m\phi)} \qquad (73)$$

$$H_{\phi 2} = -\epsilon^{-j\beta z}\sum_m \left\{ \gamma_m R_2 \left[K_m' - \frac{K_m(\gamma_m R_2)}{I_m(\gamma_m R_2)} I_m'\right]\left[J_{zm} - \frac{m\delta_m}{R\gamma_m^2} J_{\phi m}\right] I_m(\gamma_m R) \right.$$
$$\left. - m\frac{\delta_m R_1}{\gamma_m \rho}\left[K_m - \frac{K_m(\gamma_m R_2)}{I_m(\gamma_m R_2)} I_m\right] J_{zm} I_m'(\gamma_m R) \right\} \epsilon^{-j(bz - m\phi)} \quad (74)$$

$$H_{\rho 2} = -\epsilon^{-j\beta z}\sum_m \left\{ \gamma_m R_1 \left[K_m - \frac{K_m'(\gamma_m R_2)}{I_m'(\gamma_m R_2)} I_m\right] J_{\phi m} I_m'(\gamma_m R_1) \right\} \epsilon^{-j(bz - m\phi)} \quad (75)$$

$$E_{\rho 2} = \sqrt{\frac{\mu}{\epsilon}}\epsilon^{-j\beta z}\sum_m \left\{ m\frac{R\beta}{\rho\gamma_m}\left[K_m - \frac{K_m'(\gamma_m R_2)}{I_m'(\gamma_m R_2)} I_m\right] J_{\phi m} I_m'(\gamma_m R) \right.$$
$$\left. - \delta_m R \frac{\gamma_m}{\beta}\left[K_m' - \frac{K_m(\gamma_m R_2)}{I_m(\gamma_m R_2)} I_m'\right]\left[I_{zm} - \frac{m\delta_m}{R\gamma_m^2} J_{\phi m}\right] I_m(\gamma_m R) \right\} \epsilon^{-j(bz - m\phi)} \quad (76)$$

$$E_{\phi 2} = j\sqrt{\frac{\mu}{\epsilon}}\epsilon^{-j\beta z}\sum_m \left\{ \beta R_1 \left[K_m' - \frac{K_m'(\gamma_m R_2)}{I_m'(\gamma_m R_2)} I_m\right] J_{\phi m} I_m'(\gamma_m R) \right.$$
$$\left. - m\frac{\delta_m R_1}{\beta\rho}\left[K_m - \frac{K_m(\gamma_m R_2)}{I_m(\gamma_m R_2)} I_m\right]\left[J_{zm} - \frac{m\delta_m}{R_1\gamma_m^2} J_{\phi m}\right] I_m(\gamma_m R_1) \right\} \epsilon^{-j(bz - m\phi)} \quad (77)$$

$$E_{z 2} = j\sqrt{\frac{\mu}{\epsilon}}\epsilon^{-j\beta z}\sum_m \left\{ \frac{R\gamma_m^2}{\beta}\left[K_m - \frac{K_m(\gamma_m R_2)}{I_m(\gamma_m R_2)} I_m\right]\left[I_{zm} - \frac{m\delta_m}{R\gamma_m^2} J_{\phi m}\right] I_m(\gamma_m R_1) \right\} \epsilon^{-j(bz - m\phi)} \quad (78)$$

In the foregoing equations and in what follows, where the arguments of the Bessel functions are omitted, it is understood that these missing arguments are ($\gamma_m \rho$).

It can easily be demonstrated that (67) through (78) satisfy Maxwell's equation as well as the continuity conditions (41) through (45). In addition, they are single valued bounded functions having the proper form to represent the fields surrounding a uniform shielded helix. They are made up of a complete set of functions in ϕ and z assuring that the final boundary condition at $\rho = R_1$ can be met. This remaining boundary

condition is that the tangential component of the electric field be zero at the tape. That is,

$$E_\phi = 0 \tag{79}$$

$$E_z = 0 \tag{80}$$

both for $\left\{ \begin{array}{c} \rho = R_1 \\ -\frac{a}{\cos\psi} \leq \left(z - \frac{\phi}{2\pi}\tau\right) \leq \frac{a}{\cos\psi} \end{array} \right\}$

It will now be assumed that Fourier expansions exist for E_ϕ and E_z at R_1 over the interval $\left(\frac{\phi}{2\pi}\tau - \frac{a}{\cos\psi}\right) \leq z \leq \left(\frac{\phi}{2\pi}\tau + \frac{a}{\cos\psi}\right)$ and for $-\pi \leq \phi \leq \pi$ of the form,

$$E_\phi = j\sqrt{\frac{\mu}{\epsilon}}\, \epsilon^{-j\beta z} \sum_m \alpha_{\phi n}\, \epsilon^{-j\frac{r\cos\psi}{2a}(b'z - n\phi)} \tag{81}$$

$$E_z = j\sqrt{\frac{\mu}{\epsilon}}\, \epsilon^{-j\beta z} \sum_m \alpha_{zn}\, \epsilon^{-j\frac{r\cos\psi}{2a}(b'z - n\phi)} \tag{82}$$

where $\alpha_{\phi n}$ and α_{zn} are proportional to the Fourier coefficients of the electric field expansions. The coefficient b' is equal to $\frac{2n\pi}{\tau}$.

Equating corresponding components given in (71) and (72) with (81) and (82) yields,

$$\sum_m \left\{ \beta_0 R [1-G_m] J_{zm} K_m'(\gamma_m R) I_m'(\gamma_m R) - \frac{m\delta_m}{\beta_0} [1-G_m] \left[J_{zm} - \frac{n\delta_m}{R\gamma_m^2} J_{\phi m} \right] K_m(\gamma_m R) I_m(\gamma_m R) \right\} \epsilon^{-j(bz-m\phi)}$$

$$= \sum_m \alpha_{\phi n} \epsilon^{-j\frac{\tau \cos\psi}{2a}(b'z - n\phi)} \tag{83}$$

$$\sum_m \left\{ \frac{R\gamma_m^2}{\beta_0} [1-G_m] \left[J_{zm} - \frac{m\delta_m}{R\gamma_m^2} J_{\phi m} \right] K_m(\gamma_m R) I_m(\gamma_m R) \right\} \epsilon^{-j(bz-m\phi)}$$

$$= \sum_m \alpha_{zn} \epsilon^{-j\frac{\tau \cos\psi}{2a}(b'z - n\phi)} \tag{84}$$

If (83) and (84) are multiplied through by $\epsilon^{+j q \frac{\tau \cos\psi}{2a}\left(\frac{2\pi}{\ell} z - \phi\right)}$ where q is an integer and then integrated from $z = \left(\frac{\phi}{2\pi}\ell - \frac{a}{\cos\psi}\right)$ to $z = \left(\frac{\phi}{2\pi}\ell + \frac{a}{\cos\psi}\right)$ keeping ϕ constant at any particular value, it is found that for n = q the right sides of (83) and (84) are non-zero. They become respectively,

$$\frac{2a}{\cos\psi} \alpha_{\phi q} \tag{85}$$

$$\frac{2a}{\cos\psi} \alpha_{zq} \tag{86}$$

Since it is known that E_z and E_ϕ are zero over the surface of the tape, the coefficients $\alpha_{\phi q}$ and α_{zq} themselves must be identically zero. Therefore (83) and (84) become,

$$\sum_{q=1}^{\infty}\left\{ AR\left[1-G_m'\right]J_{qm}K_m'(\gamma_m R_i)I_m'(\gamma_m R_i) - \frac{m\delta_m}{A_0}\left[1-G_m\right]\left[J_{qm}-\frac{m\delta_m}{R_i\gamma_m^2}J_{qm}\right]K_m(\gamma_m R_i)I_m(\gamma_m R_i)\right\}\frac{\sin\left[q-\frac{2ma}{\tau\cos\psi}\right]\pi}{\left[q-\frac{2ma}{\tau\cos\psi}\right]\pi} = 0 \quad (87)$$

$$\sum_{q\,m}\left\{\frac{R\gamma_m^2}{A_0}\left[1-G_m\right]\left[J_{qm}-\frac{m\delta_m}{R_i\gamma_m^2}J_{qm}\right]K_m(\gamma_m R_i)I_m(\gamma_m R_j)\right\}\frac{\sin\left[q-\frac{2ma}{\tau\cos\psi}\right]\pi}{\left[q-\frac{2ma}{\tau\cos\psi}\right]\pi} = 0 \quad (88)$$

Employing matrix notation, these might be expressed

$$\| Q_{qm} \| X \| J_{qm} \| = \| R_{qm} \| X \| J_{qm} \| \quad (89)$$

$$\| S_{qm} \| X \| J_{qm} \| = \| T_{qm} \| X \| J_{qm} \| \quad (90)$$

where $\| Q_{qm} \|$, $\| R_{qm} \|$, $\| S_{qm} \|$ and $\| T_{qm} \|$ are square matrices of infinite extent and $\| J_{qm} \|$ and $\| J_{qm} \|$ are infinite column matrices. The symbol X denotes the usual row on column multiplication. The elements of the coefficient matrices are,

$$Q_{qm} = \left\{ \frac{m^2 \delta_m^2}{\gamma_m^2} [1 - G_m] K_m(\gamma_m R_1) I_m(\gamma_m R_1) + \beta_0^2 R_1^2 [1 - G_m'] K_m'(\gamma_m R_1) I_m'(\gamma_m R_1) \right\} \frac{\sin \xi_{qm}}{\xi_{qm}} \tag{91}$$

$$R_{qm} = \left\{ m \delta_m R_1 [1 - G_m] K_m(\gamma_m R_1) I_m(\gamma_m R_1) \right\} \frac{\sin \xi_{qm}}{\xi_{qm}} \tag{92}$$

$$S_{qm} = \left\{ m \delta_m R_1 [1 - G_m] K_m(\gamma_m R_1) I_m(\gamma_m R_1) \right\} \frac{\sin \xi_{qm}}{\xi_{qm}} = R_{qm} \tag{93}$$

$$T_{qm} = \left\{ \gamma_m^2 R_1^2 [1 - G_m] K_m(\gamma_m R_1) I_m(\gamma_m R_1) \right\} \frac{\sin \xi_{qm}}{\xi_{qm}} \tag{94}$$

$$\xi_{qm} = \left[q - m \frac{2a}{T \cos \psi} \right] \pi T \tag{95}$$

Assuming that the usual matrix rules for q and m finite apply, and that $\|R_{qm}\|$ is not singular, from (89) one obtains,

$$\|R_{qm}\|^{-1} \times \|Q_{qm}\| \times \|\bar{J}_{\phi m}\| = \|J_{zm}\| \tag{96}$$

where $\|R_{qm}\|^{-1}$ is the inverse of $\|R_{qm}\|$ and,

$$\| R_{qm} \|^{-1} \times \| R_{qm} \| = \| U \| \tag{97}$$

$\| U \|$ is the infinite unit matrix with all the elements on the diagonal equal to unity and all the off diagonal elements equal to zero. Upon substituting (96) into (90) there results,

$$\left\{ \left\{ \| S_{qm} \| - \| T_{qm} \| \times \| R_{qm} \|^{-1} \times \| Q_{qm} \| \right\} \right\} \times \| J_{qm} \| = 0 \tag{98}$$

In order that (98) have a nontrivial solution, the determinant of the matrix inside the braces must vanish. That is,

$$\left| \| S_{qm} \| - \| T_{qm} \| \times \| R_{qm} \|^{-1} \times \| Q_{qm} \| \right| = 0 \tag{99}$$

Since it is presumed that R_1, R_2, τ , β_0 and a are known, (99) provides an equation from which the propagation constant β can be determined.

The method by which (99) was derived is essentially the same as that used by Sensiper for a helix in free space. This method has been modified to account for the effect of the perfectly conducting shield, and (99) reduces to the determinantal equation developed by Sensiper when R_2 is allowed to approach infinity.

This infinite determinantal equation of every great complexity presents intractable difficulties in obtaining an exact solution. Even a solution using perturbation methods would be of doubtful utility because

of the transcendental nature of the equation. Approximate solutions are available, however, by specifying that the tape be anisotropic to the extent that it can conduct only in the helix direction.

D-3 The Anisotropic Tape

In this section, it will be assumed that the tape can conduct only in the helix direction. This could be achieved practically by forming the tape of a great number of very small parallel wires insulated from each other. At low frequencies in a true tape, this situation would exist since the potential difference between turns would be small and there would be no tendency for current to flow perpendicular to the tape edges. In any event, this restriction modifies the boundary conditions (79) and (80) to read,

$$E_\phi \cos\psi + E_z \sin\psi = 0 \quad \text{at,} \tag{100}$$

$$\left\{ \begin{array}{c} \rho = R_i \\ -\frac{a}{\cos\psi} \leq \left(z - \frac{\phi}{2\pi} \tau\right) \leq \frac{a}{\cos\psi} \end{array} \right\}$$

In addition, the anisotropy of the tape requires,

$$\| \sin\psi \| \times \| J_{\phi m} \| = \| \cos\psi \| \times \| J_{zm} \| \tag{101}$$

where $\| \sin\psi \|$ and $\| \cos\psi \|$ are m by m matrices which have respectively $\sin\psi$ and $\cos\psi$ on the diagonal and zero off the diagonal. Employing the same procedure used in obtaining (89) and (90), the requirement of (100) leads to,

$$\| Q_{qm}\cos\psi - S_{qm}\sin\psi \| \times \| J_{\phi m} \| = \| R_{qm}\cos\psi - T_{qm}\sin\psi \| \times \| J_{zm} \| \qquad (102)$$

where $Q_{qm} \cdots T_{qm}$ are as defined in (91) . . . (95). By eliminating $\| J_{\phi m} \|$ formally from (101) and (102), there results

$$\left\{ \| \sin\psi \| \times \| Q_{qm}\cos\psi - S_{qm}\sin\psi \|^{-1} \times \| R_{qm}\cos\psi - T_{qm}\sin\psi \| - \| \cos\psi \| \right\} \times \| J_{zm} \| = 0 \qquad (103)$$

In order that (103) have a nontrivial solution, the determinant of the coefficient matrix must be zero. This will provide a determinantal equation from which formally the propagation constant β can be found. This determinantal equation is,

$$\left| \| \sin\psi \| \times \| Q_{qm}\cos\psi - S_{qm}\sin\psi \|^{-1} \times \| R_{qm}\cos\psi - T_{qm}\sin\psi \| - \| \cos\psi \| \right| = 0 \qquad (104)$$

This is again an infinite determinantal equation and would present considerable difficulties in its solution. There are two cases which can be evaluated exactly. These are the butted tape helix and the line helix.

D-4 The Butted Tape or Sheath Helix

If the anisotropic tape of section D-3 has a width such that the edges butt together, the helix loses all of its properties of periodicity with regard to z and ϕ. This is tantamount to making

$$J_{zm} = J_{\phi m} = 0 \quad , \quad m \neq 0 \tag{105}$$

$$J_{z0} \neq 0 \quad \text{and} \quad J_{\phi 0} \neq 0 \tag{106}$$

Under these conditions,

$$Q_{qm} = R_{qm} = S_{qm} = T_{qm} = 0 \quad \text{for } m \neq c \text{ and } q \neq 0 \tag{107}$$

$$Q_{00} = \beta_0^2 R_1^2 [1 - G_0'] K_0'(\gamma R) I_0'(\gamma R_1) \tag{108}$$

$$R_{00} = S_{00} = 0 \tag{109}$$

$$T_{00} = \gamma^2 R^2 [1 - G_0] K_0(\gamma R) I_0(\gamma R) \tag{110}$$

and (104) becomes,

$$\left[\frac{\gamma^2 R^2 [1 - G_0] K_0(\gamma R) I_0(\gamma R)}{\beta^2 R^2 [1 - G_0'] K_0'(\gamma R) I_0'(\gamma R)} \cdot \frac{\sin^2 \psi}{\cos \psi} + \cos \psi \right] = 0 \tag{111}$$

This is the same as equation (32) of Chapter II which was obtained by a slightly different procedure. The solution of this equation is discussed in Chapter II, it merely being sufficient to say here that it is transcendental and must be solved by numerical or graphical procedures. The solution

shows that for the butted tape helix, the phase velocity is a function of frequency, decreasing with increasing frequency. When β_0 is allowed to approach zero in (111) it is possible to solve directly for the phase velocity in the axial direction for very low frequencies. Upon doing this, there results,

$$\frac{v_p}{v_0} = \frac{1}{\sqrt{1 - \frac{(1-R_1^2/R_2^2)\cot^2\psi}{2\log_e(R_2/R_1)}}} \tag{112}$$

D-5 The Very Narrow Tape Helix

(a) Phase Velocity

If the width of the anisotropic tape is made very small compared to the pitch, the factor ($\frac{\sin \xi_{qm}}{\xi_{qm}}$) in (71) to (74) will become approximately,

$$\frac{\sin \xi_{qm}}{\xi_{qm}} \cong \left\{ \begin{array}{ll} 1 & \text{for } q=0 \\ 0 & \text{for } q \neq 0 \end{array} \right\} \tag{113}$$

Under these conditions, Q_{qm} , R_{qm} , S_{qm} and T_{qm} become zero for q not equal to zero and,

$$Q_{om} \cong \left\{ \frac{\mu_1 \varepsilon_2 \beta_m^2}{\gamma_m^2} \left[1 - G_m \right] K_m(\gamma_m R_1) I_m(\gamma_m R_1) + \beta_0^2 R_1^2 \left[1 - G_m' \right] K_m'(\gamma_m R_1) I_m'(\gamma_m R_1) \right\} \tag{114}$$

$$R_{om} = S_{om} = \left\{ m \delta_m R_1 [1 - G_m] K_m(\gamma_m R_1) I_m(\gamma_m R_1) \right\} \tag{115}$$

$$T_{om} = \left\{ \gamma_m^2 R_1^2 [1 - G_m] K_m(\gamma_m R_1) I_m(\gamma_m R_1) \right\} \tag{116}$$

Substituting these into (102) and making use of (101), there results,

$$\sum_m \left\{ \left[\frac{m^2 \cot^2 \psi}{\gamma_m^2 R_1^2} + \left(\frac{\beta^2}{A^2} - 1 \right) \right] [1 - G_m] I_m(\gamma_m R_1) K_m(\gamma_m R_1) + \cot^2 \psi [1 - G_m'] I_m'(\gamma_m R_1) K_m'(\gamma_m R_1) \right\} J_{\phi m} = 0 \tag{117}$$

This is a determinantal equation from which β can be found provided the current density distribution across the tape is known. Since the tape is extremely narrow with respect to the pitch, it would not be too great an error to assume that the current density is uniformly distributed across the tape. Thus, $J_{\phi m}$ would have the form,

$$J_{\phi m} = \frac{\sin\left(\frac{2m\pi a}{\tau \cos\psi}\right)}{\left(\frac{2m\pi a}{\tau \cos\psi}\right)} = \frac{\sin m\xi}{m\xi} \tag{118}$$

where, $\xi = \left(\frac{2\pi a}{\tau \cos\psi}\right)$

This assumption with regard to the Fourier coefficients is tantamount to assuming that the lines of constant phase front of the current

density distribution on the helix occur for constant ϕ. This is quite satisfactory for very narrow helices. Equation (117) could also be written with J_{zm} replacing $J_{\phi m}$ and the form of (116) used for the J_{zm}, leading to the same result. Since the actual constant phase front of the current density must lie between the two extremes z = constant and ϕ = constant, it seems likely that the conditions of (117) and (118) will lead to satisfactory results. Equation (117) is essentially the equivalent of the determinantal equation arrived at by Sensiper for a helix in free space by a more cumbersome process. This can be solved for the case $\beta_0 \to 0$, that is, for the very low frequency case.

Let

$$\beta_0 = \frac{\omega}{v_0} \tag{119}$$

$$\beta = \frac{\omega}{v_z} \tag{120}$$

where v_0 is the velocity of light in a medium characterized by μ and ϵ, and v_z is the phase velocity of the propagated wave in the axial direction.

Then,

$$\frac{\beta^2}{\beta_0^2} = \frac{v_0^2}{v_z^2} \tag{121}$$

This fraction will remain finite and non-zero as β and β_0 approach zero. Equation (117) can be written in the following form by making use of the approximations available in Appendix A. It should be noted that

the $m = 0$ term has been written separately and that the summation has been performed from 1 to ∞ and multiplied by 2.

$$\left[\left(\frac{\beta^2}{\beta_0^2}-1\right)\log_e\frac{R_2}{R_1}-\frac{1}{2}\left(1-\frac{R_1^2}{R_2^2}\right)\cot^2\psi\right] + 2\sum_{m=1}^{\infty}\left[\frac{\beta^2}{\beta_0^2}\sin\psi-\frac{1}{\sin\psi}\right]\frac{\sin m\Xi}{2m^2\Xi} \tag{122}$$

This equation holds strictly for $\beta_0 = 0$, but it should be useful for low frequencies in general. From reference (2), page 58,

$$\sum_{m=1}^{\infty}\frac{\sin m\Xi}{m^2\Xi} = 1-\log_e\Xi+\frac{1}{18}\left(\frac{\Xi}{2}\right)^2+\frac{1}{900}\left(\frac{\Xi}{2}\right)^4+\cdots \tag{123}$$

For the range of Ξ from 0 to π this can be written to a high degree of accuracy as,

$$\sum_{m=1}^{\infty}\frac{\sin m\Xi}{m^2\Xi} \cong \log_e\left(\frac{e}{\Xi}\right)+\frac{\Xi^2}{e^8} \tag{124}$$

Using (124), equation (123) becomes after some algebraic manipulations,

$$\left[\left(1-\frac{v_0^2}{v_z^2}\right)S_1+1\right]\sin\psi+\left[1-\frac{v_0^2}{v_z^2}\sin^2\psi\right]S_2=0 \qquad (125)$$

where,

$$S_1=\frac{2\log_e\left(R_2/R_1\right)}{\left(1-\frac{R_1^2}{R_2^2}\right)\cot^2\psi} \qquad (126)$$

$$S_2=\frac{2\log_e\left(\frac{\epsilon}{\delta}\right)+\left(\frac{\delta^2}{34}\right)}{\left(1-\frac{R_1^2}{R_2^2}\right)\cot^2\psi} \qquad (127)$$

Upon solving (125) for $\frac{v_z}{v_0\sin\psi}$, there results,

$$\frac{v_z}{v_0\sin\psi}=\sqrt{\frac{S_1+S_2\sin\psi}{\left(1+S_1\right)\sin^2\psi+S_2\sin\psi}} \qquad (128)$$

If δ is allowed to approach T, the helix becomes a butt wound tape. In this case, S_2 becomes zero and (128) reduces to the expression in (112). On the other hand, if δ is allowed to approach zero, the helix becomes a line helix and S_2 approaches infinity. Equation (128) then becomes unity, showing that the phase velocity in the helix direction for a line helix is the speed of light. The use of (113) is actually tantamount to satisfying the condition (100) on the center line of the tape only. For this reason, it should be expected that equation (128) will favor the thin line

mode of operation over the sheath or butt mode. A study of Figure 25 shows this to be true. The true low frequency phase velocity for a thin tape is somewhere between that given by (112) and (126).

(b) Characteristic Impedance

The characteristic impedance for the narrow tape helix can be found for low frequencies by allowing β_0 to approach zero in equation (76). This expression, when integrated from $\rho = R_2$ to $\rho = R_1$ at $(bz - m\phi) = 0$ will give the difference in potential between the shield and the center line of the narrow tape. Upon dividing this by the current, the characteristic impedance results. This is,

$$Z_0 = \frac{1}{2\pi}\sqrt{\frac{\mu}{\epsilon}}\,\frac{\eta_0}{\eta_2}\left\{\log_e\frac{R_2}{R_1} + \sin\psi\left[\log_e\left(\frac{\epsilon}{\pi}\right) + \frac{\pi^2}{6\delta}\right]\right\} \tag{129}$$

This result is compared in Chapter II with the result for a wire helix having a diameter equal to the tape width.

Bibliography and References

(1) "Electromagnetic Theory" by J. A. Stratton, McGraw Hill Book Company, Inc., New York, 1941.

(2) "Electromagnetic Waves" by S. A. Schelkunoff, D. Van Nostrand Co., Inc., New York, 1943.

(3) "Electromagnetic Fields, Vol. I", by E. Weber, John Wiley & Sons, Inc. New York, 1950.

(4) "Tables of Integrals and Other Mathematical Data" by H. B. Dwight, The Macmillan Company, New York. 1947.

(5) "A Treatise on the Theory of Bessel Functions", by G. N. Watson, The Macmillan Co., New York, 1948.

(6) "Traveling Wave Tubes" by J. R. Pierce, D. Van Nostrand Co., Inc. New York, 1950.

(7) "Tables of Functions" by E. Jahnke and F. Emde, Dover Publications, New York, 1945.

(8) "British Association Mathematical Tables, Vol. X", University Press, Cambridge, 1952.

(9) "Resistance and Inductance of a Helical Conductor" by J. W. Nicholson, Philosophical Magazine, Vol. 19, page 77, 1910.

(10) "A Theoretical Investigation of Electromagnetic Wave Propagation on the Helical Beam Antenna" by J. C. Bagby, M. S. Thesis, Ohio State University, 1948.

(11) "Electromagnetic Wave Propagation on Helical Conductors" by S. Sensiper, D. Sc. Dissertation, Massachusetts Institute of Technology, 1951.

(12) "Electromagnetic Waves on Transformers" by R. Rudenberg. Journal of Applied Physics Vol. 12, page 129, 1941.

(13) "Broadband Transition from Coaxial Line to Helix" by C. Lund, R.C.A. Review Vol. XI, page 133, 1950.

(14) "Hochfrequenzkabel mit Veranderlichem Wellenwiderstand" by E. Keutner, Electriche Fernmeldetechnik, No. 67, page 3, 1943.

(15) "Electrische Stromungsfelder mit Schraubenstruktur", by H. Buchholz, Electrische Nachrictentechnik, Vol. 14, page 264, 1937.

(16) "Helix Impedance of Traveling Wave Tubes" by Ping King Tien, Stanford University E. E. L. Report No. 50. 1952.

(17) "Characteristic Impedance of Shielded Coils" by C. Susskind. T. V. E., page 26, 1951.

(18) "Static and Dynamic Electricity" by W. R. Smythe, McGraw Hill Book Company, New York, 1939.

(19) "A Note on the Inductance of Screened Single Layer Solenoids" by F. M. Phillips Proc. I.E.E. (London) Vol. 96, Part 3, page 138. 1949.

(20) "Engineering Problems in the Exponential Transmission Line Pulse Transformer Design" by J. Kukel, Ph.D Dissertation, Carnegie Institute of Technology, 1953.

(21) "Reference Data for Radio Engineers", 3rd Edition, Federal Tel[illegible]ne and Radio Corporation.

(22) "Electrical Transmission of Power and Signals" by E. W. Kimbark, John Wiley and Sons, Inc., New York, 1949.